Bulk Glass Formation and Crystallization of Zr-Ti Based Alloys

Thesis by

Xianghong Lin

In Partial Fulfillment of the Requirements

for the Degree of

Doctor of Philosophy

California Institute of Technology

Pasadena, California

1997

(Submitted October 1st, 1996)

To my parents,

my wife and son

Acknowledgments

My thesis research would not have been possible without the support of many individuals who deserve much appreciation and recognition. One of the most important, needless to say, is my advisor Prof. William L. Johnson. I joined Bill's group without any material science background. Most of the material science knowledge I have now was acquired from countless "rambling" discussions with Bill during the past four years. The intuition and the ability to grasp the quintessence of a subject passed from one of the finest scientists through these discussions cannot be learned from any class.

Bill has been an unending source of inspiration, support and encouragement. His contagious enthusiasm and optimism kept me going during the difficult and frustrating times of my research. Being a caring mentor, he was always there whenever I needed guidance and moral support, and for this I will always be grateful.

I am grateful to Prof. Brent Fultz, for his kindness, the class he taught and the x-ray differactometer he trained me to use.

I would like to thank Dr. Atakan Peker for the lab training he provided, which was essential for my research. My special thanks go to Ning Zhang, she greatly enhanced my productivity by making many specimens for me during her half year working study. I would like to thank Dr. W. Q. Rhim for letting me use the ESL in JPL. I appreciate the help of Dr. K. Osaka and S. Chung in JPL, and Dr. A. Rulison in Loral Co. with ESL experiments. I would like to thank Carol Garland for providing me TEM pictures.

I am thankful to those researchers of my senior: Drs. C. Samwer, U. Koster, M. Tenhover and C. T. Liu, for broadening my view, which benefited my research.

I would like to thank Dr. Ralf Busch for many stimulating discussions and carefully proofreading this thesis. The people in Keck Lab deserve my appreciation for various reasons: for their friendship, for discussions on various scientific and non-scientific issues, for helping in the lab, and they are: Pam Albertson, David Lee, Liubo Hong, Wenshan Liu, Haein Chi-Yim, Susane Schneider, Uli Guyer, Dale Conner, Richard Dandliker, Jianzhong Li and Andy Masuhr. I would like to thank Guanghua Gao, Xiangdong Fang, Yibo Jiang and Daqi Lu for their friendship which made my life at Caltech more colorful.

I am grateful to Prof. Xiaowei Tang at Institute of High Energy Physics of China, and Prof. Zuhe Bian at University of Science and Technology of China. Under their supervision, I had the first taste of scientific research, which led me to be at Caltech.

The financial support from the Department of Energy under grant No. DE-FG03-86ER45242 is greatly appreciated.

Finally, I would like to express my deepest gratitude to my family. I thank my parents for having sparked curiosity and imagination in a little boy, for instilling me life values, and for their support throughout my life. I thank my wife Baohong for being with me during the most difficult time of my life, for being understanding and supportive. I thank my son Steven for making my life more meaningful. I thank my parents-in law for taking care of my son.

Abstract

The first metallic glass was discovered by Pol Duwez and his colleagues at Caltech in 1960. Shortly after that, Turnbull pointed out that a high ratio of melting temperature over glass transition temperature favors glass formation based on classical nucleation theory. Using Turnbull's theory as a guideline, many alloy systems were found forming glasses. As a new state of metallic alloys, metallic glass is of scientific interest by itself as well as attractive for practical applications due to unique properties. However, since the critical cooling rates for glass formation of conventional alloys are relatively high, at least one dimension of the metallic glass is limited to a few tenths of milimeter. This severely limited the application of metallic glasses.

Recently, several multicomponent alloy systems were discovered that form bulk metallic glasses with the smallest dimension of several mm up to several cm. Two of these alloy systems are the Ti-Zr-Cu-Ni and the Zr-Ti-(Nb)-Cu-Ni-Al alloys, which were discovered during this thesis research.

In this thesis homogeneous and heterogeneous nucleation theories and their influence on glass formation are reviewed. Experimental methods for metallic glass processing are introduced. The formation of Ti-Zr-Cu-Ni and Zr-Ti-(Nb)-Cu-Ni-Al bulk metallic alloys are reported. The glass transition, crystallization behavior, and mechanical properties of these glassy alloys are presented. The optimized combinations of four or five elements in these alloys leads to very deep eutetic multicomponent alloys, in which nucleation of crystals upon undercooling becomes

increasingly improbable. Thermodynamic, kinetic and topological factors are discussed that contribute the exceptional glass forming ability of these alloys.

The very high stability of the undercooled liquids of bulk glass forming alloys makes it possible to perform studies on undercooled liquids in a time and temperature window that was not accessible thus far. In this thesis the time temperature transformation diagrams were measured for the crystallization of undercooled Zr-Ti-(Nb)-Cu-Ni-Al liquids. It has been discovered that the crystallization of the undercooled liquid is caused by heterogeneous nucleation induced by oxide particles, even when the oxygen concentration is as low as 250 atomic ppm. Overheating the melts above the liquidus temperature of the oxide particle results in maximum undercooling. Strong oxygen concentration dependence of the overheating, undercooling, and TTT diagrams was found. These results suggest that impurities play a key role in the crystallization of undercooled liquid. This first systematic study of impurity effect on crystallization of undercooled liquid will have many important implications on making bulk glasses and any study of undercooled liquids.

To summarize this thesis, important factors which affect the crystallization are revealed and discussed. Strategies on how to find new bulk metallic glasses are suggested.

Contents

List of Figures

Chapter 1

Chapter 2

List of Tables

Chapter 1
Introduction

The study of metallic glass dates back to 1960 when Klement, Willens and Duwez at Caltech rapid quenched Au-Si melts into glasses.[1] Since then, metallic glasses have been one of the focuses for scientific research.

1.1 DEFINITION OF GLASS

The first question one would ask is what is glass. A glass is a vitrified liquid. It is a solid in which the structure of liquid is preserved.

A solid has been defined as[2] a material whose viscosity exceeds $10^{13.6}$ Nsm^{-2}. This rather arbitrary division by viscosity corresponds to a relaxation time of one day. From practical view, no permanent deformation is detected during normal experimental time scales when a solid is under a reasonable stress. For comparison, the viscosities of common liquids at room temperature are of the order of 10^{-3} Nsm^{-2}.

The most common solid materials are the crystalline materials. For simplicity, a crystal is a regular assembly of atoms. Each atom has one site, which is defined by its geometrical relation with the crystal lattice. The atom undergoes thermal vibration around the mean position. The crystal lattice has long range translational periodicity. For comparison, a liquid is a more "random" array of atoms lacking translational periodicity which undergo thermal vibration. However, there are some restrictions on the randomness of liquid, such as no two atoms can be closer than the atoms "hard core" diameter and there is no space for extra atoms (the packing is

dense). A glass is a non-crystalline solid or so called amorphous solid. The atomic structure of a glass has the similar randomness to that of a liquid. There is no long range order in a glass either. The amorphous nature of glasses is most clearly shown by diffraction experiments. For example, in x-ray diffraction experiment, one observes broad diffuse haloes produced by glassy samples instead of sharp Bragg peaks produced by crystalline samples. However, the diffraction pattern of a polycrystalline material which has a grain size below a few nanometers is hard to distinguish from that of a glass.

Besides the amorphous nature of the structure, the most important characteristic of a glass is the glass transition. The glass transition is the phenomenon in which a glass exhibits a more or less abrupt change in derivative thermodynamic modulii (such as heat capacity or thermal expansivity) from crystal-like to liquid-like values with change of temperature. Fig. 1.1 shows a typical heat capacity curves of a glass, the corresponding liquid and crystalline solid as a function of temperature.[3] The temperature at which the abrupt change of heat capacity occurs is called glass transition temperature, T_g. The ratio of T_g to the melting temperature of the crystalline alloy, T_m, is called reduced glass transition temperature, T_{rg}. Below the glass transition temperature, the non-crystalline material is called glass. Above the glass transition temperature and below the melting temperature, the non-crystalline material is called undercooled liquid. Fig. 1.2[4] shows the viscosity of the undercooled liquid as a function of temperature. One notices that the viscosity value is $10^{13.6}$ Nsm^{-2} around the glass transition temperature. Using the existence of glass transition, one can distinguish a glass from an ultrafine

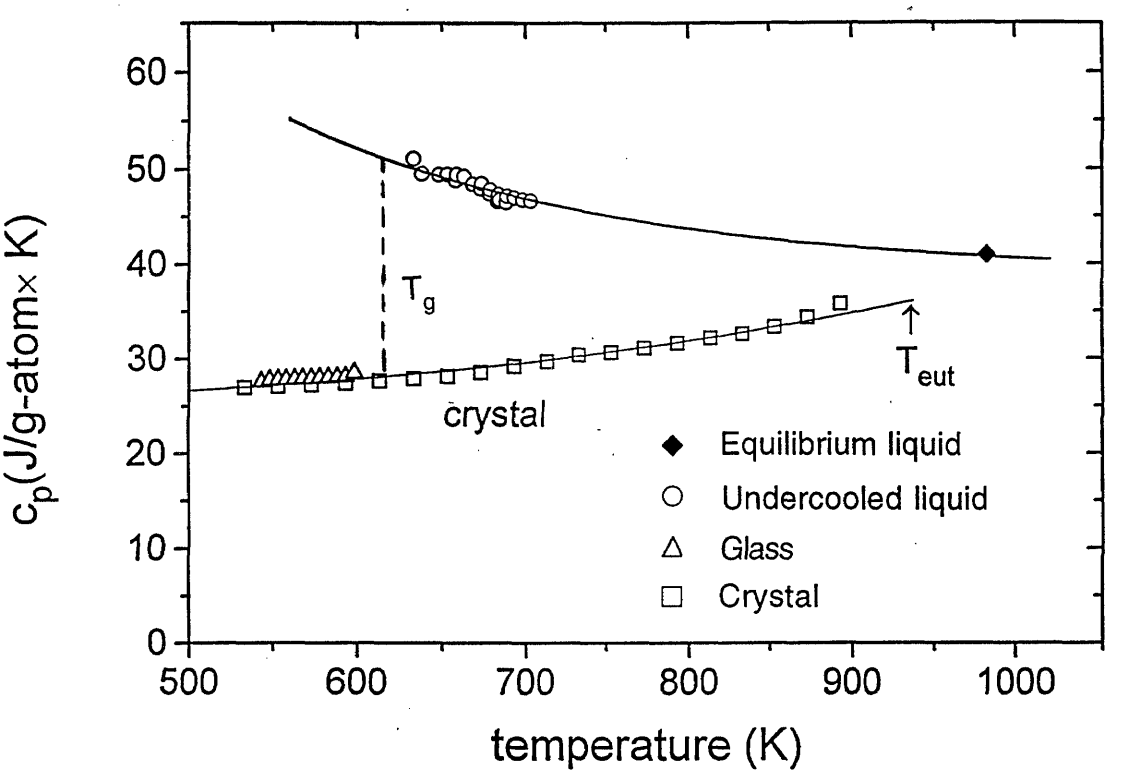

Fig. 1.1 Heat capacity curves of the $Zr_{41.2}Ti_{13.8}Cu_{12.5}Ni_{10}Be_{22.5}$ glass, the corresponding liquid and crystalline solid as a function of temperature. (reproduced from ref. 3)

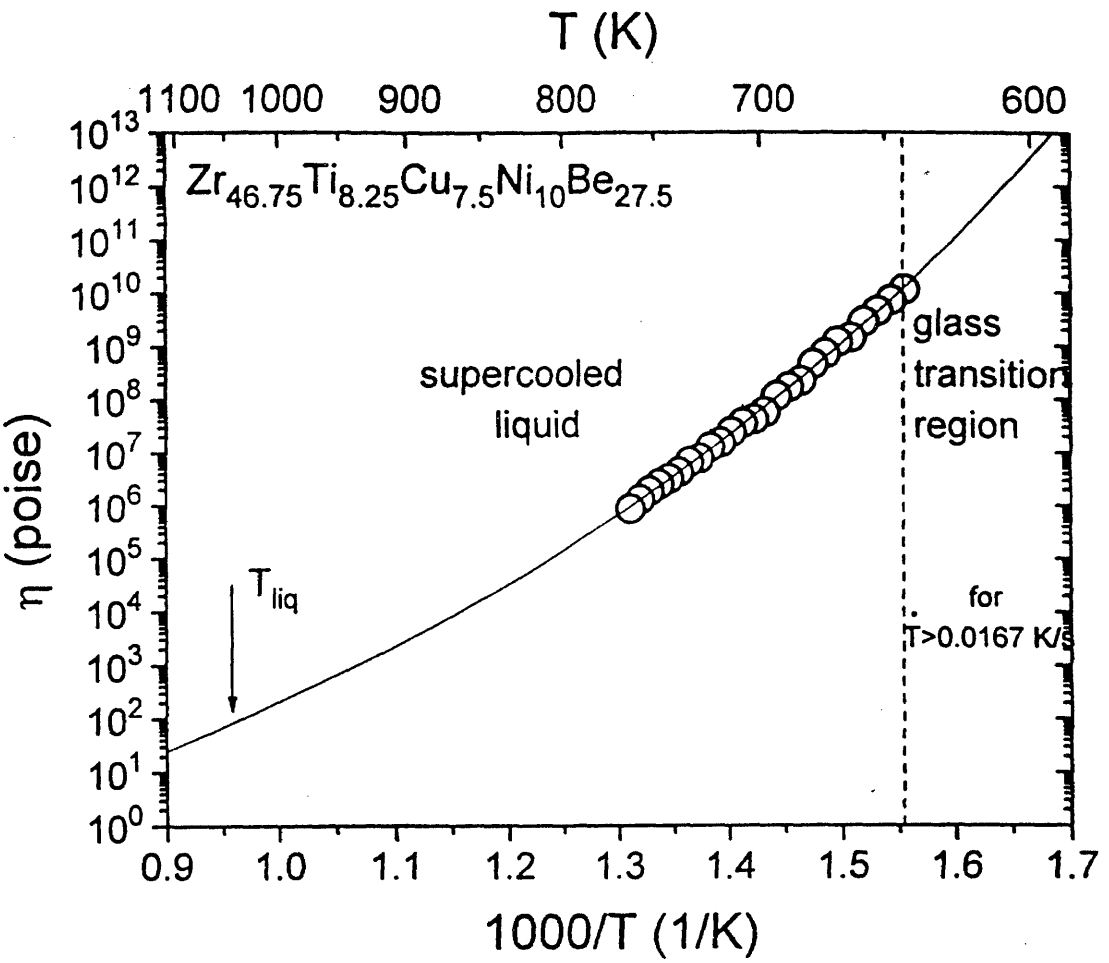

Fig. 1.2 Equilibrium viscosity as a function of temperature for the undercooled liquid of $Zr_{46.75}Ti_{8.25}Cu_{7.5}Ni_{10}Be_{27.5}$ alloy. Also shown is the Vogel-Fulcher fit to the data. (reproduced from ref. 4)

nanocrystalline material. Because of the importance of glass transition , some researchers prefer to define a glass as an amorphous solid which exhibits glass transition. Under this definition, not all amorphous solids are necessarily glasses. However, since all the amorphous alloys which I am going to discuss in this thesis exhibit a glass transition, I will use the words "amorphous" and "glassy" indistinguishably.

1.2 SOLIDIFICATION OF LIQUID

According to experiments, all glasses crystallize if they are annealed at high enough temperature and/or for long enough time. This suggests that a glass is a metastable phase comparing to corresponding equilibrium crystalline phases. Therefore, the formation of glasses is a kinetic process.

Since the most common method to obtain glasses is melt quenching, I would like to start the discussion with liquid.

For a thermodynamic system, Gibbs free energy of the system is:

$$G=H-TS \qquad (1.1)$$

where H is enthalpy of the system, S is entropy, and T is temperature. In laboratory study, the pressure and temperature are fixed. Hence, when several phases are available for a system of one composition, the one of lowest G value is the stable phase.

Since a metallic crystal has a closed-packed or nearly closed-packed structure, it has lower enthalpy than a random-packed liquid metal. On the other hand, because the atoms in the liquid have more freedom, the liquid has higher entropy. Therefore, concerning eq. 1.1, at low temperature, G for crystalline solid is smaller than that of liquid, while at high temperature, the liquid has smaller G than crystalline solid. Fig. 1.3

schematically illustrates the Gibbs free energy of crystalline solid and liquid varying with temperature. The melting temperature T_m is the temperature at which crystal and liquid have the same G value.

Cooled below the melting temperature, an energetically less stable undercooled liquid tends to transform to the more stable crystalline solid. The free energy difference between the liquid and crystal acts as the driving force for crystallization. However, to nucleate a crystalline phase out of the liquid phase, an interface between these two phases must be created. Due to the different structures of these two phases, a mismatch along the interface arises. The positive energy associated with the mismatch is called interfacial energy between the crystal and liquid phases. This interfacial energy disfavors the crystallization of the liquid. Following the approach taken by Volmer and Weber[5] to treat the problem of vapor condensation, Turnbull and his colleagues developed the classical homogeneous nucleation theory for liquid solidification (see ref. 6, 7 for review). Homogeneous nucleation is nucleation which occurs without the catalytic aid of foreign bodies. In contrast, heterogeneous nucleation is catalyzed by such bodies.

In Turnbull's treatment, it is assumed that the crystals forming have the same composition as the liquid. This is called the polymorphic approximation. The following are the major steps in the treatment.

The undercooled liquid contains some clusters of atoms, which have the structure of corresponding crystal. The free energy change associated with the existing crystalline embryos has two terms. One is the free energy decrease due to the liquid to crystal transformation, which is proportional to the volume of the embryo. The other is the free energy

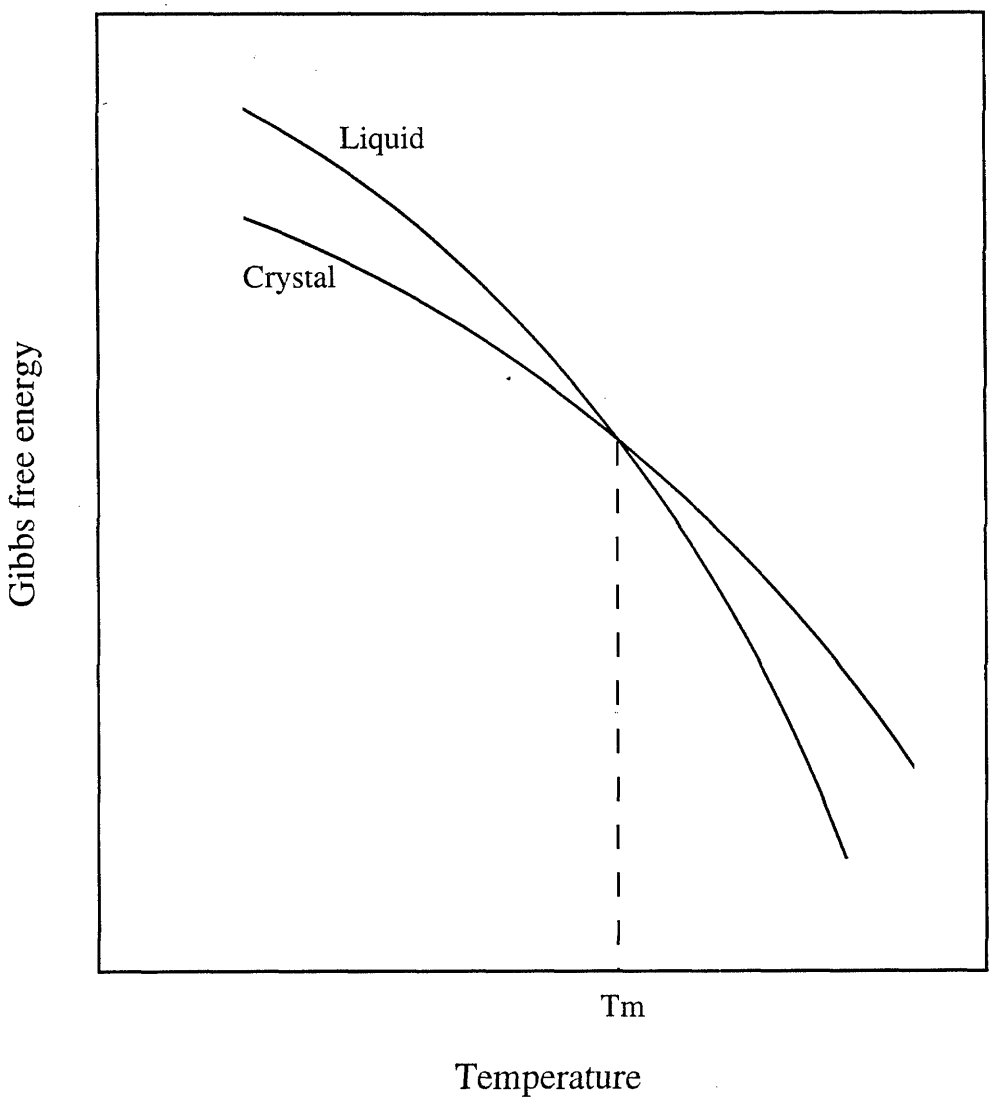

Fig. 1.3 Hypothetic Gibbs free energies for a liquid and corresponding crystal as a function of temperature.

increase due to the creation of liquid-crystal interface, which is proportional to the surface area of the embryo. As such, the free energy change due to the formation of a spherical crystal can be written as:

$$\Delta G = 4\pi r^2\sigma + \frac{4\pi}{3} r^3 \Delta G_v \tag{1.2}$$

where ΔG_v is the free energy difference between liquid and crystal per unit volume, σ is the liquid-crystal interfacial energy per unit area. Fig. 1.4 shows the volume term, surface term, and the total change of free energy, ΔG as functions of embryo radius. The competition between these two terms gives a free energy maxima:

$$\Delta G^* = \frac{16\pi}{3}\left(\frac{\sigma^3}{\Delta G_v^2}\right) \tag{1.3}$$

at a critical nucleus radius:

$$r^* = -\frac{2\sigma}{\Delta G_v} \tag{1.4}$$

ΔG^* is the nucleation energy barrier. Since σ is relatively independent of temperature and ΔG_v is approximately proportional to the undercooling, ΔG^* decreases as temperature decreasing.

In an equilibrium liquid, the population of different sized nuclei follows a thermodynamic distribution. The number of critical nuclei per unit volume is given by:

$$n^* = n\exp\left(-\frac{\Delta G^*}{kT}\right) \tag{1.5}$$

where n is total number of atoms per unit volume, k is the Boltzmann's constant. Assuming that each critical nucleus grows into a crystal, and is thereby removed from the distribution of embryo sizes, the subsequent rate of formation of nuclei is determined by the rate at which smaller embryos reach the critical size. For the small embryos to grow, atoms need to transport from the liquid side of the interface to the crystal side. Hence,

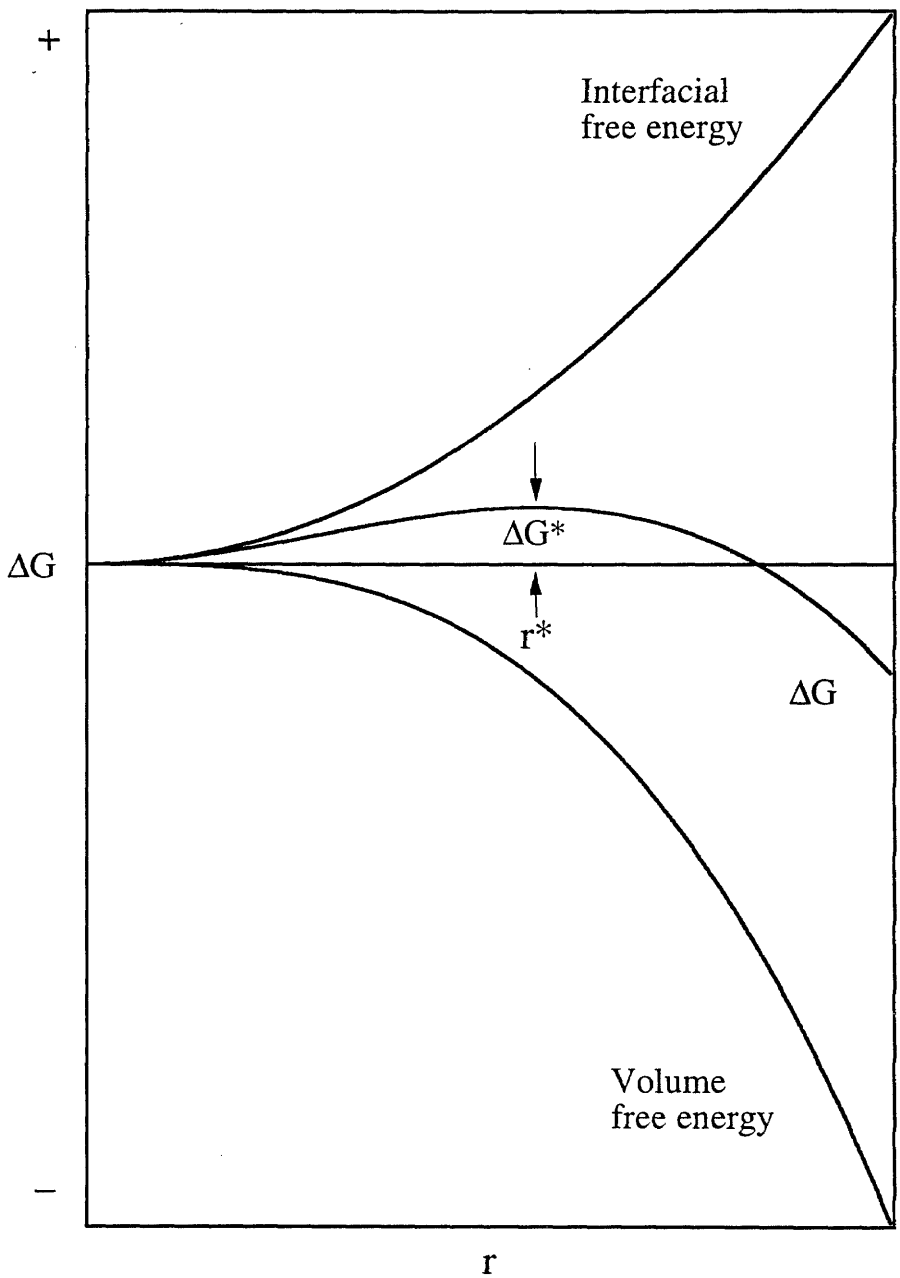

Fig. 1.4 Gibbs free energy associated with the nucleation of a crystalline embryo as a function of its radius.

the embryos growth rate is determined by the rate of atom transport. The atom transport rate is described by the atomic difusivity, which is inversely proportional to viscosity of the undercooled liquid. Therefore, the homogeneous nucleation rate was shown to be given by:

$$I_v = \frac{k_n}{\eta(T)} \exp\left(-\frac{\Delta G^*}{kT}\right) \tag{1.6}$$

where k_n is a kinetic constant, η is the viscosity. The viscosity of the undercooled liquid increases dramatically with decreasing temperature. From the melting temperature to the glass transition temperature, it is commom for the viscosity to increase more than ten orders of magnitude. The strong temperature dependence of viscosity has been described by the Vogel-Fulcher relation as:

$$\eta(T) = A \exp\left(\frac{B}{T - T_o}\right) \tag{1.7}$$

where A, B and T_o are constants.

For simplicity, using the linear approximation, the expression for ΔG becomes:

$$\Delta G = -\frac{L \Delta T_r}{V_m} \tag{1.8}$$

where L is the molar latent heat of fusion, V_m is molar volume of the crystal, and ΔT_r is the reduced undercooling defined as:

$$\Delta T_r = \frac{(T_m - T)}{T_m} \tag{1.9}$$

Thus, the homogeneous nucleation frequency becomes:

$$I_v = \frac{k_n}{\eta(T)} \exp\left(-\frac{16\pi}{3} \frac{\alpha^3 \beta}{\Delta T_r^2 T_r}\right) \tag{1.10}$$

where T_r is the reduced temperature T/ T_m, α and β are dimensionless parameters defined as:

$$\alpha = \frac{(NV_m^2)^{1/3}\sigma}{L}$$
$$\beta = \frac{L}{RT_m} \qquad (1.11)$$

where N is Avogardro's number.

According to this formula, as ΔT_r increases, I_v initially increases rapidly reflecting the increasing driving force, until, eventually, it peaks and undergoes a sharp decrease, as the increasing η becomes dominant at large ΔT_r. Taking typical values for the constants in eq. 1.11., Turnbull calculated the homogeneous nucleation frequency for alloys of varying T_{rg}, as shown in fig. 1.5.[8] The results suggest that if the cooling rate is sufficiently high, even one single nucleus can be avoided. As such, the melt vitrifies to a glass. A strong T_{rg} dependence of nucleation rate is clearly shown in fig 1.5. The reason for T_{rg} dependence of I_v can be seen in the following arguments. The higher the T_{rg}, the narrower the temperature window for η to change from a typical value for a liquid to a typical value for a solid, thus, the more rapidly η increases. Therefore, it is easier to avoid crystallization for an alloy with higher T_{rg}. For a ready glass forming alloy, T_{rg} is usually greater than 0.5. According to Turnbull, when T_{rg} approaches 2/3, the homogeneous nucleation rate is so low that crystallization can be easily avoided, which in turn results the formation of bulk glass.

In above arguments, only homogeneous nucleation is considered. However, it is frequently the case that the container wall which holds the undercooled liquid and impurities within the liquid will catalyze the nucleation. This will be discussed in chapter 5.

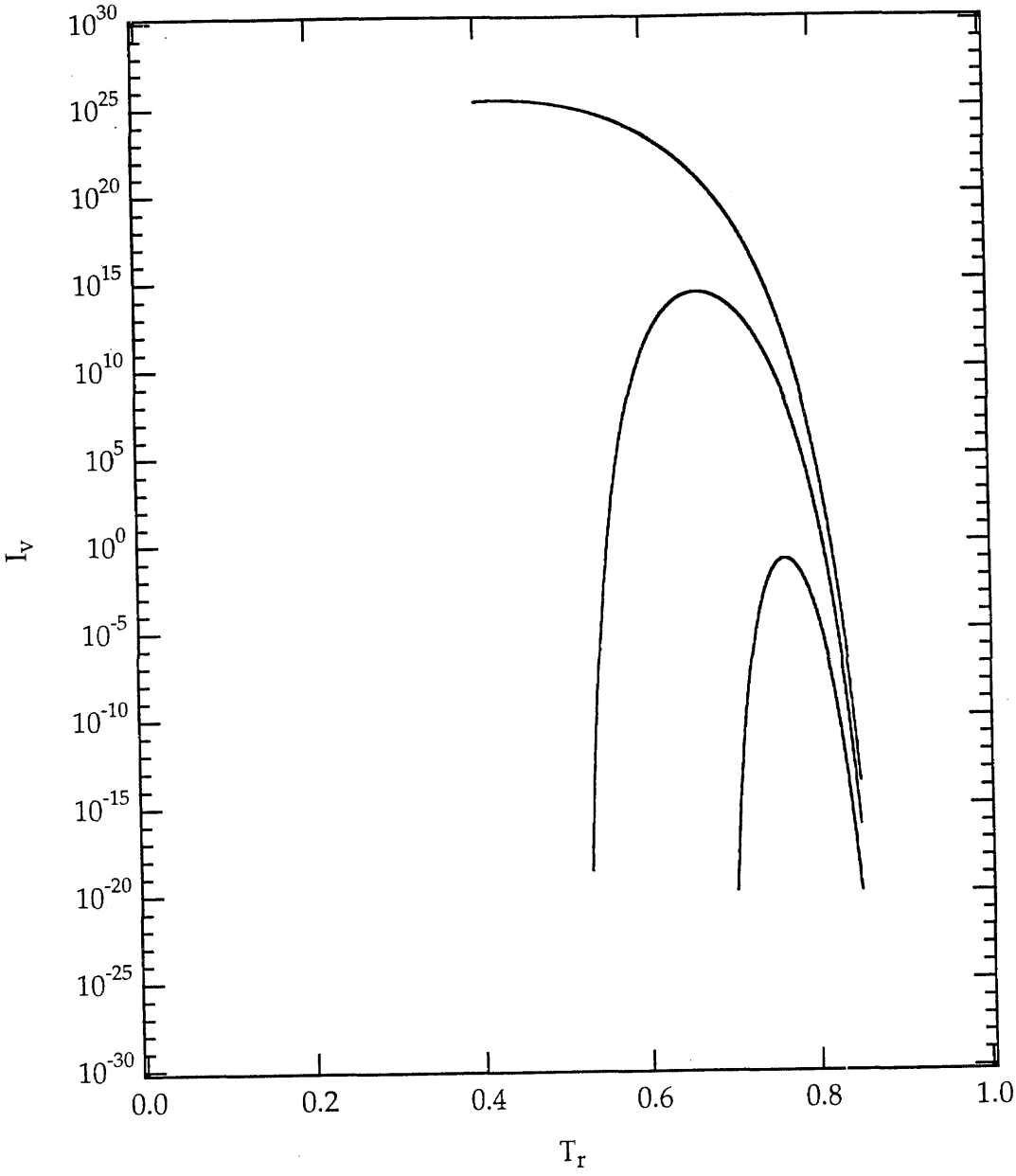

Fig. 1.5 Homogeneous crystal nucleation frequency in undercooled liquids, which have various values of reduced glass transition temperature, as functions of reduced temperature. (reproduced from ref. 8)

1.3 SYNTHESIS OF METALLIC GLASS BY RAPID QUENCHING THE MELT

By quenching a metallic alloy melt, such that the cooling rate is so high that the crystallization is avoided, a metallic glass is obtained. The lowest cooling rate for glass formation for an alloy is called the critical cooling rate. The dimension of the sample determines the rate of heat transformation from the sample to a substrate, and thus determines the cooling rate during the quench. For simplicity, we consider a infinitely large plate. Then heat conduction is only possible for one dimension. A sample of thickness R and initial temperature T_m will require a total cooling time t (to T_g) of the order of:

$$t\sim(R^2/k) \qquad (1.12)$$

where k is the thermal diffusivity of the alloy. It is given by k =K/C where K is the thermal conductivity and C is the heat capacity per unit volume. The cooling rate achieved will be of the order of:

$$dT/dt=(T_m-T_g)/\ t=K(T_m-T_g)/CR^2 \qquad (1.13)$$

Taking T_m-T_g~400 deg, K~0.1W/cm $\cdot$ s^{-1} $\cdot$ deg^{-1} (typical of a molten alloys), and C~4J/cm^3 K^{-1} (also typical of molten alloys), gives:

$$dT/dt(K/s)=10/R^2(cm) \qquad (1.14)$$

This formula shows how the cooling rate in a "one-dimensional" quench is determined by the sample thickness. Notice that one order of magnitude increase in the sample thickness is equivalent to a two orders of magnitude decrease in the cooling rate. Consequently, the maximum sizes of glassy samples are determined by the critical cooling rates of the alloys.

Since the critical cooling rates for most metallic glasses are relatively high, some special quenching equipment is needed to obtain very thin samples and thus to achieve high cooling rate. Following are some examples.

1.3.1 Gun quenching

Fig. 1.6 schematically shows a gun quenching apparatus.[9] A small alloy sample is melted in the non-reactive container. The shock wave produced by releasing high pressure inert gas to the gun atomizes the drop in to small droplets which are propelled on to a copper substrate. A cooling rate of 10^6-10^8 K/s can be achieved. The first metallic glass ($Au_{75}Si_{25}$) was produced by this equipment.[1] The flakes produced by this equipment are ideal for TEM study.

1.3.2 Piston-Anvil

Fig. 1.7 shows the schematic of a piston-anvil apparatus.[9] A falling melt drop is detected by a photocell. This releases a pneumatically-operated piston to smash the droplet to the anvil. The cooling rate of this process is of the order of 10^6 K/s. Uniform foils of thickness from 30 to 50 μm produced by this equipment are ideal for the measurement of physical properties such as electrical resistivity.

1.3.3 Melt spinning. Fig. 1.8 shows the schematic of a melt spinning apparatus.[10] The melted alloy in the nonreactive container is ejected onto a rotating drum through a nozzle. Uniform sheets having thicknesses of 15-150 μm have been produced continuously. The thickness of the sheets, and in turn the cooling rate, is controlled by the rotation speed of the drum. Commercial amounts of metallic glasses have been produced by this type of apparatus.

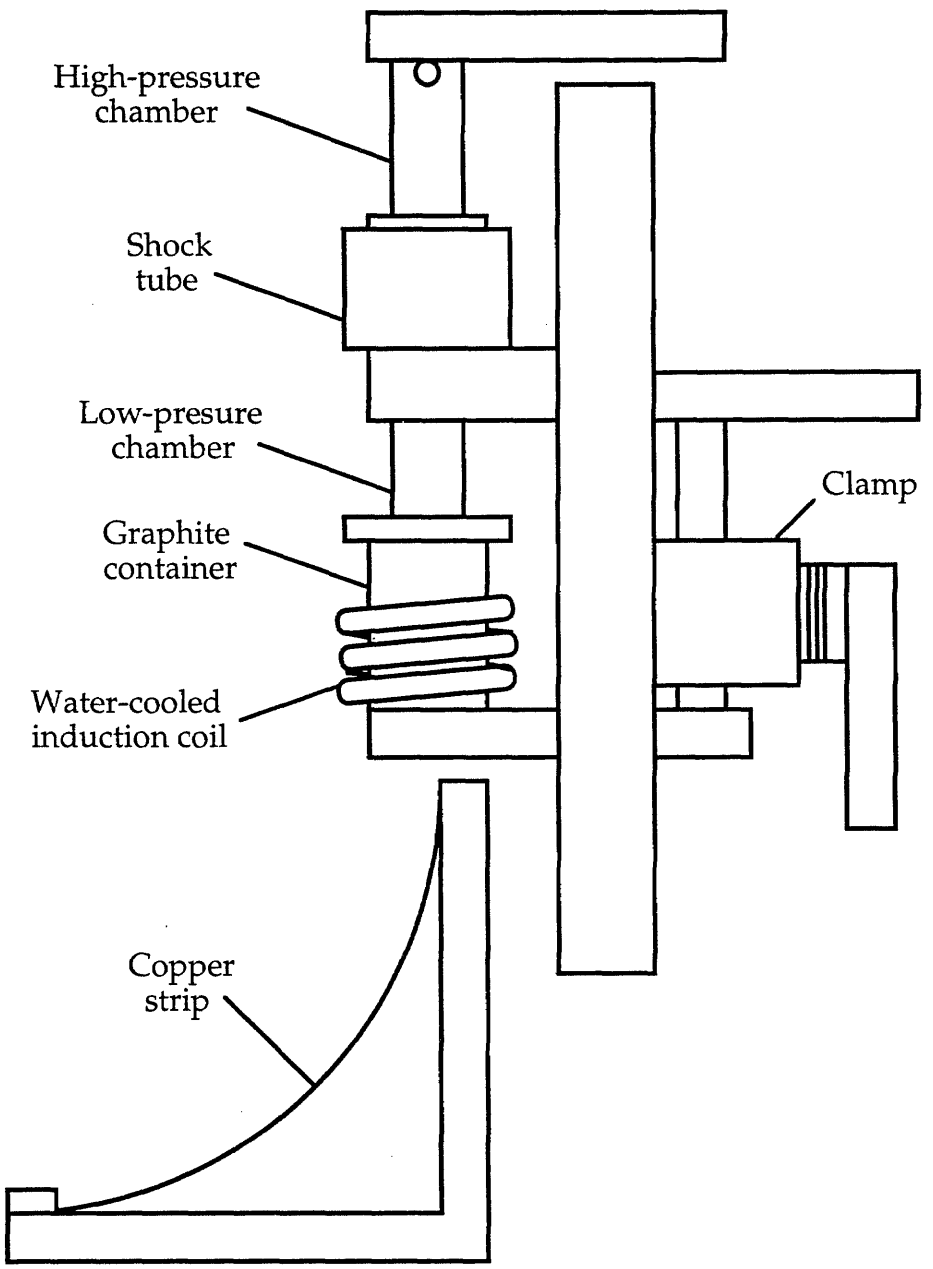

Fig. 1.6 Schematic illustration of the gun quenching apparatus. (reproduced from ref. 9)

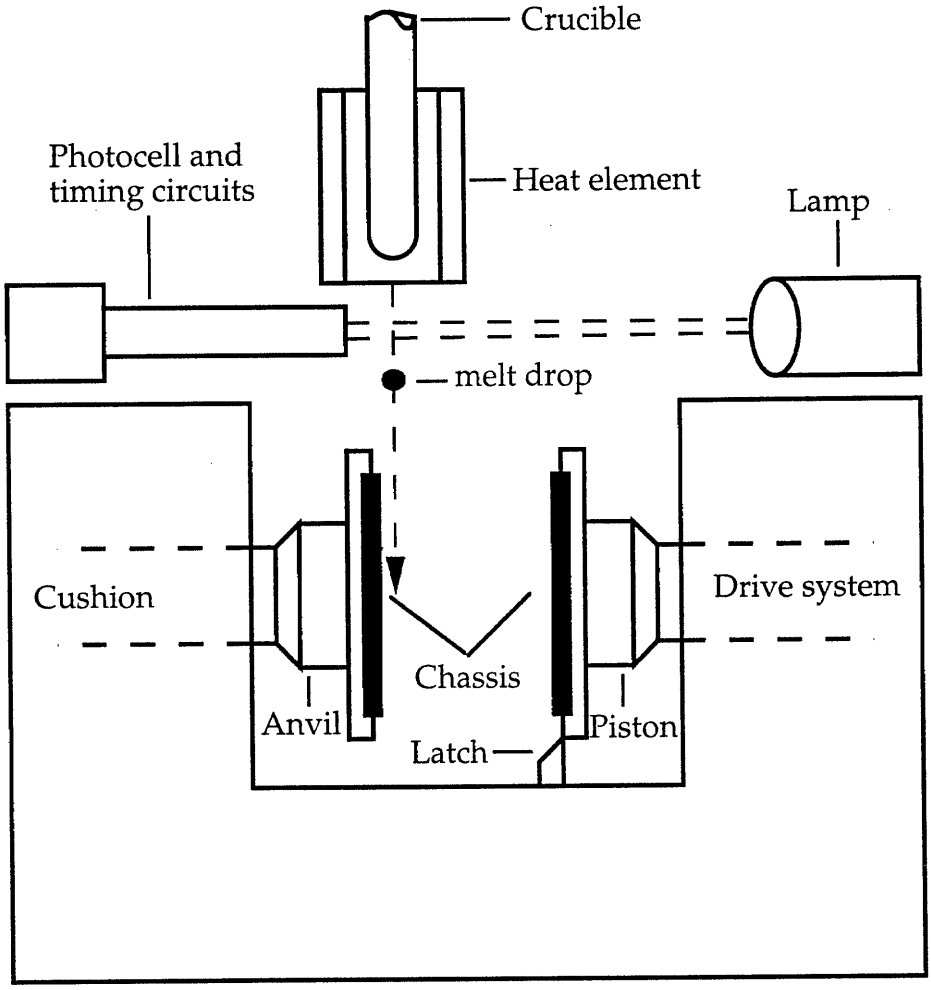

Fig. 1.7 Schematic illustration of the piston-anvil device. (reproduced from ref. 9)

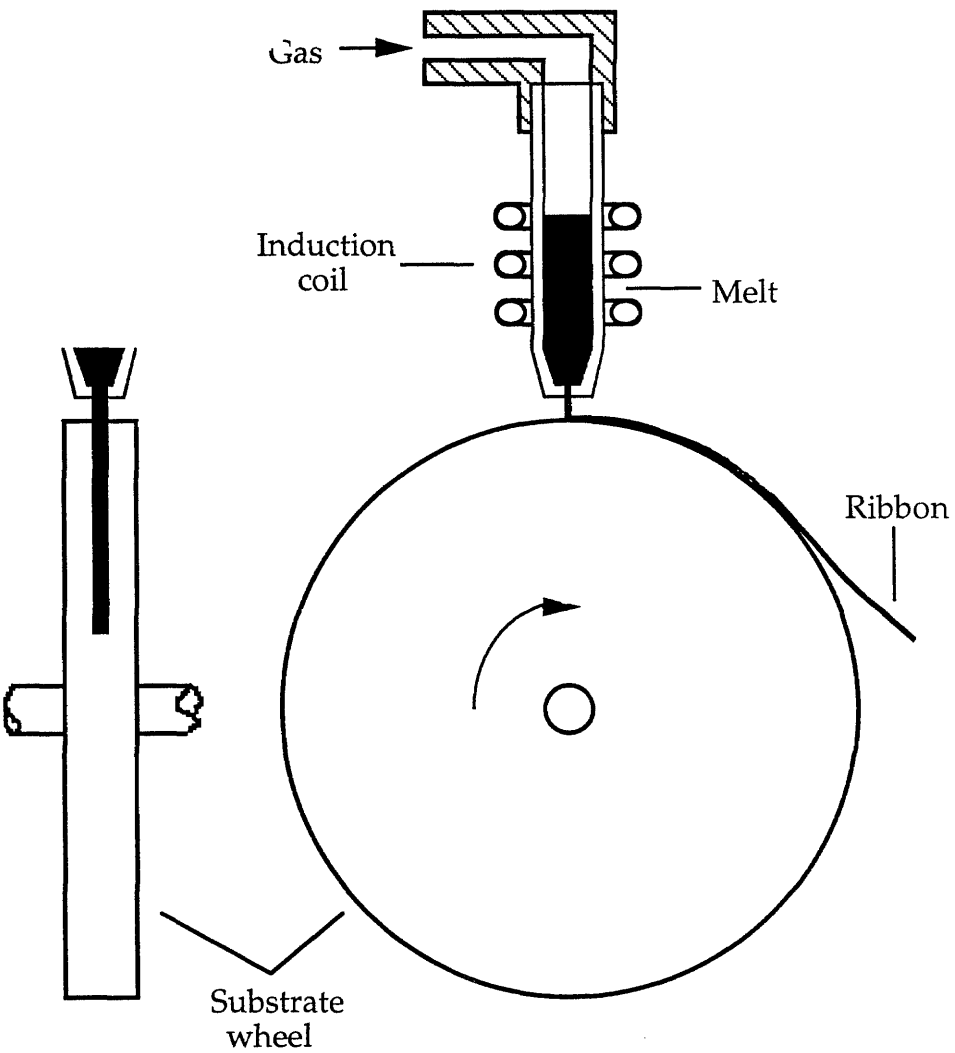

Fig. 1.8 Schematic illustration of the melt spinning device. (reproduced from ref. 10)

1.3.4 Laser surface treatment

A focused laser beam can deliver extremely high power concentration in a small spot at an alloy surface. Scanning the laser over the alloy surface yields a shallow molten layer at the alloy surface. The substrate acts as a built-in chill block. High cooling rate over 10^6 K/s can be achieved and a glassy layer can be obtained at the surface of some alloys. Fig. 1.9 shows schematic of laser treatment[10]. However, it is difficult to turn an alloy surface into a glass in general, since the present of a crystalline substrate acting as a catalyst for crystallization.

1.4 SYNTHESIS OF METALLIC GLASS FROM THE SOLID STATE

Besides rapid quenching the molten alloy, it is also possible to produce amorphous alloys from the solid state. The underlying mechanism of solid state methods was discussed by Johnson[11]. Fig. 1.10 illustrates the free energy relationship for nonequilibrium crystalline solid that undergoes a crystal-to-glass transformation. The characteristic time scales for respective transformations are also indicated. When the equilibrium crystalline state is driven to a nonequilibrium state, the nonequilibrium state will transform to glass if thermodynamic and kinetic criteria are satisfied. The thermodynamic criterion is that the free energy of the nonequilibrium crystalline is higher than that of the amorphous state. The free energy difference of nonequilibrium crystalline state and amorphous state offers the driving force for glass formation. The kinetic criteria are:

$t1<t2$, $t1<t3$ and $t1<t2'$ (1.15)

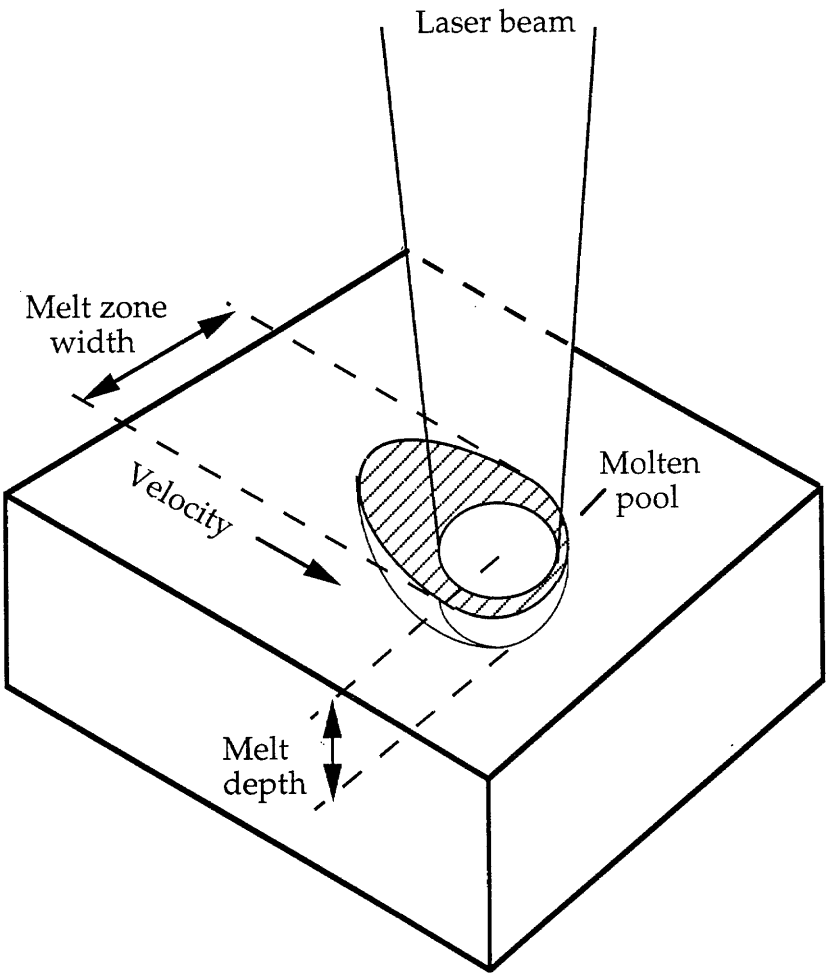

Fig. 1.9 Schematic illustration of laser beam-substrate geometry during rapid surface melting and refreezing by laser treatment. (reproduced from ref. 10)

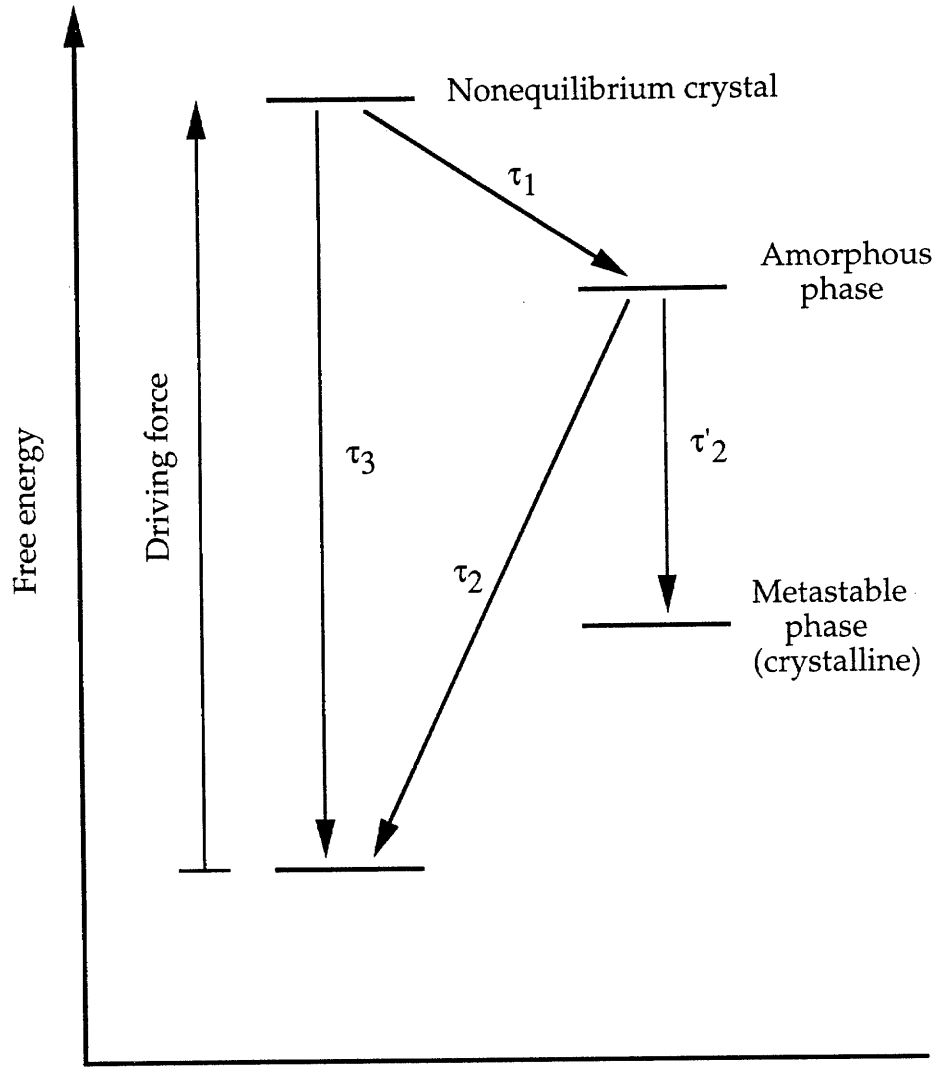

Fig. 1.10 Illustration of free energy relationship and transformation time scales (τ_1, τ_2, τ_3, τ'_2) for a nonequilibrium crystalline solid that undergoes a crystal-to-glass transformation. (reproduced from ref. 11).

These conditions ensure that neither will the nonequilibrium crystalline state transform directly to the equilibrium crystalline state nor will the formed amorphous phase transform to the equilibrium or metastable crystalline phase during the time scale of the experiment. The glassy phase is therefore formed and sustained.

One example of solid state amorphization is the diffusion couple experiment which is first reported by Schwarz and Johnson.[12] The principle is that the free energy of amorphous state is lower than that of physical mixture of the pure elements or their solid solution. Therefore a layer of amorphous is formed between the layers of the pure elements, provided the kinetic criteria are satisfied.

The other cases of solid state amorphization use high energy particles (electrons, ions, and neutrons) irradiation or mechanical attrition (such as ball milling) to produce defects in the initial crystalline phase. The free energy of the crystalline phase increases as the defect density increases. The crystalline phase transforms to an amorphous phase when the free energy of crystalline is sufficiently higher than amorphous phase, again, provided kinetic criteria are satisfied.

Hydrogen induced amorphization is another example.[13]

1.5 GLASS FORMING ALLOYS

$Au_{75}Si_{25}$ is the first alloy which was quenched to a glass from the melt.[1] Shortly after the discovery was reported, Cohen and Turnbull suggested that the formation of metallic glass in the Au-Si system around 25% Si is connected with the existence of a deep eutectic near this composition.[14] They pointed out that this gives the melt the chance to

cool easily to a low temperature at which its viscosity is quite high and thus the crystallization is sluggish enough to enable the melt to vitrify during the rapid quench. This at once provided a systematic basis for finding other glass forming alloys. Thereafter, large numbers of metallic glasses were discovered. These metallic glasses generally fall into one of two categories, metal-metalloid glasses or metal-metal glasses. The metal-metalloid glasses contain about 80 at.% of a transition metal (for example, Fe, Ni, Co, and so on) and 20 at.% of a metalloid element (for example, Si, P, B, C, and so on). The metal-metal glasses contain an early transition metal or rare earth element (for example, Zr, Ti, Nb, Ta, and so on) and a later transition metal element (for example, Cu, Ni, Co, and so on).

These metallic glasses have unique properties which are different from corresponding crystalline materials. Low coercive magnetic force and relative high permeability, combined with very high mechanical hardness and tensile strength, make Fe and Ni based glasses excellent material for power transformer cores, transducers, and etc. (for review, see ref . 15). Some alloys (for example, Fe-Cr-P-C[16]) have extraordinarily high corrosion resistance in hostile environment. This makes them excellent coating materials. The low melting temperatures of glass forming alloys makes ductile amorphous foil excellent filler for accurate brazing and soldering (for review, see ref. 17). Mechanical properties such as high hardness and close-to-theoretical-limit high strength attract applications as structure materials. However, the critical cooling rate required for glass formation in these systems remains high (10^4-10^6 K/s for most of the alloys). Heat transport requirement limits the maximum thickness of metallic glasses to between 10 and 100 μm, with a few noble metal based so

called "bulk metallic glasses" as exceptions. Au-Pb-S[18] and Pd-Ni-P[19,20] alloys are two examples. These alloys have been quenched to glasses with dimensions up to 1 to 10 mm at cooling rates in the 1-1000 K/s range. The practical applications of metallic glasses are limited by the small dimensions, especially for structure applications.

This situation did not change for decades until early 1990's, when several multicomponent bulk glass forming alloy systems, such as La-Al-Ni[21], Zr-Ni-Cu-Al[22], and Mg-Cu-Y[23] were discovered by Inoue et al. at Tohoku University in Japan. The new alloys have critical cooling rates for glass formation of the order of 100 K/s. Glassy samples can be quenched from melt up to dimensions of several mm. Encouraged by these results, Peker and Johnson at Caltech discovered an exceptionally good glass forming alloy system: Zr-Ti-Cu-Ni-Be[24]. Certain alloys in this system have a critical cooling rate for glass formation of the order of 1 K/s. This permits the formation of large three dimensional metallic glass specimens, which have the smallest dimension of several cm. With samples of such size, whole new areas of application become possible for metallic glasses. The development of these new bulk glasses has been described as "the music to the ears".[25] Further, the very high degree of resistance to crystallization of the newly developed alloys has opened new opportunities for fundamental study of the undercooled liquid state itself and glass transition.

Since "bulk metallic glasses" are so important for both scientific studies and for technical applications, it is always desirable to develop more bulk metallic glass forming systems. Further, the toxicity of beryllium in Zr-Ti-Cu-Ni-Be system is an unfortunate drawback for some

practical applications. Thus, the theme of this thesis research was to search for new bulk metallic glasses based on practically useful metals.

REFERENCES

1. W. Klement IV, R. H. Willens, and P. Duwez, Nature **187**, 869 (1960).
2. S. R. Elliott, *Physics of Amorphous Materials,* (Longman Group Ld., London, 1983), p 5.
3. R. Busch, Y. J. Kim, and W. L. Johnson, J. Appl. Phys. **77**, 4039 (1995).
4. E. Bakke, R. Busch, and W. L. Johnson, Appl. Phys. Lett. **67**, 3260 (1995).
5. M. Volmer, and A. Webber, Z. Phys. Chem. **119**, 277 (1925).
6. J. H. Holloman, and D. Turnbull, Prog. in Met. Phys. **4**, 333 (1953).
7. D. Turnbull, *Solid State Physics,* **Vol. 3**, (Academic Press, New York, 1956).
8. D. Turnbull, Contemp. Phys., **10**, 473 (1969).
9. P. Duwez, Trans. AMS **60**, 607 (1967).
10. R. W. Cahn, in **Physical Metallurgy**, edited by R. W. Cahn, and Haasen, (North-Holland Physics Publishing, Amsterdam, 1983), p 1779.
11. W. L. Johnson, in *Metals Handbook*, **Vol. 2**, 10th ed., (ASM International, 1990), p 804.
12. R. B. Schwarz, and W. L. Johnson, Phys. Rev. Lett. **51**, 415 (1983).
13. X. L. Yeh, W. L. Johnson, and K. Samwer, Appl. Phys. Lett. **42**, 242 (1983).
14. M. H. Cohen, and D. Turnbull, Nature **189**, 869 (1961).
15. C. H. Smith, in *Rapid Solidified Alloys*, edited by H. H. Liebermann,, (Marcel Dekker, New York, 1993), p. 617.
16. M. Naka, K. Hashimoto, and T. Masumoto, J. Japan Inst. Metals, **38**, 835 (1974).
17. A. Rabinkin, and H. H. Liebermann, in *Rapid Solidified Alloys*, edited by H. H. Liebermann,, (Marcel Dekker, New York, 1993), p. 691

18. M. C. Lee, J. M. Kendall, and W. L. Johnson, Appl. Phys. Lett. **40**, 382 (1982).

19. A. J. Drehman and A. L. Greer, and D. Turnbull, Appl. Phys. Lett. **41**, 716 (1982).

20. H. W. Kui, A. L. Greer, and D. Turnbull, Appl. Phys. Lett. **45**, 615 (1984).

21. A. Inoue, T. Zhang, and T. Masumoto, Mater. Trans. JIM **31**, 425 (1990)

22. T. Zhang, A. Inoue, and T. Masumoto, Mater. Trans. JIM **32**, 1005 (1991).

23. A. Inoue, T. Nakamura, N. Nishiyama, and T. Masumoto, Mater. Trans. JIM **33**, 937 (1992).

24. A. Peker, and W. L. Johnson, Appl. Phys. Lett. **63**, 2342 (1993).

25. A. L. Greer, Nature **366**, 303 (1993).

Chapter 2
Ti-Zr-Cu-Ni Quaternary Bulk Glass Forming Alloys

2.1 INTRODUCTION

According to Turnbull's homogeneous nucleation argument, a high reduced glass transition temperature T_{rg} is necessary for a good glass forming ability (GFA) of an alloy.[1] As a rough approximation, the glass transition temperature T_g of an alloy should scale with the cohesive energy of the material. In many alloy systems, the cohesive energy is mainly determined by the weighted mixture of the cohesive energy of the elemental constituents. Therefore, T_g is roughly proportional to the averaged boiling temperature, which varies slowly with composition. Experimental results generally support this expectation. On the other hand, the melting temperature of alloys changes dramatically with composition. Therefore, it is frequently the case that alloys near deep eutectics have higher T_{rg} and hence exhibit better glass forming ability.

Fig 2.1, 2.2, 2.3, and 2.4 show the binary phase diagrams for Ti-Ni, Ti-Cu, Zr-Ni, and Zr-Cu systems, respectively.[2] These binary systems all exhibit deep eutectics. Binary alloys in these systems have been known to form glass by rapid solidification for many years. On the other hand, the crystal structures of the binary intermetallic compounds which form in these binary alloys differ among the systems. Thus, one expects to find ternary or quaternary eutectics in Ti-Zr-Cu-Ni system, and the quaternary eutectic melting temperatures may be lower than those of the binary systems. As such, alloys near the quaternary eutectics may show greater glass forming ability than corresponding binary alloys.

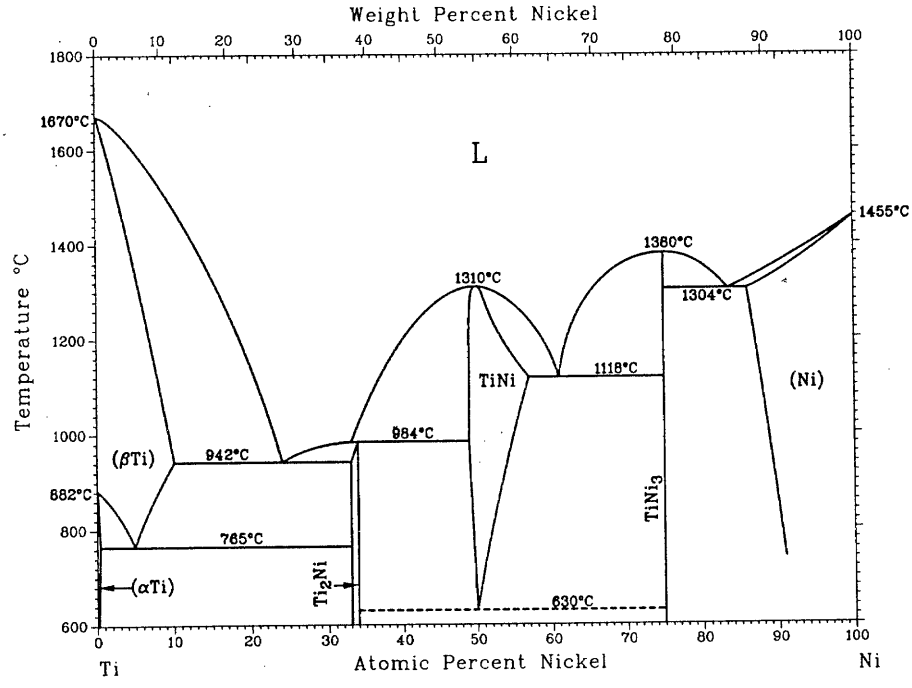

Fig. 2.1 Phase diagram of Ti-Ni. (reproduced from ref. 2)

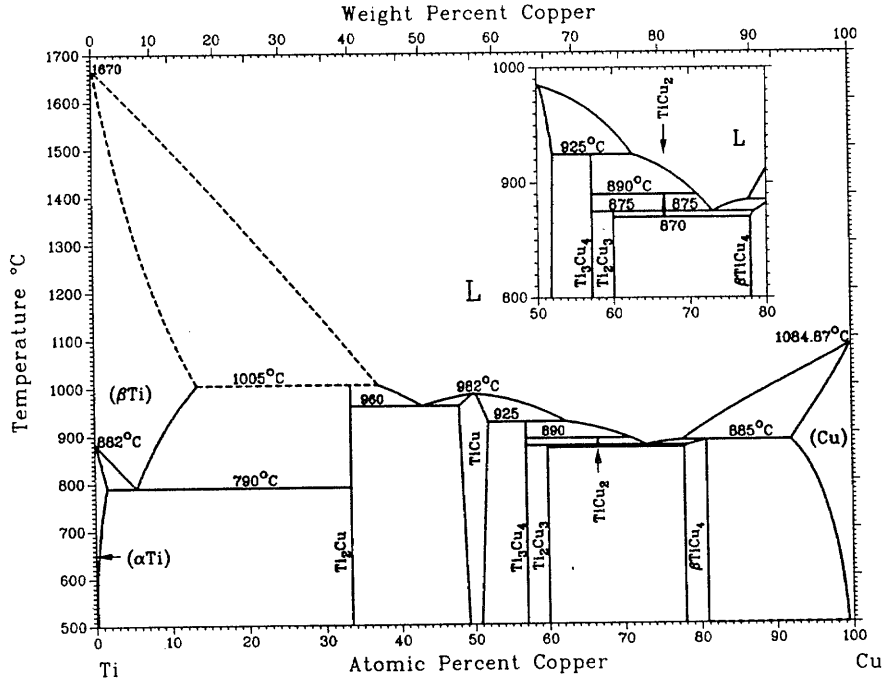

Fig. 2.2 Phase diagram of Ti-Cu. (reproduced from ref. 2)

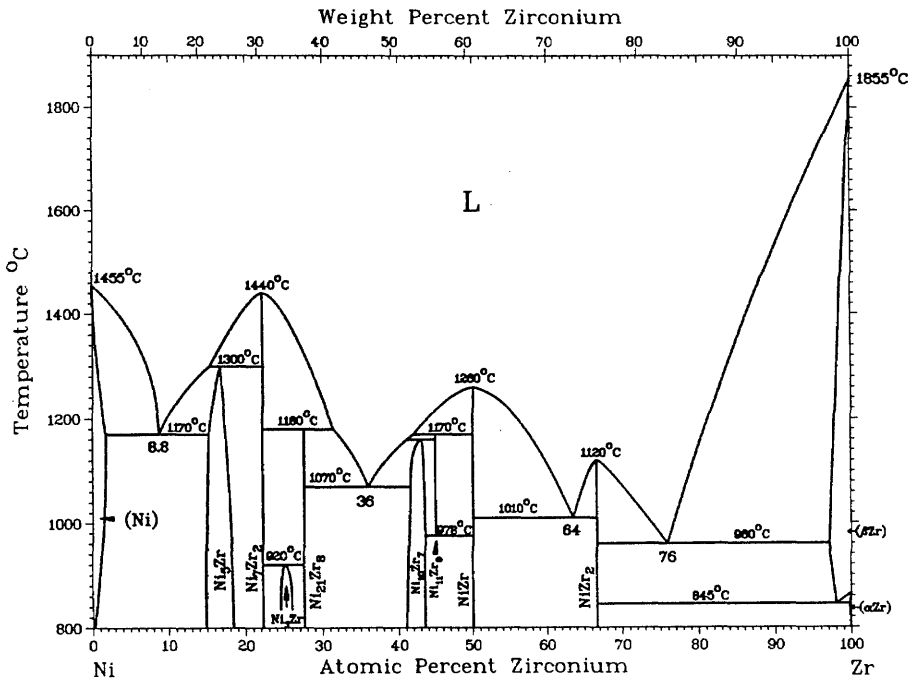

Fig. 2.3 Phase diagram of Zr-Ni. (reproduced from ref. 2)

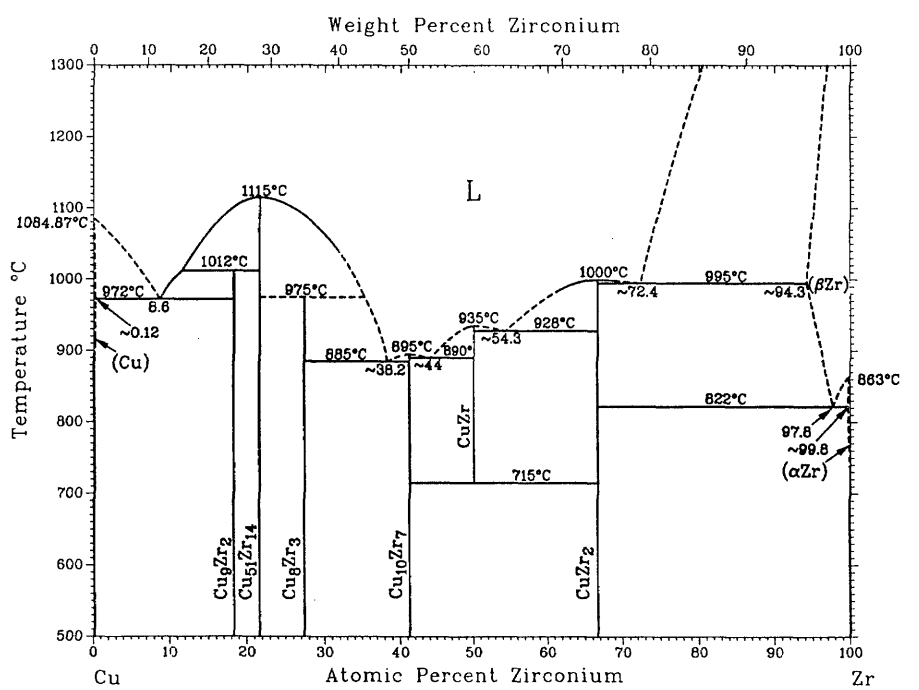

Fig. 2.4 Phase diagram of Zr-Cu. (reproduced from ref. 2)

The phase diagrams of ternary Ti-Zr-Ni and Ti-Zr-Cu have been studied respectively by two different groups. A pseudo-binary phase diagram of the Ti-Zr-Ni system is shown in fig. 2.5 at the section of Ti_2Ni-Zr_2Ni [3]. In this phase diagram, replacing Ti with Zr up to 13.5 at.% in Ti_2Ni leads to a lowering of liquidus temperature from 1273 K to 1173 K. Replacing Zr with Ti in Zr_2Ni up to 22.7 at.% Ti leads to a lowering of liquidus temperature from 1313 K to 1123 K (the melting temperature of Zr_2Ni shown here is different from the 1393K value shown in fig. 1.3). From 13.5 at.% to 44 at.% Zr, the liquidus temperature rises to 1193 K owing to the appearance of a new ternary "$MgZn_2$-type" Laves phase. Fig. 2.6 shows a part of the isothermal section of the Ti-Zr-Ni system at 973 K[4]. A large homogeneity region for the Laves phase is observed in the center of the phase diagram. The isothermal section at 976 K for Ti-Zr-Cu system is shown in fig. 2.7[5]. Near the section of TiCu-ZrCu, three eutectics were found at $Ti_{34.42}Zr_{17.98}Cu_{47.59}$, $Ti_{14.24}Zr_{37.13}Cu_{48.63}$ and $Ti_{17.37}Zr_{43.20}Cu_{39.43}$. Between these three eutectics, there is also a ternary "$MgZn_2$-type" Laves phase. Massalski et al. have reported a very broad glass forming region for ternary Ti-Zr-Cu alloys by melt-spinning[6]. The thickness of the meltspun ribbons is about 50 μm. This leads to an estimated cooling rate of about $5x10^5$ K/s.

A copper mold-casting technique was used to examine the glass forming ability of both Ti-Zr-Ni and Ti-Zr-Cu alloys. It is found that non of the Ti-Zr-Ni alloys can be cast to the amorphous state using a 300 μm thick copper mold. For the Ti-Zr-Cu system, the best glass forming alloy is found at $Ti_{35}Zr_{10}Cu_{55}$, which can be cast to the amorphous state to thickness of 500 μm. The critical cooling rate for glass formation is

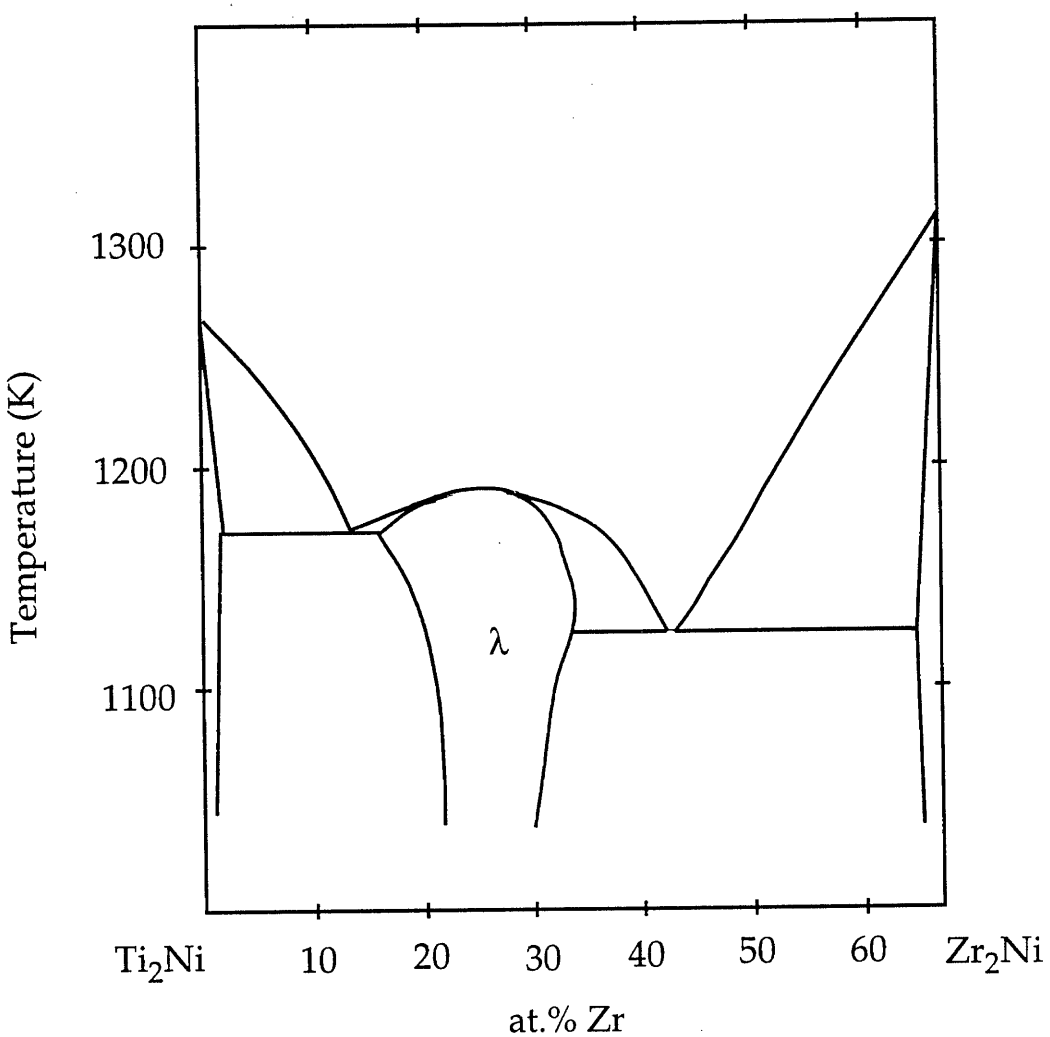

Fig. 2.5 Pseudo-binary phase diagram of Ti-Zr-Ni at the section of Ti_2Ni-Zr_2Ni. (reproduced from ref. 3)

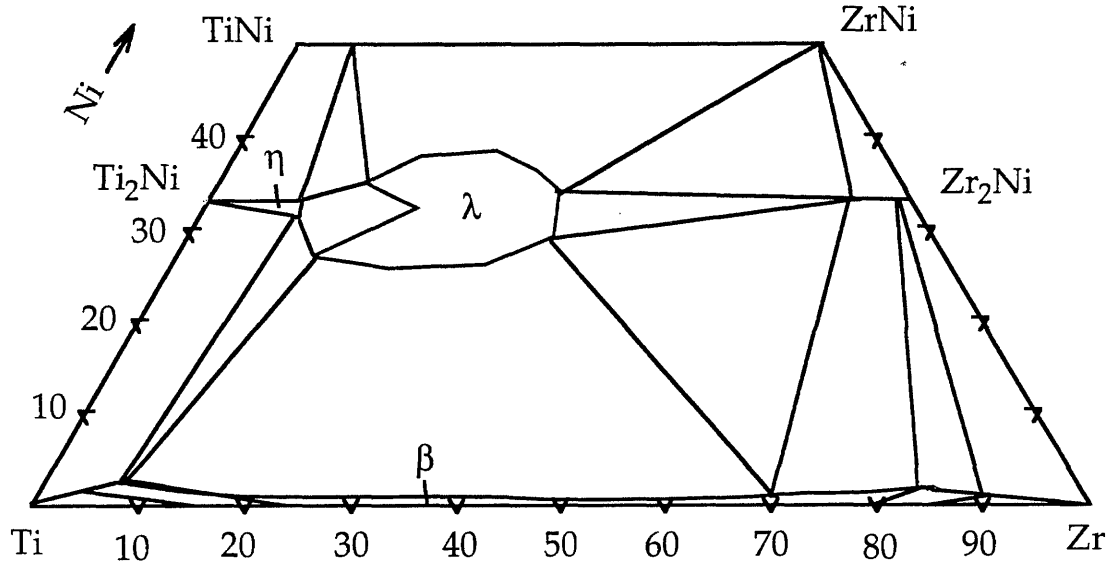

Fig. 2.6 A part of the isothermal section for Ti-Zr-Ni system at 973 K. (reproduced from ref. 4)

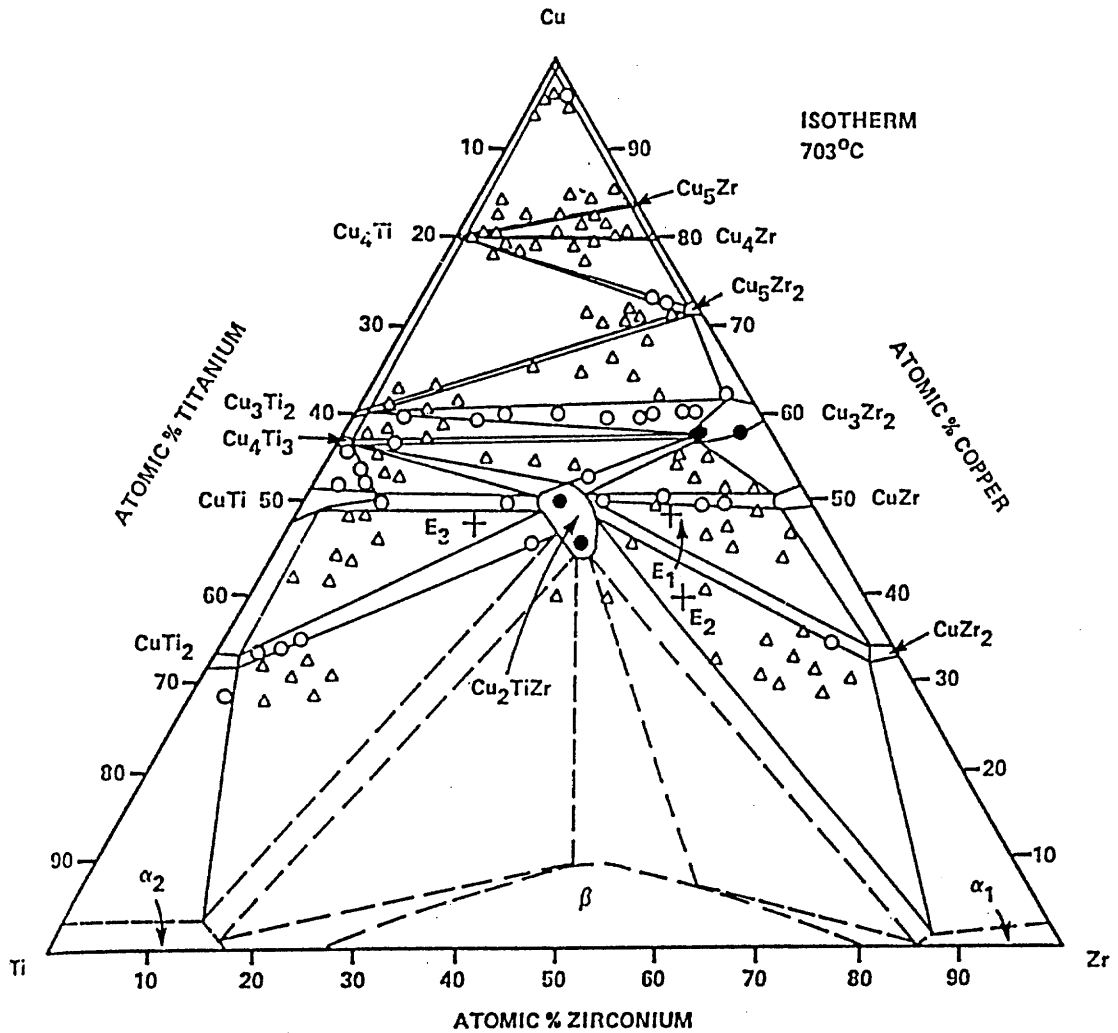

Fig. 2.7 Isothermal section for Ti-Zr-Cu system at 976 K (reproduced from ref. 5)

estimated to be $2x10^4$ K/s. In this chapter I will present two bulk glass forming regions in the Ti-Zr-Cu-Ni quaternary system. Here, I rather arbitrarily define a "bulk" metallic glass as having a minimum dimension of 1mm, equivalent to a critical cooling rate of $4x10^3$ K/s.

2.2 EXPERIMENT

Ingots of alloys were prepared by induction melting 99.99% Ti, 99.8% Zr, 99.999% Cu and 99.97% Ni on a water cooled silver or copper boat under a Ti-gettered argon atmosphere. The weight loss of the samples by alloying was less than 0.1%. Thus, the compositions of the alloys did not change significantly after melting. The alloy ingots were then remelted under vacuum in a quartz tube using a rf induction coil and then injected into a cooper mold under argon at about 1 atm. pressure. Fig. 2.8 illustrates the schematic of the mold-casting apparatus. The copper mold has strip shaped cavities of about 2 cm length, 4-6 mm width, and varying thickness of 300 μm, 500 μm, 1 mm, 2 mm, 3 mm, and 4 mm. This yields cast samples of varying strip thickness. The typical length of the resulting strips is 20 mm. The typical dimensions of the strip cross sections are 1x4 mm, 2x4 mm, 3x4 mm or 4x6 mm. The crystalline/amorphous nature of the strips was determined by x-ray diffraction using a 120° position sensitive detector (Inel) and a collimated Co-Kα x-ray source. To ensure the amorphous nature of the interior of the strips, some strips were cut longitudinally in half, and the cross-sectional surfaces were examined by x-ray diffraction. The glass transition, and crystallization behavior were studied using a Perkin Elmer Differential Calorimeter (DSC-4). The melting temperatures of the

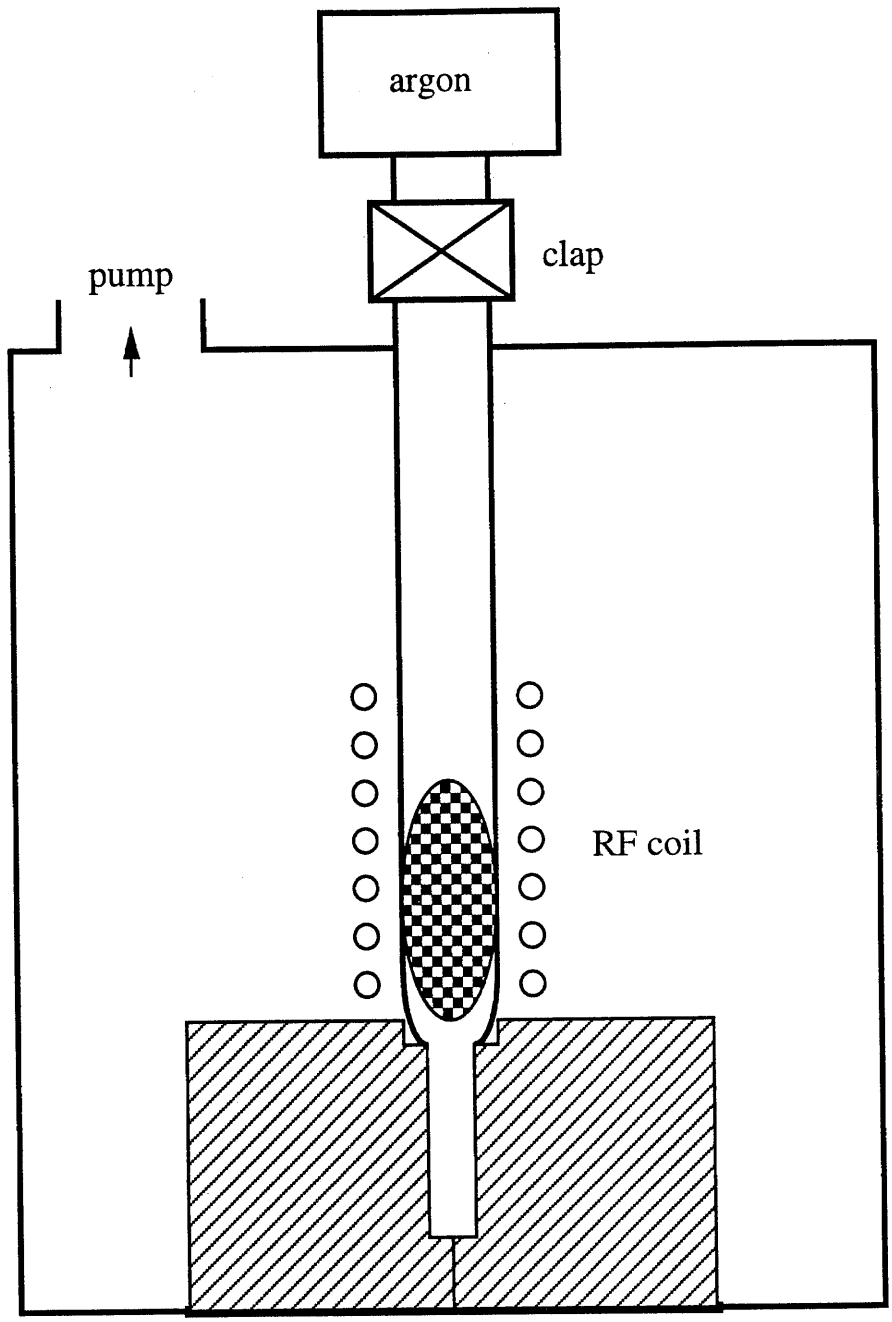

Fig. 2.8 Schematic of the mold-casting setup.

crystalline alloys were measured using a Setaram High Temperature Differential Thermal Analyzer (DTA). Vicker's hardness of the material was obtained using a Leitz micro hardness tester.

2.3 RESULTS

2.3.1 Glass forming regions

Fig. 2.9 illustrates two regions of the quaternary composition space in which bulk glass formation (>1mm thickness) was found. Notice that the diagram is pseudo-ternary. The information regarding the copper/nickel ratio is not included. Generally, the nickel concentration is about 4-12 at.% for the titanium rich region,. The glass forming region is the largest when the nickel concentration is about 8 at.%. For the zirconium rich side, copper and nickel are interchangeable when one maintains a minimum of 4 at.% of either copper or nickel. This region tends to shift downward with increasing nickel concentration. The admixture of Cu and Ni improves the glass forming ability tremendously. The best Ti-Zr-Cu amorphous alloy is $Ti_{35}Zr_{10}Cu_{55}$, having a maximum glass thickness of about 0.5 mm. $Ti_{34}Zr_{11}Cu_{47}Ni_8$ is the best quaternary Ti-Zr-Cu-Ni amorphous alloy. It can be cast at least 4 mm thick. The estimated critical cooling rate for glass formation of this alloy is about 250 K/s or lower. It is two orders of magnitude lower than that of the best ternary Ti-Zr-Cu glass former. It is also found that when an alloy was cast to a strip thicker than its maximum thickness for glass formation, the outer layer of the strip remains amorphous, while the core is crystalline. This suggests that the glass forming ability of these alloys is restricted by homogeneous or heterogeneous nucleation in the sample interior, rather

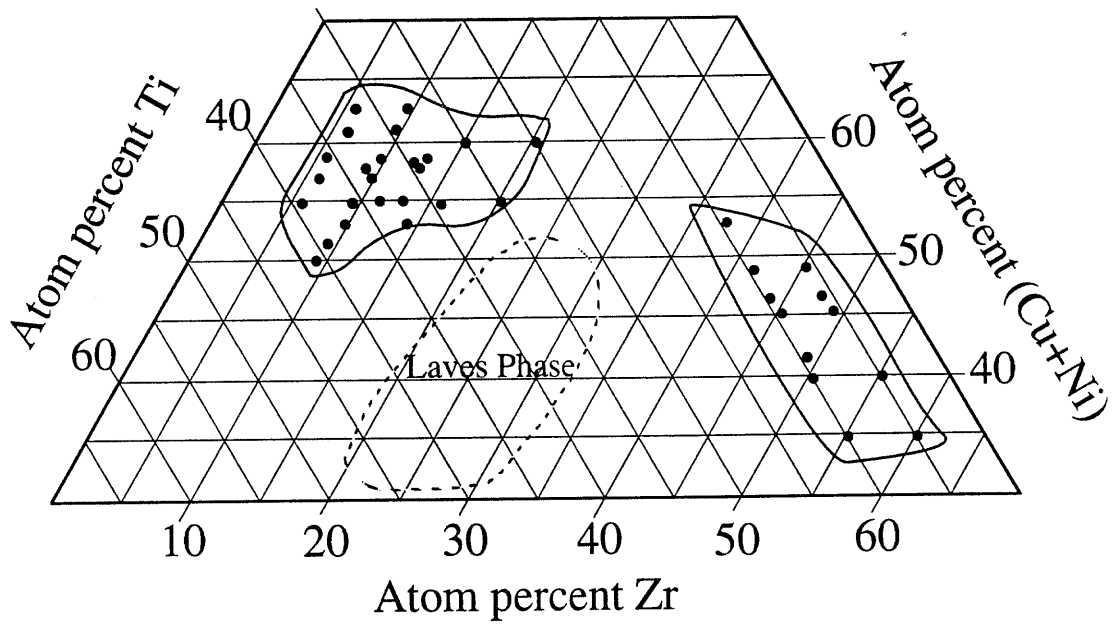

Fig. 2.9 Two bulk glass formation regions in the pseudo-ternary phase diagram. The dots represent the alloys which can be cast to amorphous strips of at least 1mm thickness. Generally for the titanium rich region, the nickel concentration is about 4-12 at.%. The glass forming region is largest when nickel concentration is about 8 at.%. For the zirconium rich region, copper and nickel are roughly interchangeable when at least 4 at.% of either copper or nickel is used. The region moves downward with increasing nickel concentration. In the center of the diagram, the quaternary Laves phase field is shown.

than by heterogeneous nucleation at the interface between the undercooled liquid and the copper mold. Fig. 2.10 shows the x-ray diffraction pattern for one of the strips. No peaks corresponding to crystalline phases can be detected, proving the amorphous state of the material.

2.3.2 Thermal Analysis of the amorphous alloys

Fig. 2.11 shows the DSC scans of two amorphous alloys taken using a heating rate of 20 K/min. They exhibit an endothermic heat event characteristic for the glass transition followed by four characteristic exothermic heat release events indicating the successive stepwise transformations from a metastable undercooled liquid state to a mixture of the equilibrium crystalline intermetallic phases at different temperatures. T_g is defined as the onset of the glass transition temperature. T_{x1} is the onset temperature of the first crystallization event, etc. ΔT, defined as T_{x1}-T_g, is referred to as the supercooled liquid region. For the $Ti_{34}Zr_{11}Cu_{47}Ni_8$ amorphous alloy, T_g=671 K, T_{x1}=717 K, and ΔT=46 K, respectively. For the $Ti_{35}Zr_{10}Cu_{55}$, T_g=668 K, T_{x1}=697 K, and ΔT=29 K, respectively. Fig. 2.12 shows a high temperature DTA scan of the crystalline alloy $Ti_{34}Zr_{11}Cu_{47}Ni_8$. The alloy begins to melt at a solidus temperature T_{sol}=1105K, followed by complete melting at the liquidus temperature T_{liq}=1160K.

2.3.3 Mechanical properties

Vicker's hardness measurements on these amorphous strips were carried out. The typical accuracy of the measurement was 3%. In terms of hardness, the composition dependence Ni>Cu>>Zr>Ti is generally observed. The value for $Ti_{34}Zr_{11}Cu_{47}Ni_8$ alloy is H_V=628$\pm$20 kg/mm^2.

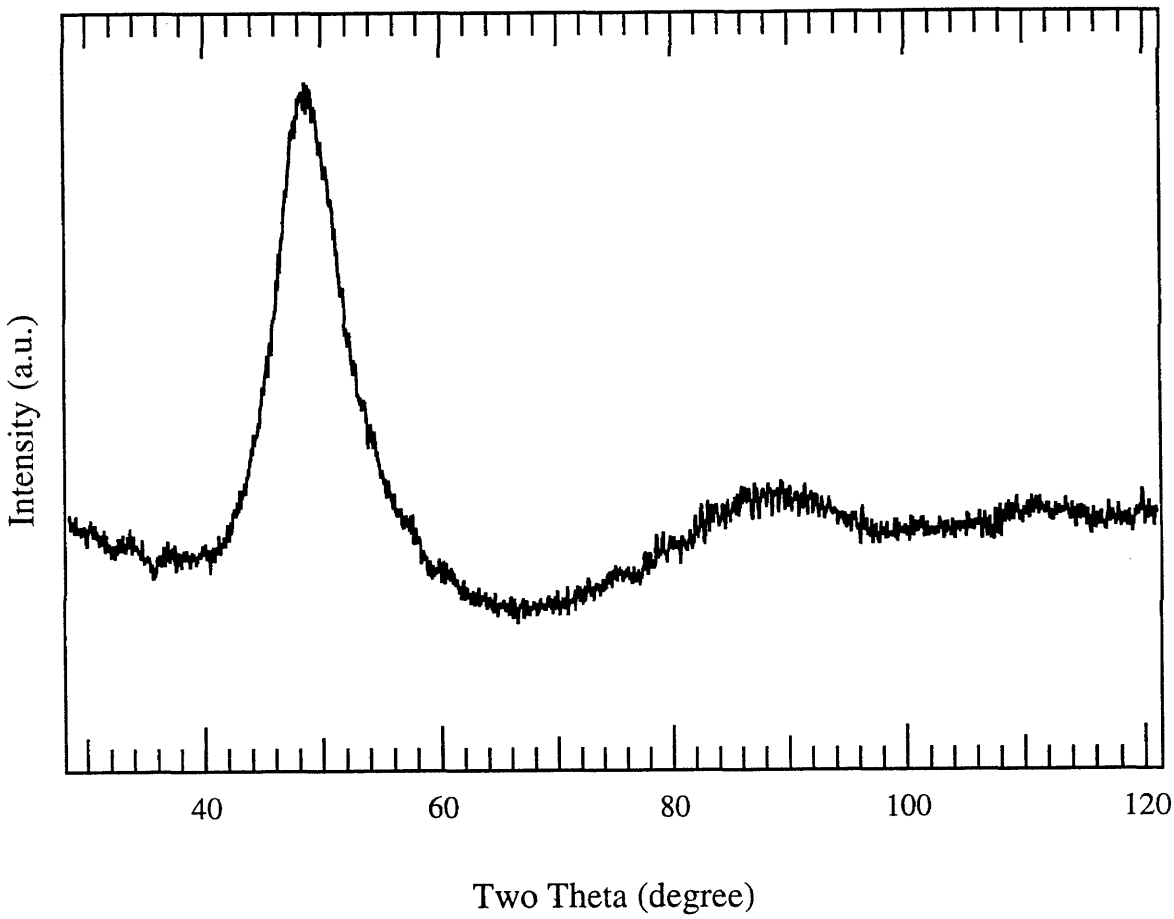

Fig. 2.10 X-ray diffraction pattern (Co Kα radiation) taken from the cross-sectioned surface of a 4x6x20 mm $Ti_{34}Zr_{11}Cu_{47}Ni_8$ strip obtained by metal mold casting.

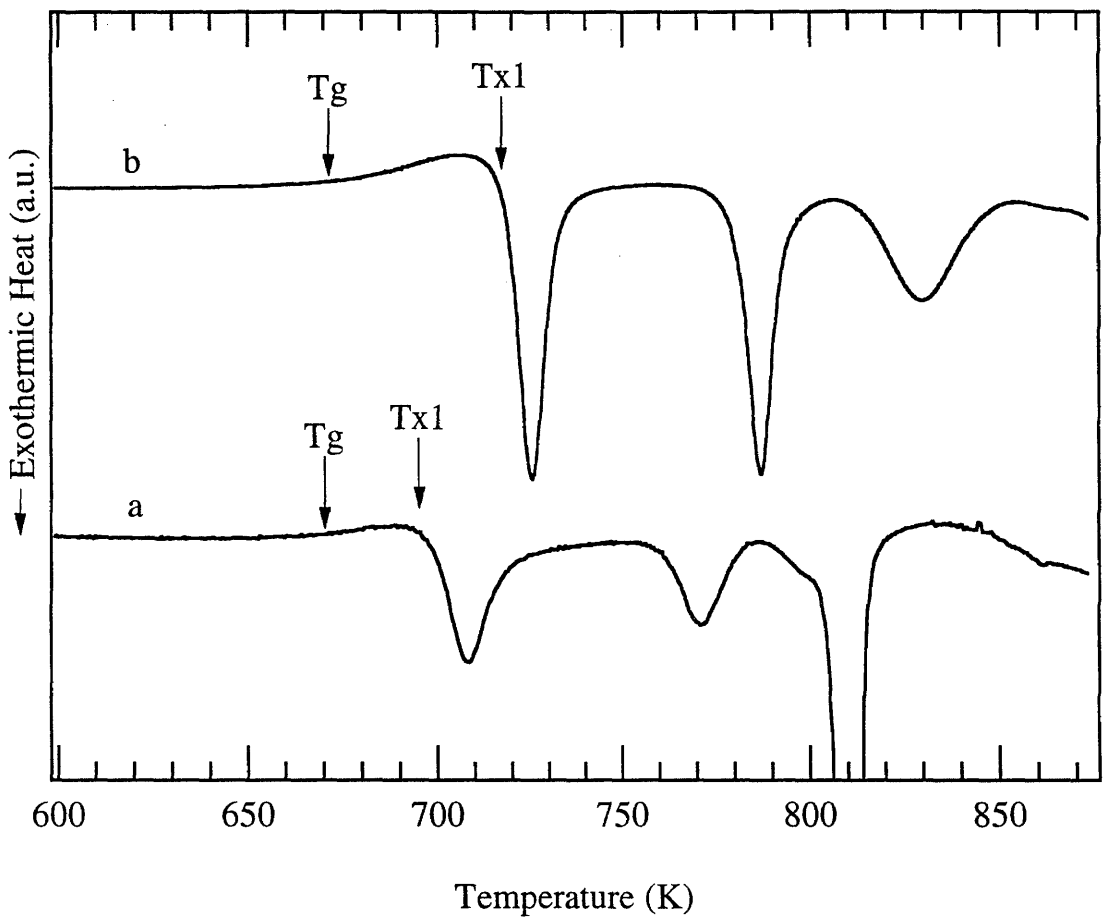

Fig. 2.11 DSC scans of amorphous alloys. T_g is the onset of glass transition temperature, T_{x1} is the onset of first crystallization temperature and so on. (a) $Ti_{35}Zr_{10}Cu_{55}$. (b) $Ti_{34}Zr_{11}Cu_{47}Ni_8$

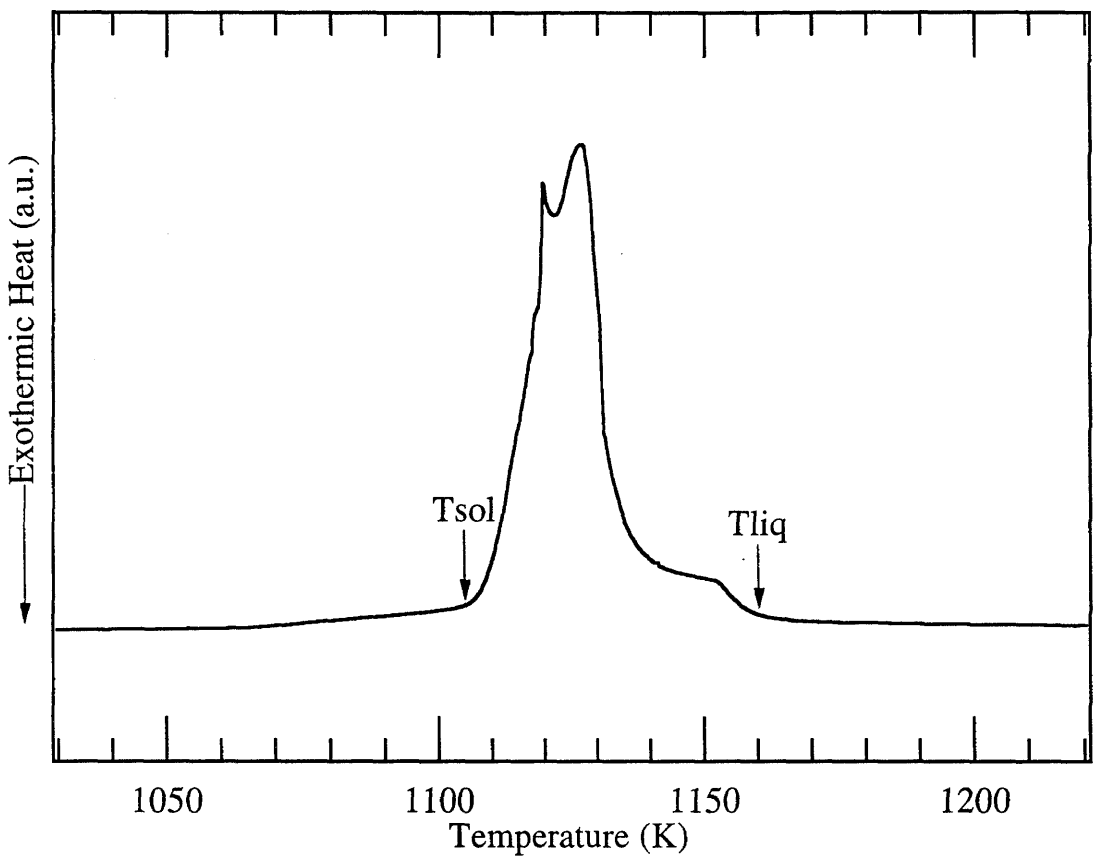

Fig. 2.12 High temperature DTA scan of a crystalline $Ti_{34}Zr_{11}Cu_{47}Ni_8$ alloy. T_{sol} is the solidus temperature, T_{liq} is the liquidus temperature.

Using the well known relation $H_V=3\sigma_y$[7], the yield strength of this amorphous alloy is estimated to be around 2 GPa. This agrees with experimental data obtained in compression and tensile test.[8]

One 2 mm thick $Ti_{34}Zr_{11}Cu_{47}Ni_8$ amorphous strip was successively rolled at room temperature using a thickness reduction of 1.5% deformation per step down to a 0.15 mm thick ribbon without cracking. This demonstrates the ductile behavior of the amorphous material when deformation occurs under a confined geometry. The resulting ribbon can be further bent 180° without failure. The Vicker's hardness of the resulting ribbon was also measured and agrees with that of the initial strip within the experiment accuracy. This indicates that there is no work-hardening as is expected for an amorphous material.

2.4 DISCUSSION

Fig. 2.13 shows the critical cooling rates for glass formation for some alloys versus the reduced glass transition temperature T_{rg}. A strong T_{rg} dependence of the glass forming ability of metallic alloys is seen. High values of T_{rg} are associated with good glass forming ability. For example, $Au_{55}Pb_{22.5}Sb_{22}$ alloy has $T_{rg}=0.63$. The critical cooling rate is about 1000 K/s.[10] $Pd_{40}Ni_{40}P_{20}$ alloy has $T_{rg}=0.66$,[11] its critical cooling rates are 1 K/sec.[12] The recently discovered $Zr_{41.2}Ti_{13.8}Cu_{12.5}Ni_{10}Be_{22.5}$ alloy has $T_{rg}=0.67$,[13] and has critical cooling rate of 1 K/sec.[14] The T_{rg} of $Ti_{34}Zr_{11}Cu_{47}Ni_8$ is 0.578, by comparison not a very high value. According to Fig. 2.13, the estimated critical cooling rate for an alloy of $T_{rg}=0.578$ would typically be of the order of 10^5 K/sec. Therefore, from the point of view of reduced glass transition temperature, the glass forming ability of Ti-Cu-Zr-Ni alloys such as

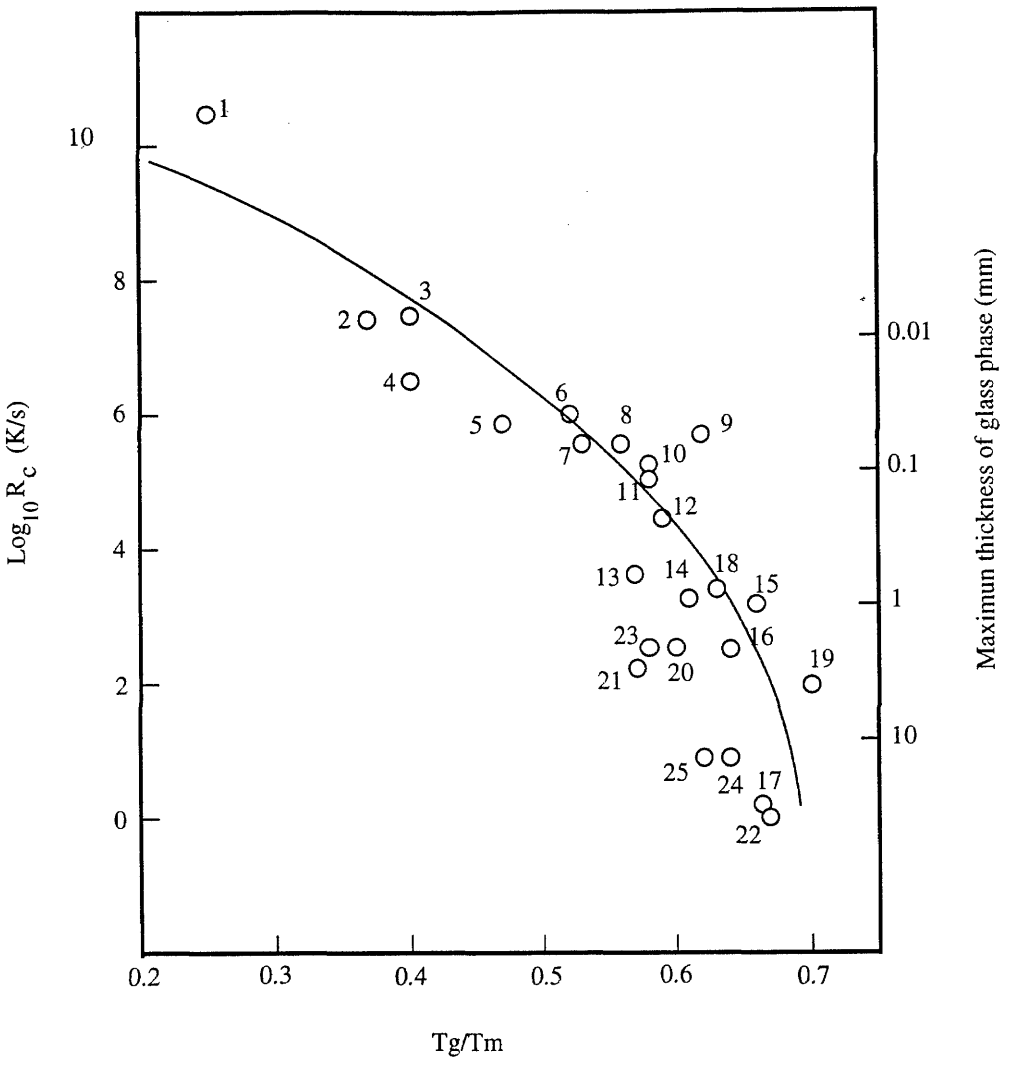

Fig. 2.13 Critical cooling rates for glass formation and corresponding maximum thickness of glass phases. Key to the alloys: (1) Ni; (2) $Fe_{91}B_9$; (3) $Fe_{89}B_{11}$; (4) Te; (5) $Au_{77.8}$ $Ge_{13.8}Si_{8.4}$; (6) $Fe_{83}B_{17}$; (7)$Fe_{41.5}Ni_{41.5}B_{17}$; (8) $Co_{75}Si_{15}B_{10}$; (9) Ge: (10)$Fe_{79}Si_{10}B_{11}$; (11) $Ni_{75}Si_8B_{17}$; (12)$Fe_{80}P_{13}C_7$ (13)$Pt_{60}Ni_{15}P_{25}$; (14) $Pd_{82}Si_{18}$; (15) $Ni_{62.4}Nb_{37.6}$; (16)$Pd_{77.5}Cu_6Si_{16.5}$ (above from ref. 9); (17) $Pd_{40}Ni_{40}P_{20}$ (ref. 11,12); (18) $Au_{55}Pb_{22.5}Sb_{22.5}$ (ref. 10); (19) $La_{55}Al_{25}Ni_{10}Cu_{10}$ (ref. 15); (20) $Mg_{65}Cu_{25}Y_{10}$(ref. 16); (21) $Zr_{65}Cu_{17.5}Ni_{10}Al_{7.5}$ (ref. 17); (22) $Zr_{41.2}Ti_{13.8}Cu_{12.5}Ni_{10}Be_{22.5}$ (ref. 13, 14); (23) $Ti_{34}Zr_{11}Cu_{47}Ni_8$ (24) $Zr_{52.5}Ti_5Cu_{17.9}Ni_{14.6}Al_{10}$; (25) $Zr_{57}Nb_5Cu_{15.4}Ni_{12.6}Al_{10}$.

$Ti_{34}Zr_{11}Cu_{47}Ni_8$ is better than expected. In fact, this is not unique. Some newly found multicomponent alloys, such as $Mg_{65}Cu_{25}Y_{10}$[16] and $Zr_{65}Cu_{17.5}Ni_{10}Al_{7.5}$,[17] also show better glass forming ability than expected from T_{rg}. Three factors, a significantly different atomic size among the constituent elements, a large negative heat of mixing, and the necessity of substantial redistribution of the component elements for the progress of crystallization, have been cited and used to interpret the unexpected good glass forming ability of these systems.[18] In fact, the first two factors, large atomic size ratios and large negative heat of mixing, are already reflected by the relatively low lying eutectic melting temperatures of these alloys. As such, these factors give, at best, a qualitative glass forming criteria, whose role is not quantified. In conventional homogenous nucleation theory, one evaluates glass forming ability by considering the competition between a decreasing nucleation barrier and an increasing viscosity with increasing undercooling of the liquid. If the nucleating crystalline phase has a composition very different from that of the undercooled liquid, only when the composition of a local liquid region the size of a critical crystalline nucleus satisfies the composition requirements of the crystalline phase (either by fluctuation or liquid decomposition) can crystallization occur. For higher order multicomponent systems, it is more difficult for the concentrations of all elements to simultaneously satisfy the composition requirements of crystalline phase than for lower order systems. As such, the crystallization process of the multicomponent undercooled liquid will tend be more sluggish than for simpler systems. The multicomponent alloys will thus exhibit better glass forming ability than predicted from the point of view of the reduced glass transition

temperature alone. The fundamental argument used here has been loosely called the "confusion principle".[19] The concept is that as the number of components in a liquid alloy is increased, crystallization becomes confused or frustrated. Recently, Desre has quantified this argument[20]. He considered a multicomponent system with n equally concentrated component elements. For n=2 to n=10, the addition of each additional component to the alloy is predicted to lower by an order of magnitude the probability of the concentration fluctuation within a cluster of 600 atoms for crystallization. The probability of achieving a critical nucleus of the required composition is lowered by an order of magnitude with the addition of each new component. Thus the more complex an alloy is, the better the glass forming ability it has. This argument may explain the extraordinary good glass forming ability of present Ti-Zr-Cu-Ni system and the Zr-Cu-Ni-Al[17] and Mg-Cu-Y[16] systems as well. One piece of evidence in support of this argument is that all good glass forming alloys in these systems show a large undercooled liquid region, as indicated by the temperature interval between glass transition and first crystallization event during sample heating. The nucleation of crystalline phases from the undercooled liquid phases requires substantial atomic diffusion and composition redistribution. In this situation, the undercooled liquid is relative stable against the crystallization. Note that for the $Ti_{34}Zr_{11}Cu_{47}Ni_8$ amorphous alloy, the supercooling liquid region is ΔT=46 K, while for the $Ti_{35}Zr_{10}Cu_{55}$ alloy, ΔT=29 K is found. ΔT correlates with the relative glass forming ability of these two alloys. However, since the crystallization of a multicomponent alloy is a complicated process, the correction between

glass forming ability and ΔT should not be over emphasized. This issue will be discussed in following chapters.

It is noteworthy that a large number of early transition metal/late transition metal systems exhibit the $MgZn_2$-type or the $MgCu_2$-type Laves phases. Examples are: $TiMn_2$, $ZrMn_2$, $TiFe_2$ and $TiZn_2$ (of $MgZn_2$-type structure), and $ZrFe_2$, $ZrCo_2$ and $ZrZn_2$ (of $MgCu_2$-type structure). The congruent melting temperatures of these Laves phases are generally above 1600 K and the liquidus curves are relatively flat (with respect to composition). The Laves phase homogeneity ranges are often as large as 10 at.% or more[2]. These factors suggest that the Gibbs free energy function of the Laves phases varies slowly with composition. In this sense, the Laves phases are somewhat similar to liquid or glassy phase. They are both "forgiving" of composition variation. On the other hand, there are no equilibrium binary Ti-Cu, Ti-Ni, Zr-Cu, or Zr-Ni Laves phases. The melting temperature of Ti_2Ni is lowered by adding Zr, and the melting temperature of Zr_2Ni is lowered by adding Ti. One would expect an extremely low lying liquidus temperature in the center of Ti_2Ni-Zr_2Ni section if there were no ternary Laves phase. In the actual ternary Ti-Ni-Zr system, the Laves phase enters the diagram with a homogeneity range from 21 to 30 at.% Zr at 1193 K[3]. One expects similarly large homogeneity ranges for the ternary Ti-Cu-Zr Laves phase as well as the quaternary Ti-Zr-Cu-Ni Laves phase. Because of the relative insensitivity of the Laves phase to composition variations, it may nucleate more easily than the other competing crystalline phases from the undercooled liquid. It has been determined that there are two quaternary eutectics near the compositions of $Ti_{37}Zr_{17}Cu_{42}Ni_4$ and $Ti_{17}Zr_{40}Cu_{28}Ni_{15}$ respectively.

Interestingly, these two alloys cannot be cast to 0.5 mm thick amorphous strips. By comparison, $Ti_{34}Zr_{11}Cu_{47}Ni_8$ can be cast to 4 mm thick amorphous strips and $Ti_{10}Zr_{49}Cu_{33}Ni_8$ can be cast to at least 2 mm thick amorphous strips. Their reduced glass transition temperatures are in fact lower than those of the two eutectic alloys, but their critical cooling rates for glass formation are at least one and possibly two orders of magnitude lower than those of the two eutectic alloys. They are much better glass formers. This may be due to the compositions being relatively far from that of the Laves phase. To obtain a good glass forming composition in Ti-Zr-Cu-Ni system, one must consider two factors. First, one should be close to the eutectic compositions to obtain a high reduced glass transition temperature. Second, one must avoid nucleating the Laves phase which apparently forms relatively more easily than other competing crystalline phases. The best glass forming alloys of the present Ti-Zr-Cu-Ni system are examples of simultaneously satisfying these two conditions.

The main obstacle which prevents us from getting better glass formability in the Ti-Zr-Cu-Ni system is the existence of the quaternary Laves phase. To improve the glass forming ability of the Ti-Zr-Cu-Ni system, one must find a way to eliminate or at least destabilize the Laves phase to obtain an alloy with a lower melting temperature in the center of the quasi-ternary phase diagram. It is found that transition metals which have a high melting temperature Laves phase with Ti or Zr tend to stabilize the Laves phase of the quaternary alloy and thus degrade the glass forming ability. On the other hand, substituting Cu or Ni by Zn or Co does not degrade the glass forming ability. If a metalloid element like B or Si is added, the alloy loses its glass forming ability. Fig. 2.14 shows the phase

diagram of Ti-B.[2] From extrapolation, the metastable liquidus of the TiB phase should be around 1650 K as the B concentration approaching zero, which is much higher than the melting temperature of the alloys. The phase diagram of Zr-Si shows a similar feature. Therefore, crystallization of B or Si bearing Ti-Zr-Cu-Ni alloys is apparently triggered by the precipitation of very stable Ti boride or Zr silicide. One very efficient way to improve the glass forming ability of current Ti-Zr-Cu-Ni system is to add Be as has already been proven.[13,14] Apparently the very small atomic radius of Be is incompatible with the preferred atomic size ratio of the Laves phase. As such, Be acts to destabilize the quaternary Laves phase resulting in further depression of the alloy liquidus curve in the center portion of the quaternary phase diagram. This yields a pentiary alloy with a eutectic at 943 K[13]. From this point of view, we can understand why Zr-Ti-Cu-Ni-Be system is such an exceptional glass former.

2.5 CONCLUSIONS

Bulk metallic glass formation in the ternary Ti-Zr-Cu-Ni system is presented in this chapter. Bulk samples of metallic glass can be prepared by metal mold casting up to dimensions of several millimeters. The critical cooling rate for glass formation is of the order of 500 K/sec. For the particular amorphous alloy $Ti_{10}Zr_{49}Cu_{33}Ni_8$, the hardness is about 628 kg/mm^2, while the tensile strength is estimated to be about 2 GPa. Comparing with the Zr-Ti-Cu-Ni-Be system, the quaternary alloys have relatively poorer glass forming ability. On the other hand, the absence of Be in these glasses may make them of interest from the point of view of applications.

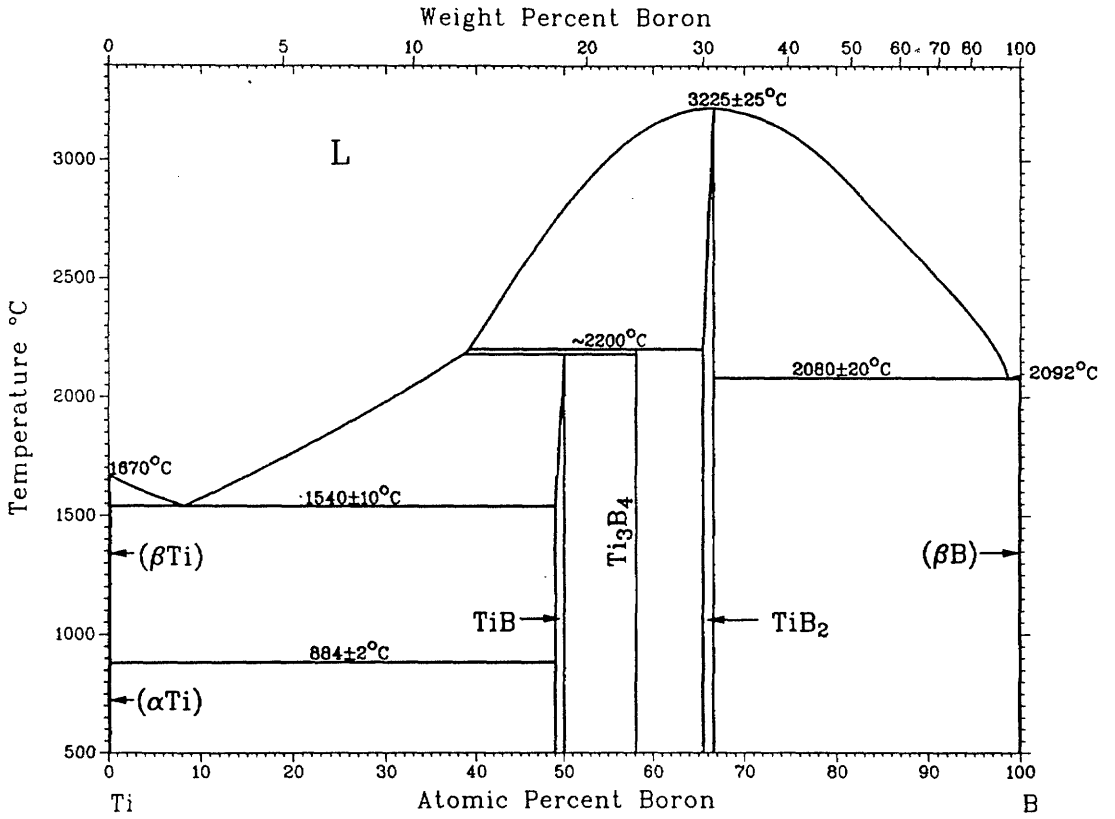

Fig. 2.14 Phase diagram of Ti-B. (reproduced from ref. 2)

It has been noted that the glass forming ability of the quaternary alloys is better than might be expected based on their reduced glass transition temperature alone. This suggests that while the reduced glass transition temperature still plays a dominant role in determining the glass forming ability of metallic alloys, the requirement that the crystallization involve large composition fluctuations in the liquid phase also tends to enhance the glass forming ability tremendously.

The greatly enhanced glass forming ability obtained by adding a few percent of fourth element in the present alloy system suggests that making a system more complex is a practical way to search for new bulk glass forming alloy systems.

REFERENCES:

1. D. Turnbull, Contemp. Phys. **10**, 473 (1969).
2. T. B. Massalski ed., *Binary Alloy Phase Diagrams*, 2nd edition, (ASM International, 1990).
3. V.V. Molokanov, V. N. Chebotnikov, and Yu. K. Kovneristyi, Inorganic Materials **25**, 46 (1989).
4. V. N. Eremenko, E. L. Semennova, and L. A. Tretyachenko, Dopovidi Akademii Nauk Ukrains'koi RSR **A50**, 76 (1988)
5. C. G. Woychik and T. B. Massalski, Z. Metal. **79**, 149 (1988).
6. T. B. Massalski, C. G. Woychik, and J. Dutkiewicz, Metal. Transactions **19A**,1853 (1988).
7. L. A. Davis, in *Mechanical Behavior of Rapidly Solidified Materials*, edited by S. M. L. Sastry, and B. A. MacDonald, (the Metallurgical Society, Inc., 1986).
8. H. Choi-Yim, D. Conner, and W. L. Johnson, unpublished results.
9. H. A. Davies, *Rapidly Quenched Metals III*, B. Cantor (ed.), (Metals, Soc., London, 1978), Vol.1, p. 1.
10. M. C. Lee, J. M. Kendall, and W. L. Johnson, Appl. Phys. Lett. **40**, 382, (1982).
11. A. J. Drehman and A. L. Greer, Acta. Metal. **32**, 323, (1984).
12. A. J. Drehman and A. L. Greer, and D. Turnbull, Appl. Phys. Lett. **41**, 716 (1982).
13. A. Peker and W. L. Johnson, Appl. Phys. Lett. **63**, 2342 (1993).
14. Y. J. Kim, R. Busch, W. L. Johnson, A. J. Rulison, and W. K. Rhim, Appl. Phys. Lett. **65**, 2136 (1994).

15. A. Inoue, T. Nakamura, T. Sugita, T. Zhang, and T. Masumoto, Mater. Trans., JIM **34**, 351, (1993).

16. A. Inoue, A. Kato, T. Zhang, S. G. Kim, and T. Masumoto, Mater. Trans., JIM **32**, 609, (1990).

17. A. Inoue, T. Zhang, N. Nishiyama, K Ohba, and T. Masumoto, Mater. Trans., JIM **34**, 1234, (1993).

18. A Inoue, T. Zhang and T. Masumoto, J. Non-Cryst. Solids **156-158**, 473 (1993).

19. A. L. Greer, Nature **366**, 303 (1993).

20. P. J. Desre, presentation on Int. Conf. of Non-crystal Mat., Grenoble, France, 1994, to be published in Materials Forum.

Chapter 3
Zr-Ti(Nb)-Cu-Ni-Al Bulk Glass Forming Alloys

3.1 INTRODUCTION

In order to improve the glass forming ability (GFA) of Ti-Zr-Cu-Ni alloys, many elements besides Be have been added to the alloys, but most of the elements did not have a positive effect on the GFA. However, adding Al to some of the alloys shows improvement of the GFA. Comparing the Zr rich side bulk glass forming region for Ti-Zr-Cu-Ni alloys as shown in fig. 2.9 with the glass forming region of Zr-Cu-Ni-Al as shown in fig 3.1,[1] one notices the analogy between these two regions immediately. Both systems have 45-65 at.% Zr, 5-10 at.% Ti or Al, and Cu and Ni in balance, for bulk glass formation. A logical next step is to combine these two systems and make Zr-Ti-Cu-Ni-Al pentiary alloys. This results the discovery of a better bulk glass forming alloy system as will be demonstrated in this chapter.

3.2 EXPERIMENT

Ingots of alloys were prepared by induction or arc melting 99.99% Ti, 99.5% Zr, 99.99% Ti, 99.9% Nb, 99.999% Cu , 99.97% Ni and 99.999% Al on a water cooled copper hearth under a Ti-gettered argon atmosphere. The weight loss of the samples by alloying was less than 0.1%. Thus, the compositions of the alloys did not change significantly after melting. Typical ingots weigh from 5 to 25 grams. For some of the compositions, samples were found to freeze without crystallization resulting in glassy ingots, after the power of the melter was turned off. In the case of the

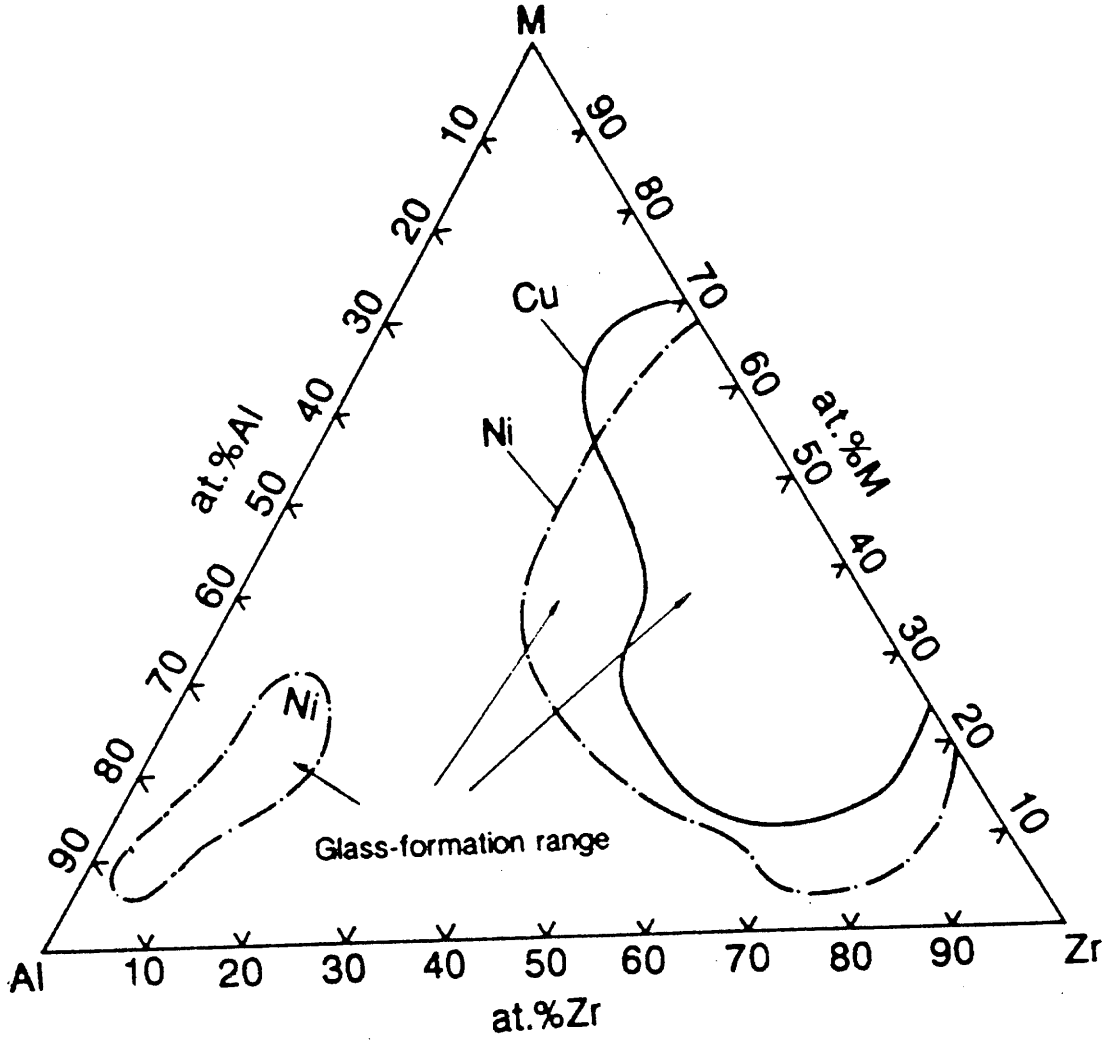

Fig. 3.1 Composition regions for glass formation by melt-spinning in Zr-Al-Ni and Zr-Al-Cu systems. (reproduced from ref. 1). The cooling rate used here is of the order of 10^5 K/s. The Al-poor bulk glass forming regions (using 10^3 K/s cooling rate) are much smaller than that shown here. Alloys in Al-rich region do not form bulk glass.

other alloys, ingots were remelted and cast into a copper mold resulting in glassy strips or rods of different sizes up to a dimension of 9 mm. The crystalline/amorphous nature of the ingots, strips and rods was determined by x-ray diffraction using a 120° position sensitive detector (Inel) and a collimated Co-Kα x-ray source. To ensure the amorphous nature of these sample, both outer surface and the cross-sectional surface were examined by x-ray diffraction. The glass transition and crystallization behavior were studied using a Perkin Elmer Differential Calorimeter (DSC-7). The melting temperatures of the crystalline alloys were measured using a Seteram High Temperature DTA (DSC-2000). The Vicker's hardness of the materials was determined using a Leitz micro hardness tester.

3.3 RESULTS

Fig. 3.2 illustrates the region of the quinary composition space in which bulk glass formation (thicker than 6 mm by mold casting, corresponding to critical cooling rate of 100 K/s or less) was found. Notice that the diagram is pseudo-ternary, the optimum Al/Ti or Al/Nb ratio is 2:1, and Cu/Ni ratio is 11:9. The dots represent the composition of alloys which form at least 5 gram glassy ingots in the induction or arc melter. The best glass forming alloys are those around the compositions $Zr_{52.5}Ti_5Cu_{17.9}Ni_{14.6}Al_{10}$ and $Zr_{57}Nb_5Cu_{15.4}Ni_{12.6}Al_{10}$. Formation of glassy ingots of 1 cm thickness by cooling from one side is found for the alloys around these two compositions. This reflects a critical cooling rate of 10 K/s. Fig. 3.3 shows typical examples of glassy ingots and cast rods. A typical X-ray diffraction pattern for the cross-section of a 25 g ingot is

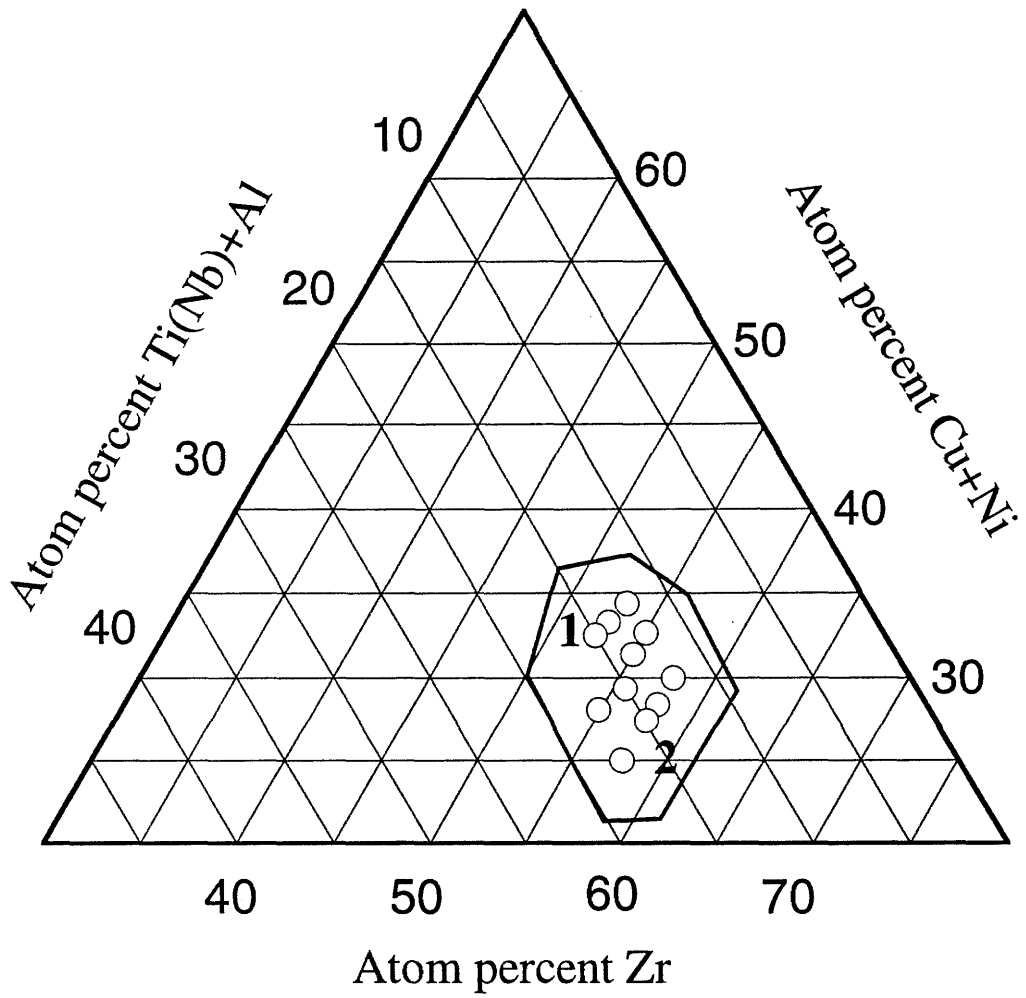

Fig. 3.2 Bulk glass forming region in the pseudoternary phase diagram. The region corresponding to critical cooling rates of 100 K/s or less. The circles represent the alloys which freeze to amorphous ingots in the induction or arc melter. (1) $Zr_{52.5}Ti_5Cu_{17.9}Ni_{14.6}Al_{10}$, (2) $Zr_{57}Nb_5Cu_{15.4}Ni_{12.6}Al_{10}$.

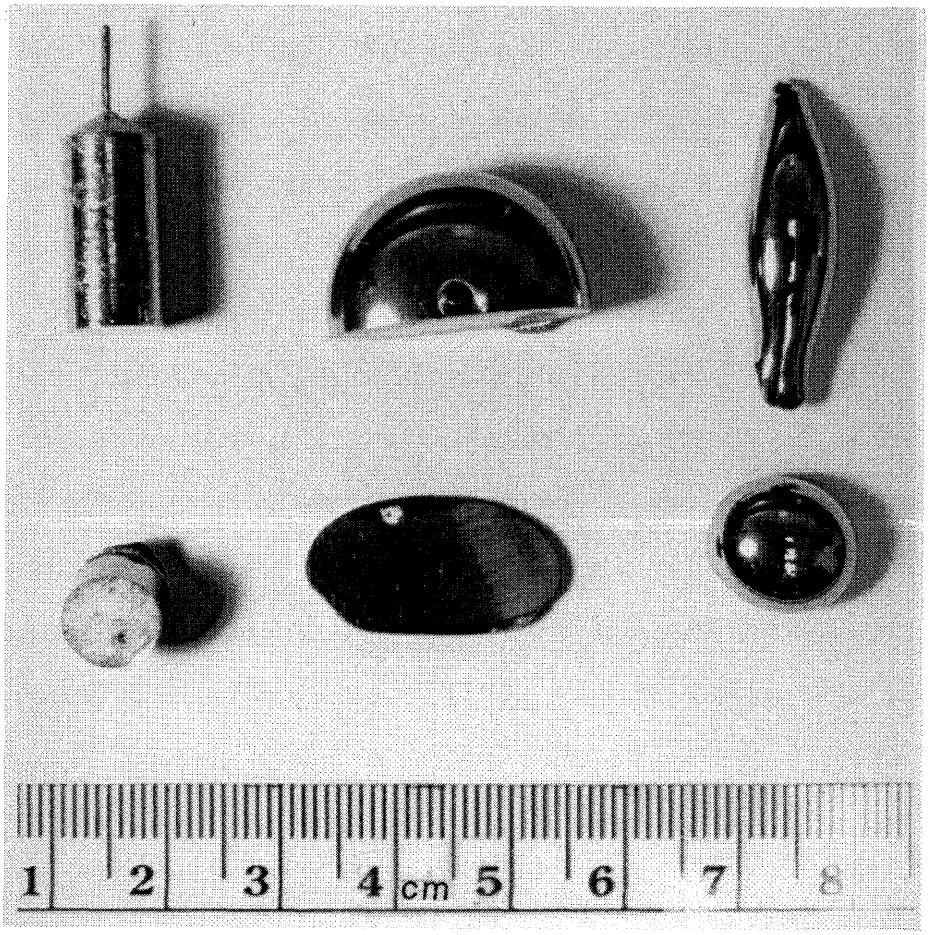

Fig. 3.3 Samples of glassy alloys prepared by various processes. From left to right: mold cast 9-mm-diam rod and its cross section, half of an 25 g and 12 mm thick arc melted ingot and its cross section, an induction melted ingot and an arc melted ingot of 5 g each and 8 mm thick.

depicted in fig. 3.4. No peaks corresponding to crystalline phases can be detected.

Fig. 3.5 shows the DSC scans of $Zr_{52.5}Ti_5Cu_{17.9}Ni_{14.6}Al_{10}$ and $Zr_{57}Nb_5Cu_{15.4}Ni_{12.6}Al_{10}$ amorphous alloys taken at a heating rate of 20 K/min. They both exhibit an endothermic heat event characteristic of the glass transition followed by two characteristic exothermic heat release events indicating the successive stepwise transformations from a metastable undercooled liquid state to the mixture of the equilibrium crystalline intermetallic phases at different temperatures. T_g is defined as the onset of the glass transition temperature. T_{x1} is the onset temperature of the first crystallization event. ΔT, defined as T_{x1}-T_g, is referred to as the supercooled liquid region. For the $Zr_{52.5}Ti_5Cu_{17.9}Ni_{14.6}Al_{10}$ amorphous alloy, T_g=682 K, T_{x1}=739 K, and ΔT=57 K, respectively, are observed. For the $Zr_{57}Nb_5Cu_{15.4}Ni_{12.6}Al_{10}$ amorphous alloy, T_g=678 K, T_{x1}=748 K, and ΔT=70 K, are found. Fig. 3.6 shows a high temperature DTA scan of the crystalline $Zr_{52.5}Ti_5Cu_{17.9}Ni_{14.6}Al_{10}$ and $Zr_{57}Nb_5Cu_{15.4}Ni_{12.6}Al_{10}$ alloys. The widths of the melting peaks are almost identical with that of pure Al and Au standards. This indicates that these two alloys are likely to be very close to the pentiary eutectics. Therefore, it is appropriate to describe the melting temperature by using one single value T_m. The values are T_m=1069 K for $Zr_{52.5}Ti_5Cu_{17.9}Ni_{14.6}Al_{10}$ alloy, and T_m=1093 K for $Zr_{57}Nb_5Cu_{15.4}Ni_{12.6}Al_{10}$ alloy, respectively. Hence, one finds T_{rg}=0.638 for $Zr_{52.5}Ti_5Cu_{17.9}Ni_{14.6}Al_{10}$ alloy and T_{rg}=0.620 for $Zr_{57}Nb_5Cu_{15.4}Ni_{12.6}Al_{10}$ alloy, respectively.

Vicker's hardness measurements on mold cast amorphous strips have been carried out. The typical accuracy of the measurement is 5%.

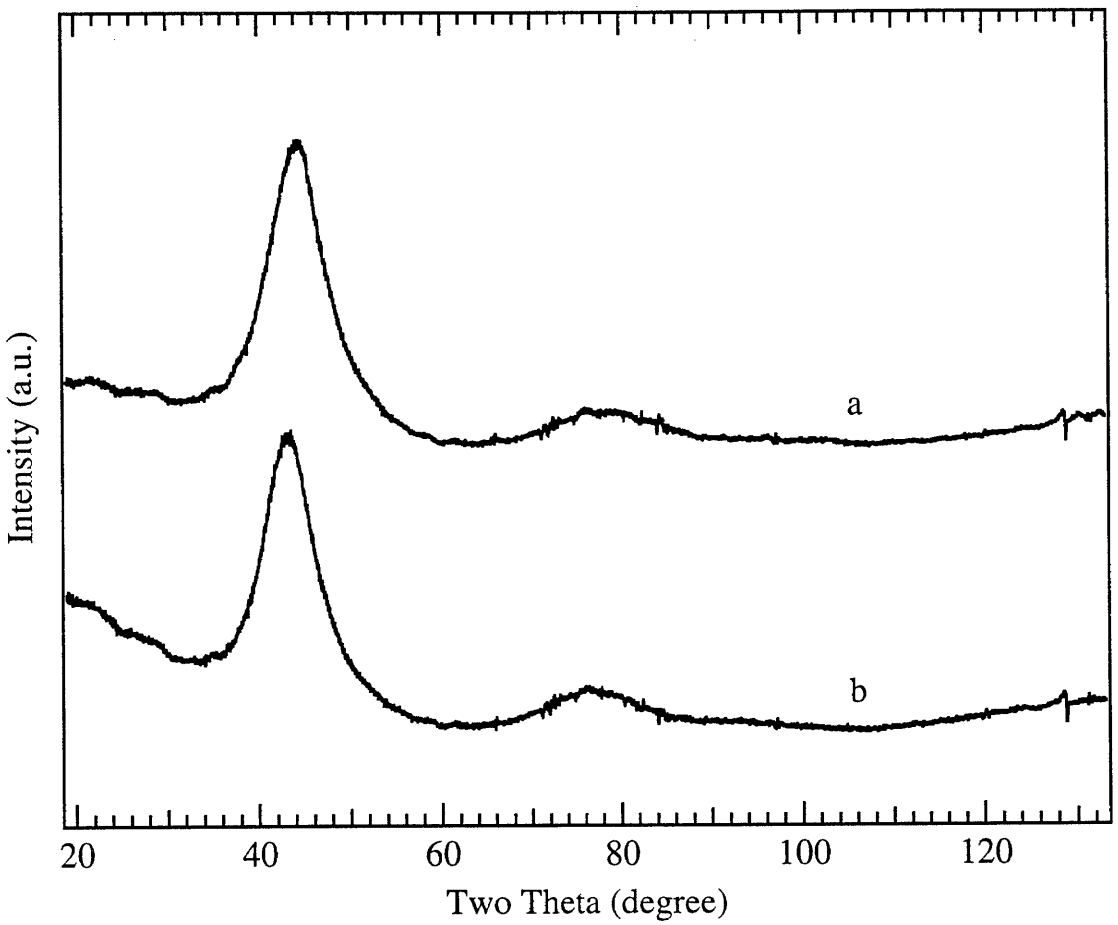

Fig. 3.4 X-ray diffraction patterns (Co Kα radiation) taken from the cross-sectioned surfaces of glassy ingots. (a) $Zr_{52.5}Ti_5Cu_{17.9}Ni_{14.6}Al_{10}$, (b) $Zr_{57}Nb_5Cu_{15.4}Ni_{12.6}Al_{10}$.

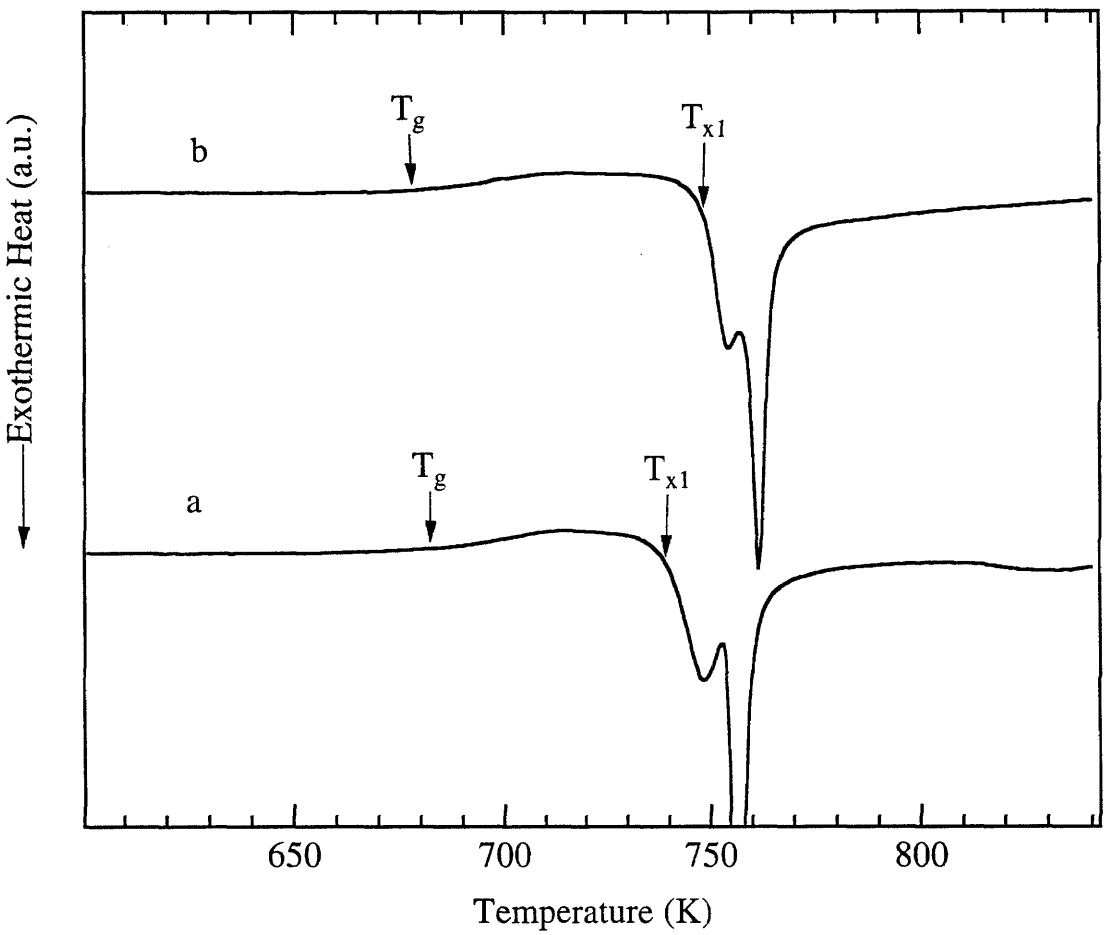

Fig. 3.5 DSC scans of glassy alloys. T_g is the onset of glass transition temperature, T_{x1} is the onset of first crystallization temperature. (a) $Zr_{52.5}Ti_5Cu_{17.9}Ni_{14.6}Al_{10}$, (b) $Zr_{57}Nb_5Cu_{15.4}Ni_{12.6}Al_{10}$.

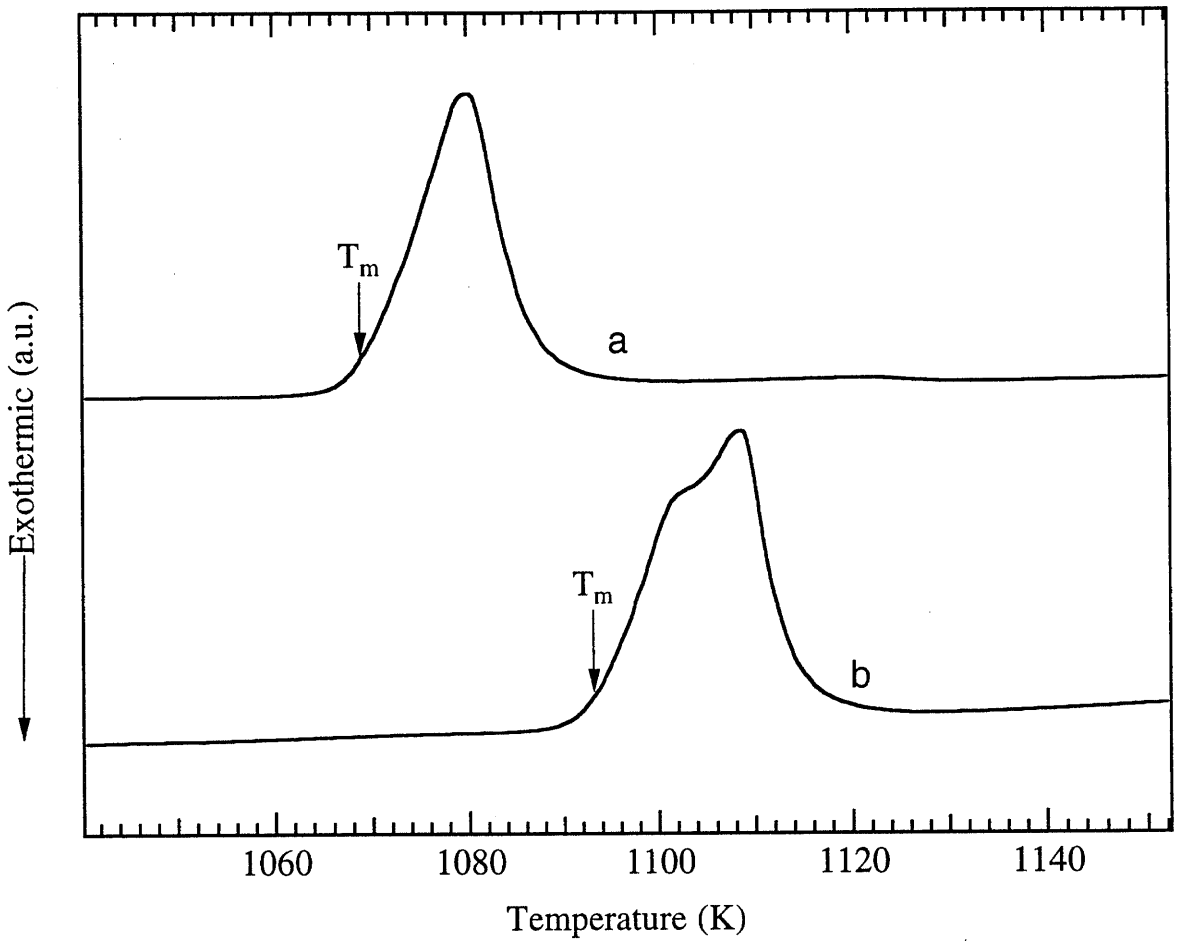

Fig. 3.6 High-temperature DTA scan of crystalline alloys. T_m is the onset of melting temperature. (a) $Zr_{52.5}Ti_5Cu_{17.9}Ni_{14.6}Al_{10}$, (b) $Zr_{57}Nb_5Cu_{15.4}Ni_{12.6}Al_{10}$.

The value for $Zr_{52.5}Ti_5Cu_{17.9}Ni_{14.6}Al_{10}$ alloy is H_v=568±30 kg/mm^2. The value for $Zr_{57}Nb_5Cu_{15.4}Ni_{12.6}Al_{10}$ alloy is H_v=560±30 kg/mm^2. The tensile strength for these glasses is about 1.7 GPa[2].

3.4 ORIGINS OF THE EXCEPTIONAL GLASS FORMING ABILITY

As discussed in chapter 2, the enhanced GFA of Zr-Ti-Cu-Ni alloys compared to Zr-Cu-Ni alloys can be understood by studying the phase diagrams of ternary Ti-Zr-Ni and Ti-Zr-Cu systems. Generally speaking, replacing Zr with Ti in the ternary alloys lowers the melting temperature. The melting temperature of the alloy decreases continuously with increasing Ti concentration until the Laves phase forms. This results in bulk glass formation of the Zr-rich alloys as shown in fig. 2.9, with the present of 5-10 at.% of Ti. On the other hand, the GFA of the Zr-Ni-Cu-Al[1] alloys and the Zr-Ti-Cu-Ni alloys are comparable. It is found[3] that the melting temperature of the alloys decreases when an increasing amount of Al up to 10 at.% is added to Zr-Cu-Ni alloys. Apparently, Al has the same effect as Ti for reducing the melting temperature of Zr-Cu-Ni alloys due to its similar atomic radius to that of Ti. When more than 10 at.% Al is added to the alloys, the melting temperature increases again. This suggests the formation of a new multicomponent phase, just as the Laves phase in the case of adding more than 10 at.% Ti to the alloys. Therefore, the role which Ti and Al play in the glass formation of Zr-Cu-Ni-Ti and Zr-Cu-Ni-Al alloys is to lower the melting temperature of the alloys until their concentrations reach upper limit, which are determined by the formation of new quaternary phases. However, the new Zr-Cu-Ni-Al phase may not be the Laves phase. As such, adding Ti and Al together to Zr-Cu-Ni alloys

lowers the melting temperature as adding Ti or Al alone does. However, the upper limit of the total amount of Ti and Al is greater than that of adding Ti or Al alone. Therefore, the lowest melting temperature of Zr-Cu-Ni-Ti-Al alloy is lower than that of Zr-Cu-Ni-Al and Zr-Cu-Ni-Ti alloys. Hence, the five component alloys have better GFA from the T_{rg} point of view. The complexity of the alloy may also enhance the GFA due to the "confusion principle"[4]. Apparently, the combination of Nb and Al has the same effect to enhance glass formation.

Inoue et al. have been using large ΔT as an indicator for good GFA of alloys.[1,5] However, one notices that ΔT=57 K for the $Zr_{52.5}Ti_5Cu_{17.9}Ni_{14.6}Al_{10}$ alloy and ΔT=70 K for the $Zr_{57}Nb_5Cu_{15.4}Ni_{12.6}Al_{10}$ alloy. Both of these values are lower than that of the $Zr_{65}Cu_{17.5}Ni_{10}Al_{7.5}$ alloy,[5] which has a ΔT=126 K. However, the $Zr_{52.5}Al_{7.5}Co_{2.5}Ni_{10}Cu_{15}$ and the $Zr_{57}Nb_5Cu_{15.4}Ni_{12.6}Al_{10}$ alloys are better glass formers than the $Zr_{65}Cu_{17.5}Ni_{10}Al_{7.5}$ alloy. In fact, this is not a unique case. $Zr_{41.2}Ti_{13.8}Cu_{12.5}Ni_{10}Be_{22.5}$ and $Zr_{46.75}Ti_{8.25}Cu_{7.5}Ni_{10}Be_{27.5}$ alloys are another pair of examples.[6,7] ΔT=80 K for the $Zr_{41.2}Ti_{13.8}Cu_{12.5}Ni_{10}Be_{22.5}$ alloy and ΔT=125 K for the $Zr_{46.75}Ti_{8.25}Cu_{7.5}Ni_{10}Be_{27.5}$ alloy, but the $Zr_{41.2}Ti_{13.8}Cu_{12.5}Ni_{10}Be_{22.5}$ alloy has a better GFA than the $Zr_{46.75}Ti_{8.25}Cu_{7.5}Ni_{10}Be_{27.5}$ alloy. This is because a large ΔT indicates a good stability of the undercooled liquid at low temperature close to T_g, whereas an undercooled liquid is least stable in a temperature range which usually is in the middle between T_g and T_m. The GFA is mainly determined by the stability of the alloy at this temperature. The more stable an alloy is at this temperature, the lower the critical cooling rate for glass formation and the better the GFA. For a

multicomponent alloy, the crystallization mechanism is much more complicated than polymorphic crystallization, which will be discussed in chapter 4 in detail. The relative stability of two alloys may vary with temperature. Therefore, a larger ΔT does not necessary correspond to a lower critical cooling rate and a better GFA.

3.5 CONCLUSIONS

In this chapter, an extremely good glass forming system: Zr-Ti(Nb)-Cu-Ni-Al is presented. The GFA of this system is much better than that of either Ti-Zr-Cu-Ni system or Zr-Cu-Ni-Al system. $Zr_{52.5}Ti_5Cu_{17.9}Ni_{14.6}Al_{10}$ and $Zr_{57}Nb_5Cu_{15.4}Ni_{12.6}Al_{10}$, as two examples, have a critical cooling rate for glass formation of 10 K/s, which is at least one order of magnitude lower than that of best Ti-Zr-Cu-Ni and Zr-Cu-Ni-Al alloys. The combination of Ti or Nb with Al ultimately lowers the melting temperature of the alloys. This in turn makes Zr-Ti(Nb)-Cu-Ni-Al an exceptional good glass forming system. The discovery of these alloys shows again that a few percent addition of a "right" component can induce large improvement in glass forming ability. Hence, finding new metallic glasses is a subtle task.

REFERENCES

1. A. Inoue, T. Zhang, and T. Masumoto, J. Non-cryst. Solids **156-158**, 473 (1993).
2. H. Choi-Yim, D. Conner, and W. L. Johnson, unpublished results.
3. X. H. Lin, and W. L. Johnson, unpublished results.
4. A. L. Greer, Nature **366**, 303 (1993).
5. Zhang, A. Inoue, and T. Masumoto, Mater. Trans. JIM **32**, 1005 (1991).
6. A. Peker, and W. L. Johnson, Appl. Phys. Lett. 63, 2342-2344 (1993).
7. A. Peker, Ph.D. thesis, California Institute of Technology, 1994.

Chapter 4
Time Temperature Transformation Diagrams of Zr based Bulk Glass Forming Alloys

4.1 INTRODUCTION

Based on classical nucleation theory, Davies et al.[1] adopted an approach used by Uhlmann[2] to account for a limited degree of crystal growth in undercooled metallic melts. Time temperature transformation (TTT) curves were computed for Ni, $Au_{78}Ge_{14}Si_8$, $Pd_{82}Si_{18}$, and $Pd_{78}Cu_6Si_{16}$ as shown in fig. 4.1[3]. In this diagram, the time to form a barely detectable fraction (which is arbitrarily set to be 10^{-6} here) of crystals for the undercooled liquids is shown as a function of reduced temperature. However, since the crystallization time for conventional material is very short and the sample container tends to cause heterogeneous nucleation, the TTT curves for crystallization of undercooled liquids of metallic alloys are generally hard to access experimentally.

The novel bulk glass forming alloys have extremely good glass forming ability. Associated with this, extremely high stability against crystallization of the undercooled molten alloys is expected. Thus, the crystallization time scale becomes comparable to experimentally accessible time scales. Hence, it is possible to study the crystallization kinetic experimentally in the deeply undercooled melts. On the other hand, the high temperature high vacuum electrostatic levitation (HTHVESL) processing technique[4] is a ideal tool to eliminate the role of the container wall as a heterogeneous nucleation site as well as the role of contamination by ambient gaseous impurities to study undercooling and

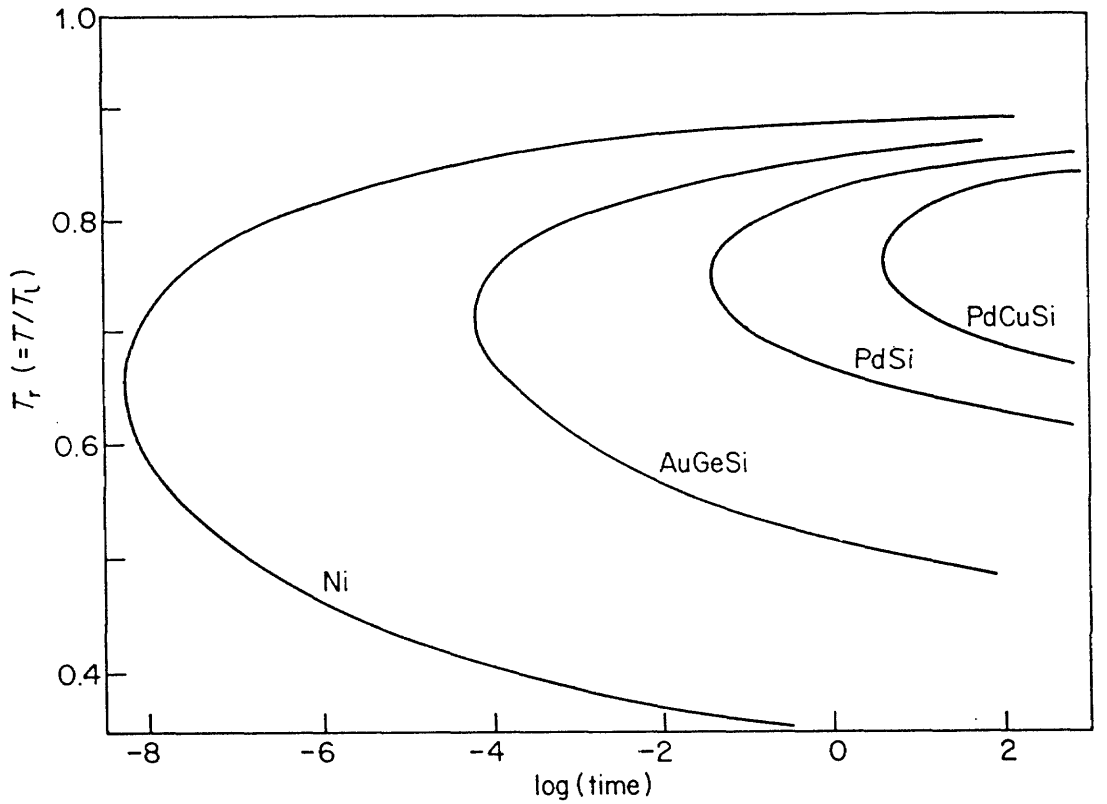

Fig. 4.1 Calculated time temperature transformation curves for a fraction crystal of 10^{-6} for Ni, $Au_{78}Ge_{14}Si_8$, $Pd_{82}Si_{18}$ and $Pd_{78}Cu_6Si_{16}$. (reproduced from ref. 3).

crystal nucleation in the undercooled melt. Using HTHVESL, Kim et al. determined the complete TTT diagram for crystallization of the undercooled $Zr_{41.2}Ti_{13.8}Cu_{12.5}Ni_{10}Be_{22.5}$ liquid.[5] This is the first TTT measurement for crystallization of an alloy for the whole temperature range of undercooled liquid. The measured diagram exhibits a significantly higher "nose" temperature compared to the calculated diagram based on the classic theory that assumes polymorphic solidification. Kim et al. attributed the observation to the fact that crystallization in such a multicomponent alloy involving large concentration fluctuation of several alloy components as well as phase separation. In fact, many factors, such as composition redistribution (which was discussed in chapter 2), phase separation,[6-8] strong glass behavior,[9] and impurity-triggered heterogeneous nucleation (which will be discussed in next chapter) have been discovered involving in the crystallization of multicomponent glass forming alloys. The relative importance of these factors varies with temperature as well as composition of alloys. Thus, each multicomponent alloy has its unique way to crystallize. The shape of the TTT diagram may be different for all the alloys. It would be a surprise if one could fit the TTT curve with one simple model. Therefore, it is interesting to determine the TTT diagram for each new bulk glass forming alloy when this is allowed by the stability of the undercooled melts. By measuring the TTT diagrams, one can also determine the critical cooling rates for vitrification of the glass forming alloys. In addition, since the emissivity and specific heat of the undercooled liquid of $Zr_{52.5}Ti_5Cu_{17.9}Ni_{14.6}Al_{10}$ alloy will be studied by using a micro-gravity facility, measuring the TTT diagram in the

HTHVESL provides valuable information for sample processing and experiment design. In this chapter, the results of TTT diagram measurements for $Zr_{52.5}Ti_5Cu_{17.9}Ni_{14.6}Al_{10}$ and $Zr_{57}Nb_5Cu_{15.4}Ni_{12.6}Al_{10}$ alloys by using HTHVESL at high temperature and by using DSC at low temperature will be presented.

4.2 SAMPLE PREPARATION

As described in chapter 3, high purity elemental materials were melted and mixed by a plasma arc on a water cooled hearth under a Ti-gettered argon atmosphere. Glassy ingots of about 5 g each were obtained after the power of the arc-melter was turned off. To prepare the HTHVESL samples for the TTT diagram measurements, the glassy ingots were crystallized intentionally in an induction melter by heating the ingots above the crystallization temperature for a short time. The crystallized ingots were very brittle. Thus it was easy to cut them into small pieces of about 30 mg each without contamination. These small specimens were remelted in the arc melter very briefly (shorter than one second). The surface tension of the melt caused the samples to assume the shape of nearly perfect spheres. These spherical samples were introduced into the HTHVESL chamber for TTT diagram measurement.

4.3 ELECTROSTATIC LEVITATION PROCESSING

Fig. 4.2 shows the schematic of the high temperature high vacuum electrostatic levitator at JPL. A sufficient electric charge is maintained on the sample. The electric field between the top electrode and bottom electrode generates a levitation force on the charged sample to offset the

gravitational force. The sample position is detected by three-dimensional position sensors. A feed back circuit is applied to actively control the sample position. In comparison, an electromagnetic levitator (EML) relies on eddy currents induced in the sample by an rf magnetic field, which restricts the applicability to electrically conductive materials. An electrostatic levitator (ESL), however, can be used for a broad range of materials including alloys, semiconductors, and insulators. Most importantly, in an electromagnetic levitation processing, the levitation field generates heat in the sample. It is very hard to control sample temperature and levitation independently. However, in an electrostatic levitation processing, sample temperature can be easily controlled by an external heating source, since the levitation field does not generates any heat in the sample. Furthermore, the electrostatic lavitator provides quiescent positioning during sample processing due to the employment of a feedback control. A more open view in ESL allows a full access of the non-contact optical diagnostic instruments such as a pyrometer for thermal analysis and a video camera for image analysis.

The sample and electrodes are contained in a stainless steel vacuum chamber as schematically shown in fig. 4.3, which was pumped down to a pressure of $5x10^{-8}$ tor, and was baked by an ultraviolet lamp to reduce the water partial pressure. During the experiment, the sample was heated by a 1 kW UV-rich high pressure xenon arc lamp after being levitated. The sample temperature was measured by an E^2T pyrometer. The pyrometer was calibrated by the melting temperature of the sample. During isothermal measurement, the sample was first melted, then cooled radiatively by blocking the iris of the xenon lamp. When the sample

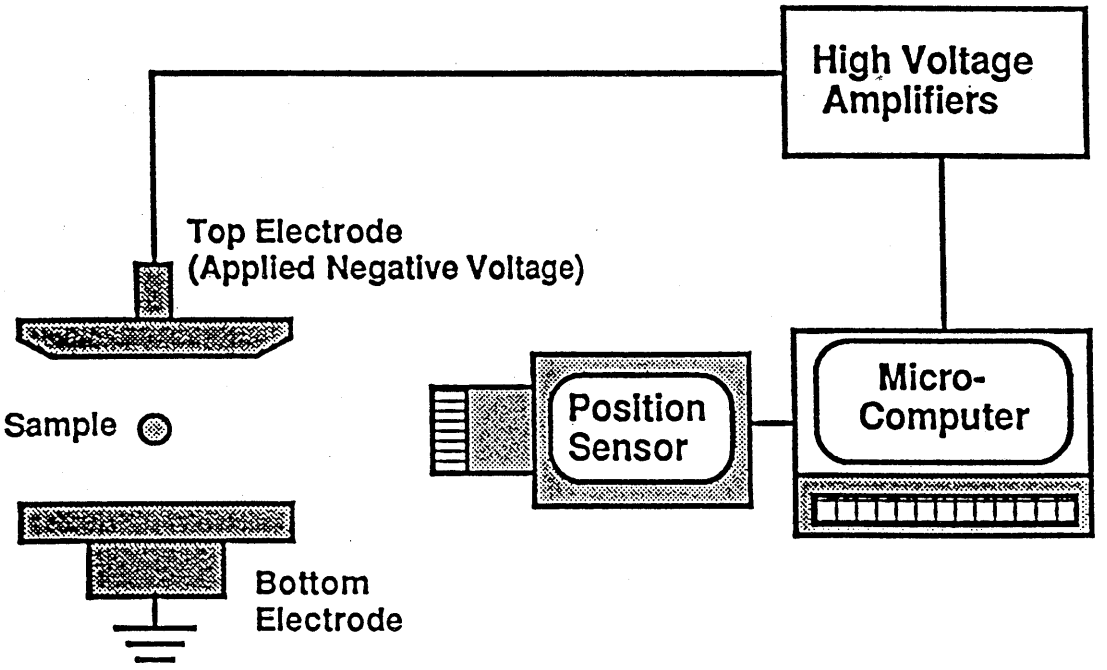

Fig. 4.2 Schematic illustration of an electrostatic levitator in which the sample is levitated by maintaining the charge induced by the applied negtive voltage. Sample position is actively controlled by using a feed-back control to correct any deviation from a preset position.

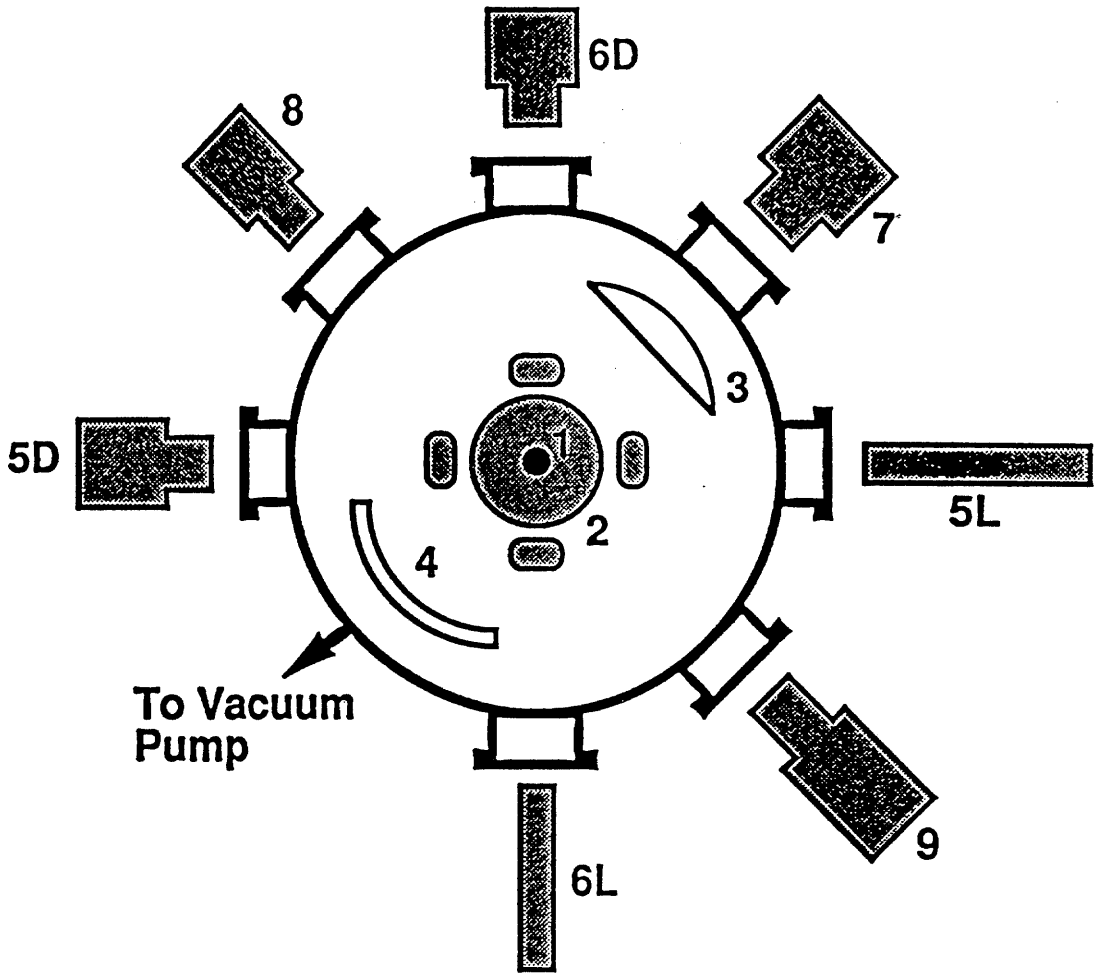

Fig. 4.3 Schematic of an electrostatic levitator. 1 is the sample, 2 is the electrode assembly, 3 is the focusing lens, 4 is the spherical reflector, 5D and 6D are the position detectors, 5L and 6L are the He-Ne lasers, 7 is the 1 kW UV-rich Xenon lamp, 8 is the video camera, and 9 is the single color E^2T pyrometer.

reached a pre-set undercooling temperature, the iris of the lamp was re-opened to a pre-tested width for which the balance between input power and radiative heat loss yields isothermal conditions. Using this method, the sample could be radiatively cooled to a pre-set temperature and then maintained isothermally with an accuracy of ± 4 K. The time for the onset of recalescence was then recorded as a function of undercooling temperature (under isothermal conditions).

The low temperature branches of TTT diagrams were measured by differential scanning calorimeter (DSC). Isothermal measurements were carried out on glassy samples, following a rapid heating at heating rate of 100 K/min.

4.4 RESULTS

Fig. 4.4 shows a cooling curve for an 27.4 mg $Zr_{52.5}Ti_5Cu_{17.9}Ni_{14.6}Al_{10}$ sample. After being heated to 1300 K and staying at this temperature for 1 min, the sample was allowed to cool radiatively by blocking the xenon lamp. Because the radiation power loss is proportional to the fourth power of the sample temperature, the cooling rate decreases as the sample is cooled. The typical cooling rate is 3-7 K/s for the interesting temperature range. The sample recaleses at T_{recl}=869 K, which is indicated by a sudden increasing of sample temperature due to the enthalpy released by the crystallization. For a 26.6 mg $Zr_{57}Nb_5Cu_{15.4}Ni_{12.6}Al_{10}$ alloy, T_{recl}=886 K. Fig. 4.5 shows a typical isothermal curve of the 27.4 mg $Zr_{52.5}Ti_5Cu_{17.9}Ni_{14.6}Al_{10}$ sample at 966 K. The sample crystallizes 270 s after reaching the pre-set temperature.

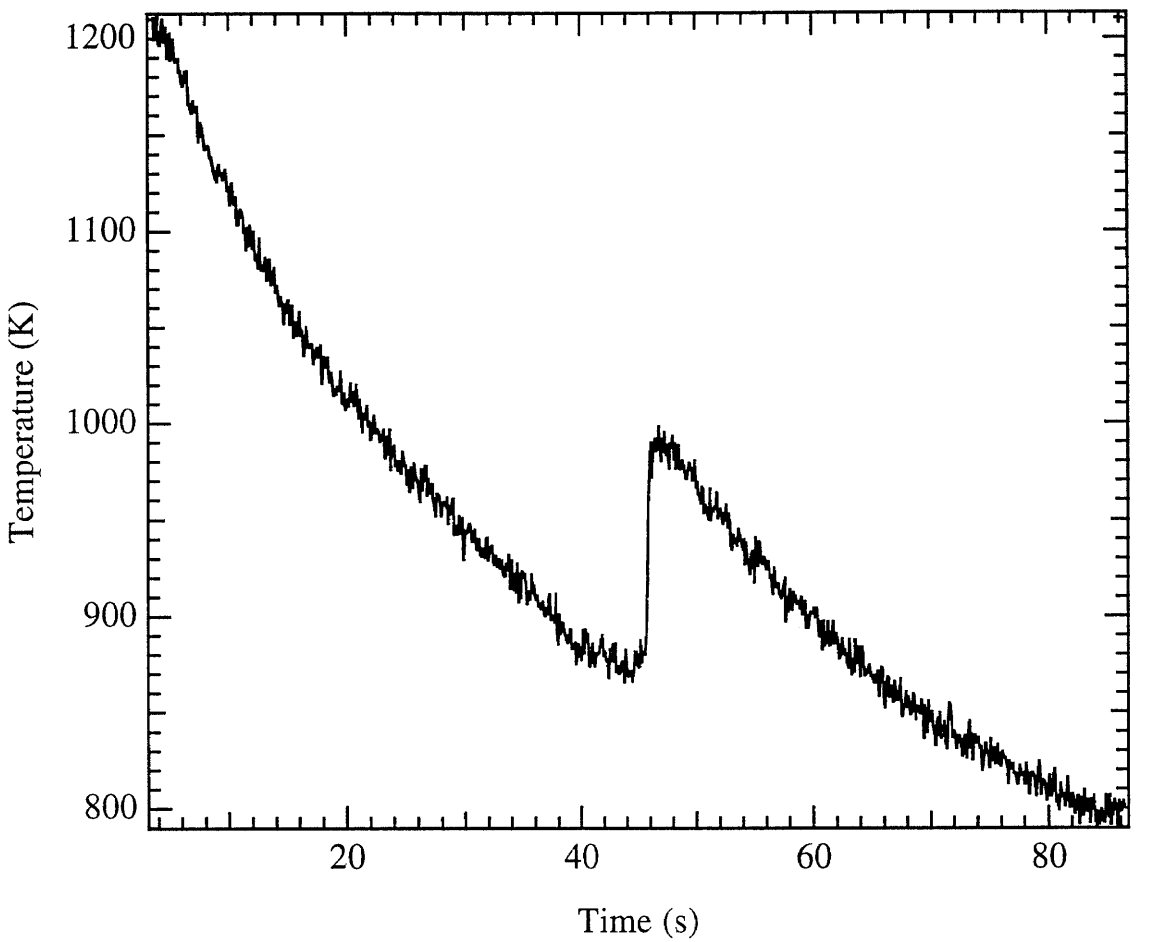

Fig. 4.4 Radiative cooling curve of a 27.4 mg $Zr_{52.5}Ti_5Cu_{17.9}Ni_{14.6}Al_{10}$ alloy. Recalescence event is observed at 869 K and the temperature increases to 978 K.

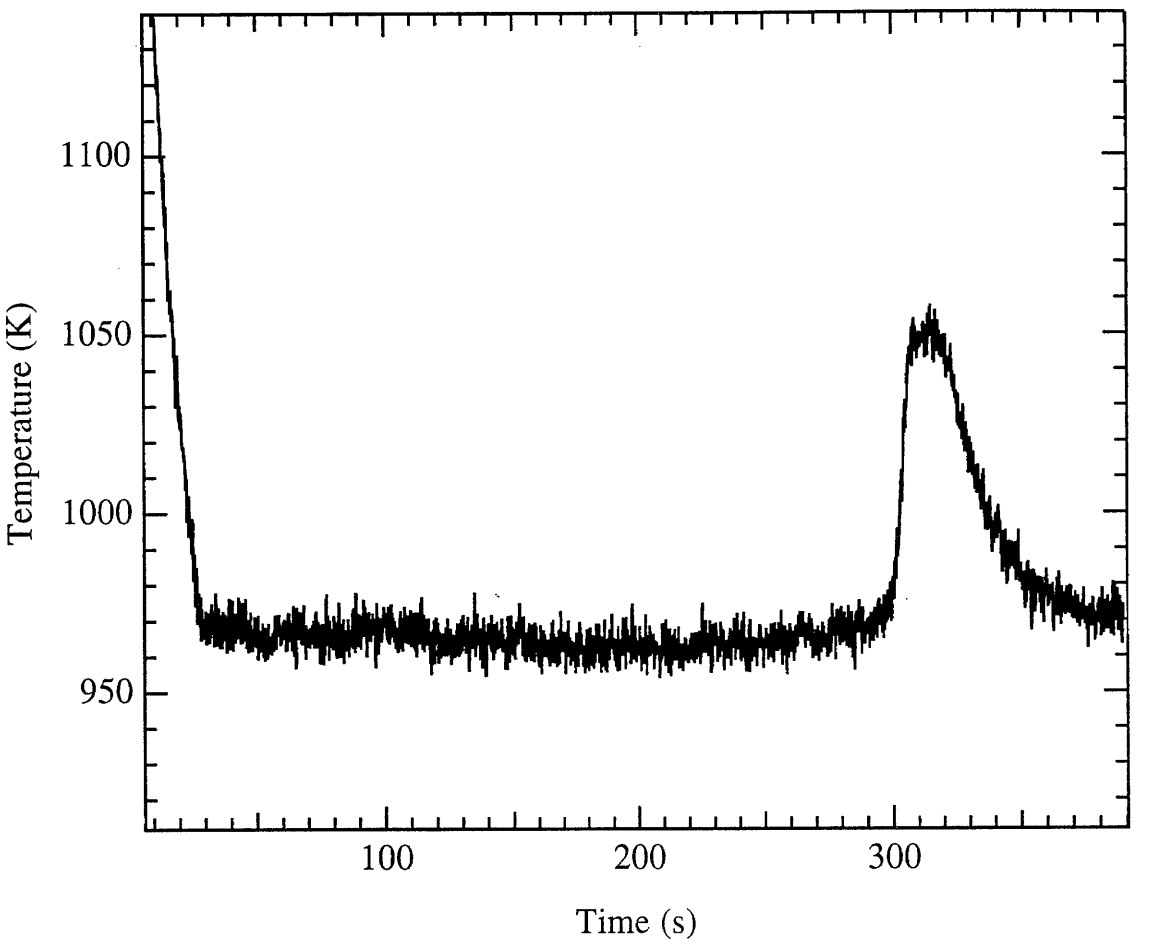

Fig. 4.5 Temperature-time profile for a 27.4 mg $Zr_{52.5}Ti_5Cu_{17.9}Ni_{14.6}Al_{10}$ alloy under isothermal treatment at 966 K. The recalescence event occurs at 270 s, which leads to a temperature increase up to 1049 K.

At relatively high temperature, the cooling time from melting temperature to the pre-set temperature is negligible comparing to the isothermal time. The isothermal time can be taken as the incubation time for crystallization. However, at low temperature, the cooling time is comparable to the isothermal time. Then the isothermal time should be corrected by the cooling time to yield the real incubation time for crystallization. For first order approximation, we assume that each time interval the sample spends at any temperature below the melting temperature has a contribution to the final crystallization. The relative contribution of a time interval at each temperature is determined by the ratio of the time interval and characteristic crystallization time for that temperature. For example, if a sample stays at temperature T_1 for a time t_1, and subsequently stays at another temperature T_2 and crystallizes after time t_2, t_2 is determined by the equation:

$$\frac{t_1}{\tau_1(T_1)} + \frac{t_2}{\tau_2(T_2)} = 1 \qquad (4.1)$$

where τ_1 and τ_2 are crystallization times at T_1 and T_2 respectively. Therefore, if τ_1 is known, t_1 and t_2 are measured, one can calculate the τ_2 value using equation:

$$\tau_2 = \Big/ \left(1 - \frac{t_1}{\tau_1}\right)^{1} \qquad (4.2)$$

Thus, one defines $c=1/(1- t_1/ \tau_1)$ as the correction coefficient for t_2. In the case of continuous cooling before the isothermal heat treatment, we have:

$$\frac{t(T_{iso})}{\tau(T_{iso})} = 1 - \int_{Tm}^{Tiso} \frac{dT}{\tau(T)\frac{dT}{dt}} \approx 1 - \sum_{Tm}^{Tiso} \frac{\Delta T}{\tau(T)\frac{dT}{dt}} \qquad (4.3)$$

where T_{iso} is the isothermal temperature, dT/dt is the slope of the cooling curve. For good approximation, we took ΔT=2 K. Then, the correction coefficient becomes:

$$c(T_{iso}) = \frac{1}{1 - \sum_{Tm}^{Tiso} \frac{\Delta T}{\tau(T)\frac{dT}{dt}}} \tag{4.4}$$

This means that the crystallization time at any temperature can be corrected, if the crystallization time and cooling rate for higher temperatures are known. In fact, because the crystallization time is long near T_m, one only has to do the summation in eq. 4.4 starting from a relatively low temperature. At the starting temperature, one assumes $\tau_1=t_1$. Then one computes c_2 for next lower temperature. Thus one obtains $\tau_2= c_2t_2$. Using τ_1 and newly obtained τ_2, one can compute c_3. Step by step, all the isothermal times are corrected to the real crystallization times. To verify the correction, using dT/dt data and obtained τ data, the recalescence temperature T_{recl} is evaluated, which satisfies:

$$\sum_{Tm}^{Trecl} \frac{\Delta T}{\tau(T)\frac{dT}{dt}} = 1 \tag{4.5}$$

The calculated T_{recl} are 871 K and 877K for $Zr_{52.5}Ti_5Cu_{17.9}Ni_{14.6}Al_{10}$ alloy and $Zr_{57}Nb_5Cu_{15.4}Ni_{12.6}Al_{10}$ alloy respectively, which agree with the measured values reasonably well. This means that the correction of crystallization is valid.

Fig. 4.6 shows the corrected TTT diagram for undercooled liquid of $Zr_{52.5}Ti_5Cu_{17.9}Ni_{14.6}Al_{10}$ alloy. In fig. 4.7 the corrected TTT diagram for undercooled liquid of $Zr_{57}Nb_5Cu_{15.4}Ni_{12.6}Al_{10}$ alloy is depicted. The noses of the TTT diagram are observed at a temperature of about 920 K for $Zr_{52.5}Ti_5Cu_{17.9}Ni_{14.6}Al_{10}$ alloy, and approximately 930 K for

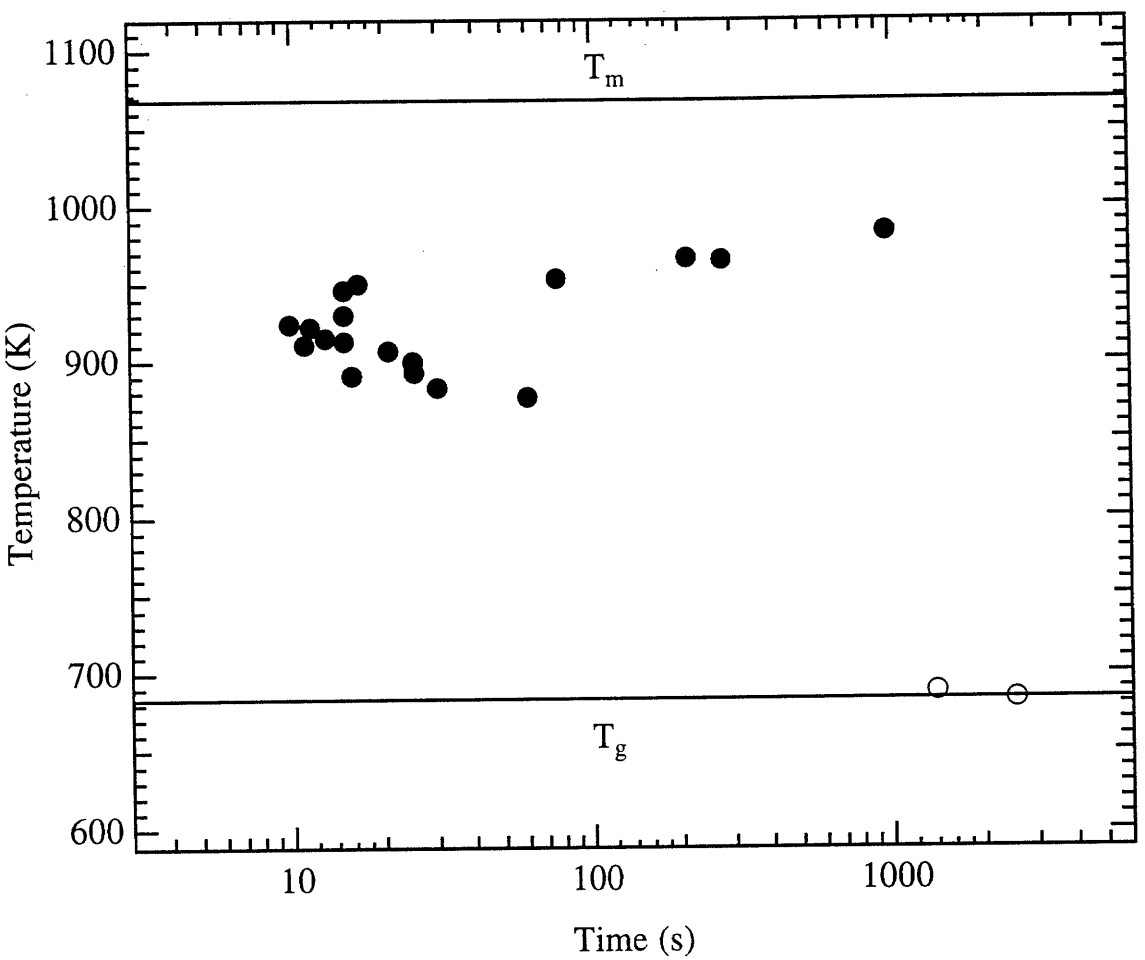

Fig. 4.6 TTT diagram reflecting the onset of crystallization measured by HTHVESL (●) and DSC (○) for $Zr_{52.5}Ti_5Cu_{17.9}Ni_{14.6}Al_{10}$ alloy.

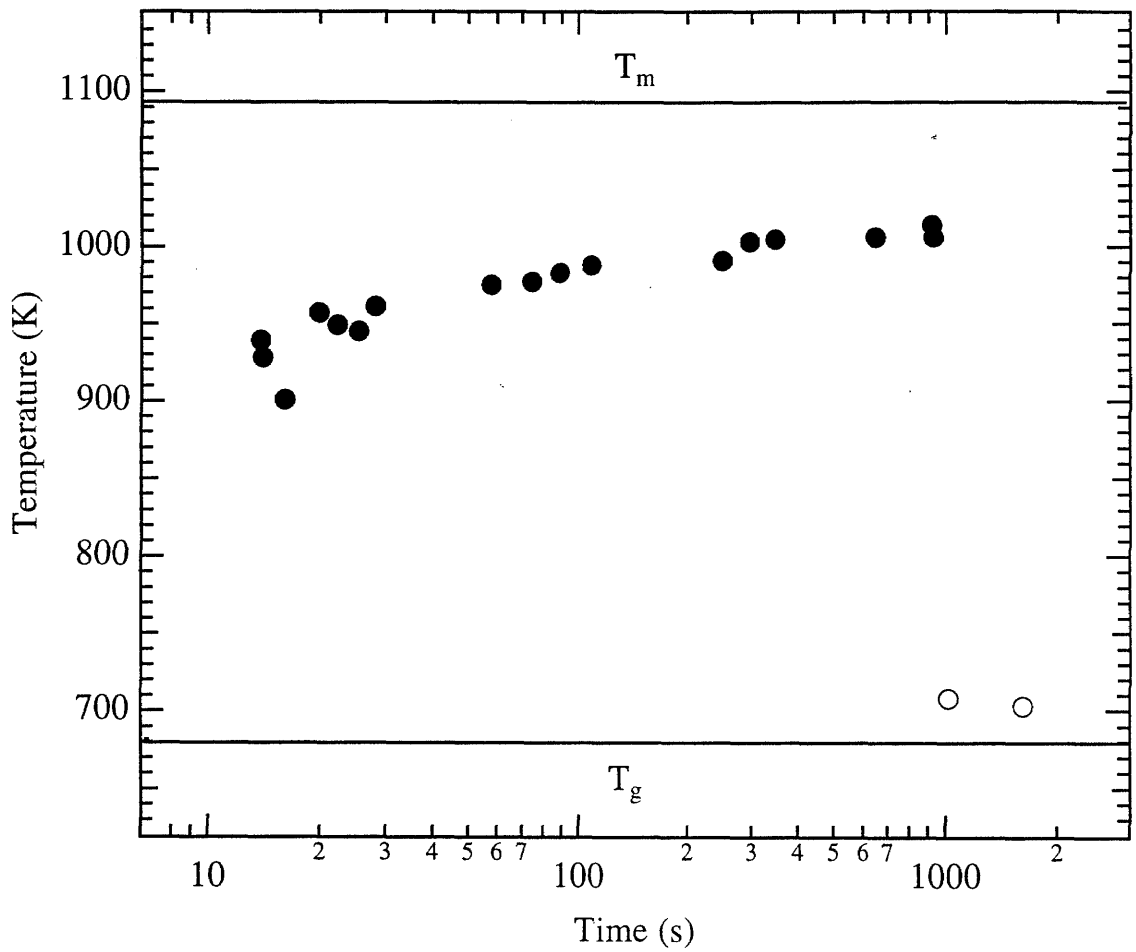

Fig. 4.7 TTT diagram reflecting the onset of crystallization measure by for HTHVESL (●) and DSC (○) for $Zr_{57}Nb_5Cu_{15.4}Ni_{12.6}Al_{10}$ alloy.

$Zr_{57}Nb_5Cu_{15.4}Ni_{12.6}Al_{10}$ alloy, respectively. Despite the fact that the noses can be "passed" during free radiative decay, the samples recalesce at temperature below the noses, due to the decreasing cooling rate (with undercooling) and to the cumulative nucleation effect during continuous cooling. As such, fully glassy spheres were not able to be obtained by free radiative cooling as in the earlier reported experiments of Kim et al.[5] One would expect that a modest increase in cooling rate would lead to glass formation under free radiative cooling. Based on analysis, a critical cooling rate of about 10 K/s is determined for the nominally "clean" alloy, which agrees with the fact that 1-cm-thick glassy ingots were obtained in the arc melter. It is also noticed that at low temperature near T_g, the $Zr_{57}Nb_5Cu_{15.4}Ni_{12.6}Al_{10}$ alloy is more stable than $Zr_{52.5}Ti_5Cu_{17.9}Ni_{14.6}Al_{10}$ alloy. This is consistent with the factor that the former has larger ΔT than the latter one in continuous heating experiments.

4.5 DISCUSSION AND CONCLUSION

For a multicomponent system, the crystallization mechanism is much more complicated than polymorphic crystallization. First, the composition of a multicomponent good glass forming alloy is usually near a eutectic point. The equilibrium state at low temperature is a mixture of several crystalline phases. The primary crystallization is the result of the competition among these phases. Since the composition of each crystalline phase is deferent from that of the liquid, the nucleation and growth of these crystalline phases is diffusion controlled. Second, decomposition may occur in the undercooled liquid, which triggers the crystallization. The free energy of a liquid is: G=H-TS, where H is

enthalpy, T is the temperature, and S is the entropy. Short range order in the liquid state may have lower H value at certain composition. At high temperature, the TS term has a high value, which smears out the local minimums of H. The liquid composition is homogeneous above the melting temperature. When the liquid is deeply undercooled, TS term decreases, free energy G may show local minimum values corresponding to some energetic more stable short range orders. Therefore, the decomposition occurs. This process has no energy barrier. The resulting decomposed domains then may crystallize polymorphically. Decomposition was reported in a large variety of metallic glasses. $Zr_{41.2}Ti_{13.8}Cu_{12.5}Ni_{10}Be_{22.5}$[6] and Mg-Y-Cu-Li[7] are two examples. Diffusion controlled and decomposition preceded crystallization frequently results in formation of nanocrystals, as in the cases for $Zr_{41.2}Ti_{13.8}Cu_{12.5}Ni_{10}Be_{22.5}$[8] and $Ti_{34}Zr_{11}Cu_{47}Ni_8$.[10] Third, it is found that the crystallization of $Zr_{52.5}Ti_5Cu_{17.9}Ni_{14.6}Al_{10}$ and $Zr_{57}Nb_5Cu_{15.4}Ni_{12.6}Al_{10}$ undercooled melts starts with heterogeneous nucleation triggered by oxide particles in the melts, which will be presented in chapter 5. Further, viscosity measurements in the undercooled $Zr_{46.75}Ti_{8.25}Cu_{7.5}Ni_{10}Be_{27.5}$ liquid shows that bulk metallic glass forming alloy exhibits "strong" as opposed to "fragile" glass behavior.[9] This behavior is in stark contrast to that reported earlier for metallic glass forming alloys and contributes the good GFA of bulk glass forming alloys. All of these observations make it impossible to predict the TTT diagram for crystallization by using a universal model. Thus, every alloy has its unique TTT diagram.

REFERENCES

1. H. A. Davies, J. Aucot, and J. B. Hull, Scripta Met. **8**, 1179 (1974).
2. D. R. Ulhmann, J. Non-cryst. Solids **7**,337 (1972).
3. H. A. Davies, in *Amorphous Metallic Alloys*, edit by F. E. Luborsky, (Butterworth & Co, 1983), p8.
4. W. K. Rhim, S. K. Chung, D. Barber, K. F. Man, G. Gutt, A. J. Rulison, and R. E. Spjut, Rev. Sci. Instrum. **64**, 2961 (1993).
5. Y. J. Kim, R. Busch, W. L. Johnson, A. J. Rulison, and W. K. Rhim, Appl. Phys. Lett. **68**, 1057 (1996).
6. R. Busch, S. Schneider, A. Peker, and W. L. Johnson, Appl. Phys. Lett. **67**, 1544 (1995).
7. W. S. Liu, and W. L. Johnson, J. Mater. Res., (1996) in press
8. S. Schneider, P. Thiyagarajan, and W. L. Johnson, Appl. Phys., Lett. **68**, 493 (1996)
9. E. Bakke, R. Busch, and W. L. Johnson, Appl. Phys. Lett. **67**, 3260 (1995).
10. X. H. Lin, and W. L. Johnson, unpublished results.

Chapter 5
Oxygen Impurity Effects on the Crystallization of Zr based Bulk Metallic Glass Forming Alloys

5.1 HETEROGENEOUS NUCLEATION THEORY

According to classical homogeneous nucleation theory, all melts should show a large degree of undercooling. However, this is contradictory to most experimental observations. To solve this puzzle, Turnbull proposed that the formation of a nucleus of the critical size can be catalyzed by a suitable surface in contact with the liquid.[1] The process is called heterogeneous nucleation. The nucleation catalyst or nucleant may be either a solid particle suspended in the liquid, the surface of the container, or a solid film, such as oxide, on the surface of the liquid. The heterogeneous nucleation theory will be discussed briefly in the following.

When a peripherical embryo is formed on the surface of a substrate, as shown in fig. 5.1[2], the balance for the horizontal components of the surface tensions requires:

$$\sigma_{sl} - \sigma_{sc} = \sigma_{lc}\cos\theta \qquad (5.1)$$

where σ_{sl} , σ_{sc}, and σ_{lc} are the interfacial energies between substrate and liquid, substrate and crystal, and liquid and crystal, respectively. θ is called the wetting angle. It is easy to see that this equation is not always satisfied. For convenient, a parameter m is defined as:

$$m = \frac{\sigma_{sl} - \sigma_{sc}}{\sigma_{lc}} \qquad (5.2)$$

If m>1, then there is no stable angle of contact and the interfacial energy decreases continuously as the embryo spreads over the substrate. In this case, the liquid wets the substrate entirely. If m<-1, again there is no stable

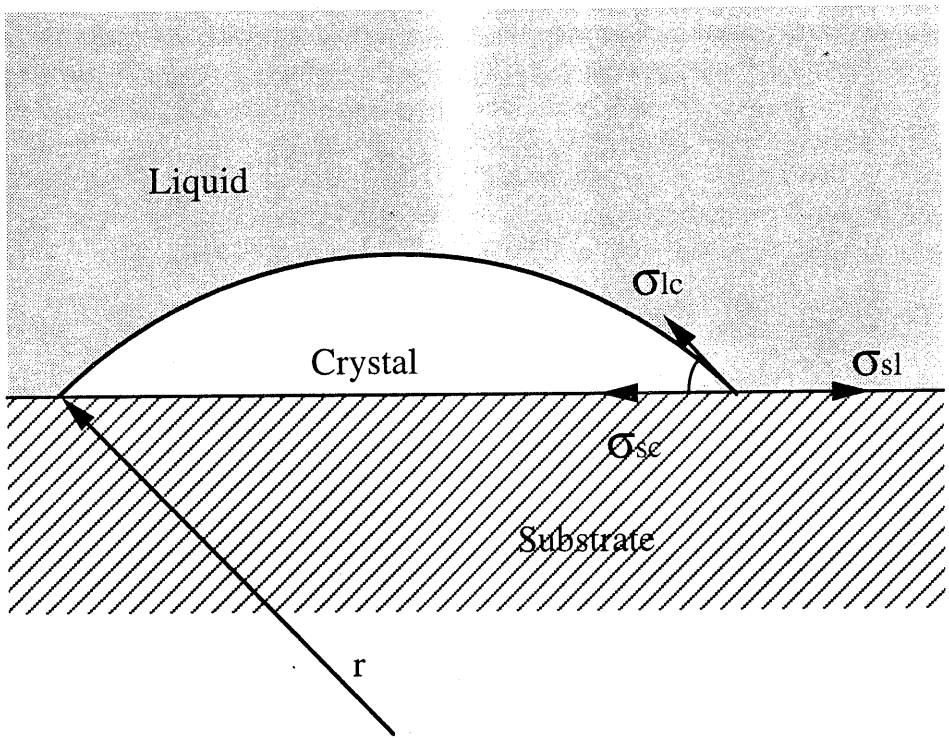

Fig. 5.1 Stability of an spherical cap shaped embryo on a substrate. (reproduced from ref. 2)

angle of contact, and any contact between embryo and substrate causes an increase of interfacial energy. Any value of m between +1 and -1 corresponds to a stable contact angle. In this case, the surface area of the spherical cap is:

$$A = 2\pi(1-\cos\theta)r^2 \tag{5.3}$$

The volume of the spherical cap is:

$$V = \frac{1}{3}\pi(1-\cos\theta)^2(2+\cos\theta)r^3 \tag{5.4}$$

Therefore, the free energy change associated with the formation of a spherical cap shaped embryo on a substrate is:

$$\begin{aligned}\Delta G &= 2\pi(1-\cos\theta)r^2\sigma_{lc} + \pi(r\sin\theta)^2(\sigma_{sc}-\sigma_{sl}) \\ &\quad + \frac{1}{3}\pi(1-\cos\theta)r^3\Delta G_v \\ &= f(\theta)\Delta G\end{aligned} \tag{5.5}$$

where ΔG is the energy change for homogeneous nucleation, f(θ) is a function of θ defined as:

$$f(\theta) = \frac{(1-\cos\theta)^2(2+\cos\theta)}{4} \tag{5.6}$$

Fig. 5.2 shows the value of f(θ) as a function of wetting angle. Therefore, the radius of critical spherical cap for heterogeneous nucleation is the same as the radius of critical nucleus for homogeneous nucleation. However, the volume of the critical spherical cap is only a fraction of f(θ) of the critical nucleus, and the energy barrier for heterogeneous nucleation is also reduced by a factor of f(θ) comparing to homogeneous nucleation. That is:

$$\Delta G_{het}^* = f(\theta)\Delta G^* \tag{5.7}$$

Similar to equation 1.6, the heterogeneous nucleation rate is given by:

$$I_{het} = \frac{k_n}{\eta(T)}\exp\left(-\frac{f(\theta)\Delta G^*}{kT}\right) \tag{5.8}$$

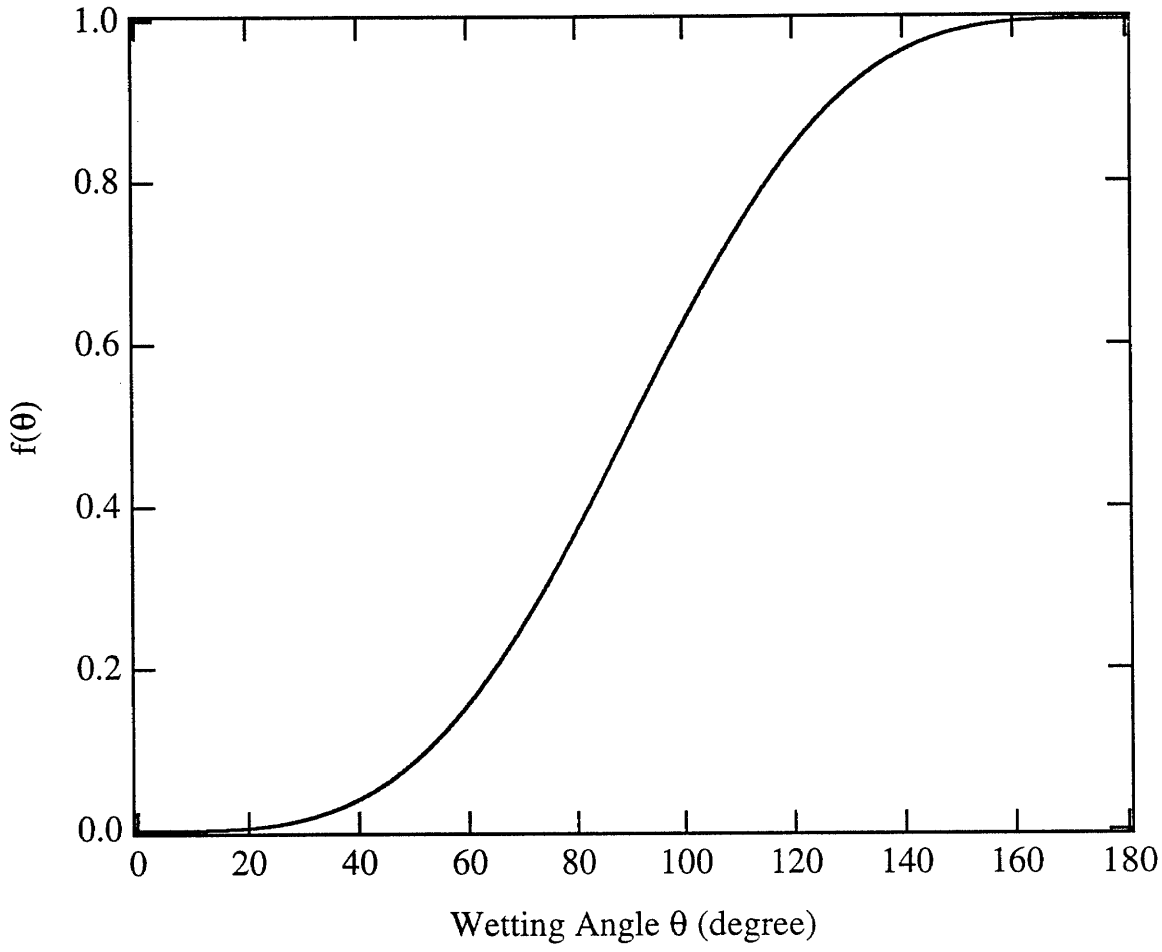

Fig. 5.2 The value of f as a function of wetting angle.

A $f(\theta)$, which is less than one can cause heterogeneous nucleation rates that are orders of magnitude larger than homogeneous nucleation rates.

5.2 HETEROGENEOUS NUCLEATION AND GLASS FORMATION

If crystal embryos wet the substrate, heterogeneous nucleation is favored over homogeneous nucleation. If the density of heterogeneous nucleants is high enough, the crystallization of undercooled melt will be dominated by heterogeneous nucleation. It is common that molten alloys contain some impurities. Thus, it is not surprising that heterogeneous nucleation may become the controlling factor that determines the glass formation and the critical cooling rate, when a high density of impurities is presented. As a matter of fact, by using boron oxide fluxing to suppress the role of heterogeneous nucleation, Kui et al. have obtained centimeter-sized ingots of Pd-Ni-P glassy material at a cooling rate in the 1-10 K/s range[3], which is much lower than the critical cooling rate for glass formation of the alloy without fluxing treatment. This experiment demonstrated that heterogeneous nucleation can be the dominant factor in determining the glass forming ability of some alloys. However, quantitative information, such as how much impurity will cause heterogeneous nucleation or how much change of crystallization kinetic will be caused by certain impurity concentration, is not known.

More recently, several families of multicomponent glass forming alloys have been reported exhibiting such enhanced glass forming ability. These include the La-Al-Ni[4], Zr-Ni-Cu-Al[5], Mg-Cu-Y[6], Zr-Ti-Ni-Cu-Be[7], Zr-Ti-Cu-Ni[3], and Zr-Ti(Nb)-Cu-Ni-Al[9] with critical cooling rates for glass formation in the range of 1-100 K/s. Specimens of these bulk glass

forming alloys with smallest dimensions up to several mm to several cm have been cast at cooling rates as low as 1-100 K/s. It has opened not only technological opportunities, but also has facilitated the study of the undercooled liquid state in metallic systems. The fundamental underlying factors which control the glass forming ability of these systems has, nevertheless, remained rather poorly understood. It is not known, for example, whether glass formation and cooling rate requirements are controlled by homogeneous or heterogeneous nucleation. If the later controls crystallization, then substantial improvement in glass forming ability could be expected by removal of the active heterogeneous nucleants. In this chapter, $Zr_{52.5}Ti_5Cu_{17.9}Ni_{14.6}Al_{10}$ was chosen to study the impurity effect on crystallization due to its exceptional glass forming ability.

The high temperature high vacuum electrostatic levitation (HTHVESL) processing technique[10] has been applied to eliminate the role of the container wall as a heterogeneous nucleation site as well as the role of contamination by ambient gaseous impurities to study undercooling and crystal nucleation in the undercooled melt. The onset of crystallization can be readily detected by its accompanying recalescence effect. The use of the HTHVESL method has permitted the controlled introduction of impurity (i.e., oxygen) into the starting alloy and the investigation of its influence on crystal nucleation. It will be shown that changing the oxygen content of the alloy over the range of 250-5250 ppm (atomic concentration) changes crystal nucleation kinetics dramatically. It is observed that undercooling was dependent on initial overheating of the sample in an unexpected manner. A very well defined critical level of

overheating leads to enhanced undercooling. This critical level of overheating depends on oxygen impurity content. For insufficiently overheated samples undercooling is limited to a well defined temperature independent of oxygen content. For samples sufficiently overheated, deeper undercooling is achieved with the extent of undercooling sensitively and systematically depending on oxygen content. This latter effect has been quantified by direct HTHVESL measurements of the isothermal TTT diagram for crystallization as a function of oxygen impurity content. The TTT diagram is a systematic function of oxygen content.

5.3 SAMPLE PREPARATION AND EXPERIMENT METHODS

Two master ingots of nominal composition $Zr_{52.5}Ti_5Cu_{17.9}Ni_{14.6}Al_{10}$ were prepared by arc melting from the purest available Zr, Ti, Cu, Ni, and Al on a water cooled cooper hearth under a Ti-gettered argon atmosphere. The dominant non-metallic impurity in the alloy is oxygen with a concentration of 250 atomic ppm. The oxygen comes mainly from oxygen present in the high purity Zr crystal bar used (350-400 ppm oxygen). An additional 5000 ppm oxygen was added to one master ingot by dissolving the appropriate amount of ZrO_2 during remelting. The oxide is readily dissolved by the alloy during melting at elevated temperature. Smaller ingots of varying oxygen content were subsequently prepared by melting various portions of these two master ingots in predetermined ratios. The HTHVESL samples of 27.4 ± 1.0 mg were cut from the smaller ingots. Special care was taken to ensure that no contamination was introduced during the sample preparation. The

HTHVESL chamber was pumped down to a pressure of 10^{-8} torr, and baked with an ultraviolet lamp to reduce the partial pressure of H_2O. The sample was levitated and then heated by a 1 kW UV-rich high pressure xenon arc lamp. The sample temperature was measured using an E^2T infrared pyrometer. The pyrometer was calibrated using the known melting temperature of the alloy.

5.4 OXYGEN CONCENTRATION DEPENDENCE OF UNDERCOOLING AND OVERHEATING EFFECTS

During the undercooling measurement, the sample was first melted and maintained at a temperature above the melting point (1069 K) for several minutes. This is referred to as the "soak" temperature. The sample was then allowed to cool by thermal radiation by blocking the lamp. Fig. 5.3 shows two free radiative cooling curves of a 27.4 mg "clean" sample containing 250 atomic ppm oxygen. The cooling curves were started after "being soaked" at two different temperatures. Since radiative power loss is proportional to the fourth power of temperature, the cooling rate is seen to rapidly decrease with increasing undercooling. The cooling rate is about 3-7 K/s for the typical temperature range studied. The sudden increase of the sample temperature can be identified with enthalpy released during recalescence which follows the onset of crystallization. For the higher initial "soak" temperature, the sample recalesces at T_{recl} = 869 K. For the lower initial "soak" temperature, T_{recl} = 1015 K.

Fig. 5.4 shows the dependence of T_{recl} on the "soak" temperature. A very well defined "threshold" effect is seen with a minimum "soak" temperature of about 1215 K required to achieve a discontinuously larger

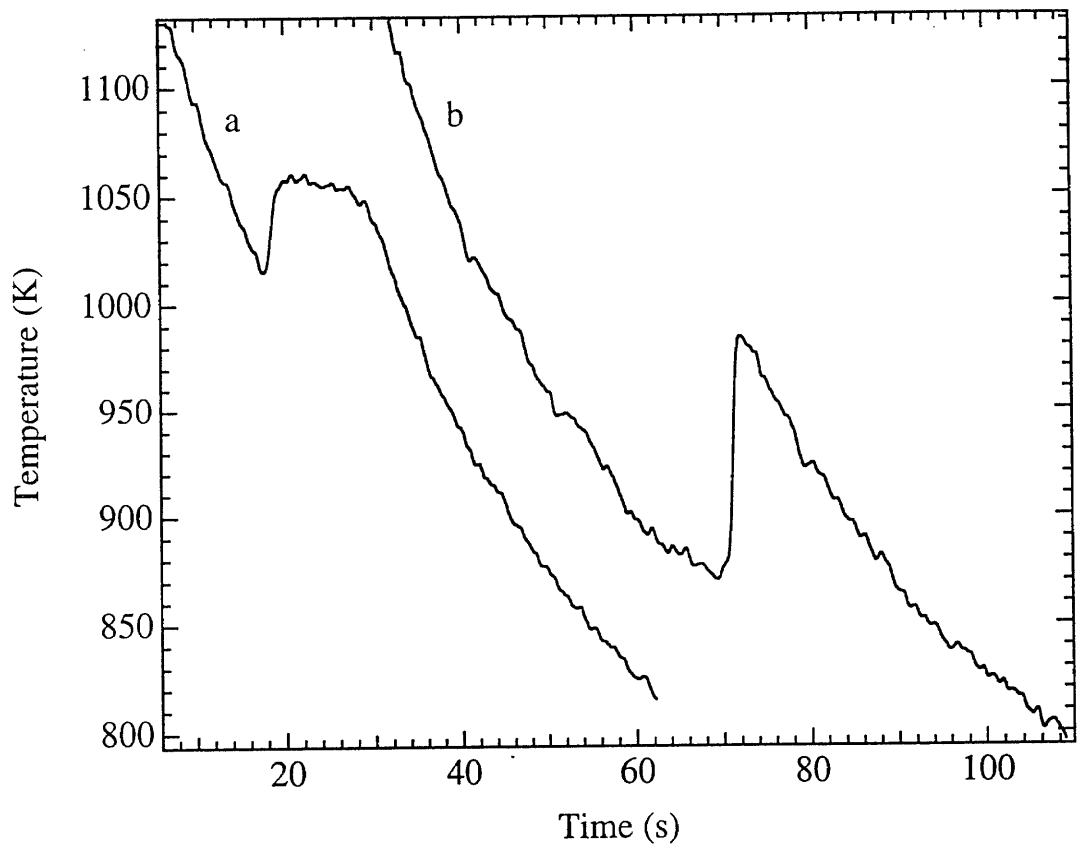

Fig. 5.3 Typical cooling curves of a 27.4 mg $Zr_{52.5}Ti_5Cu_{17.9}Ni_{14.6}Al_{10}$ sample with 250 atom ppm oxygen. a: cooled from 1212 K, the sample recalesces at 1015 K. b: cooled from 1219 K, the sample recalesces at 869 K.

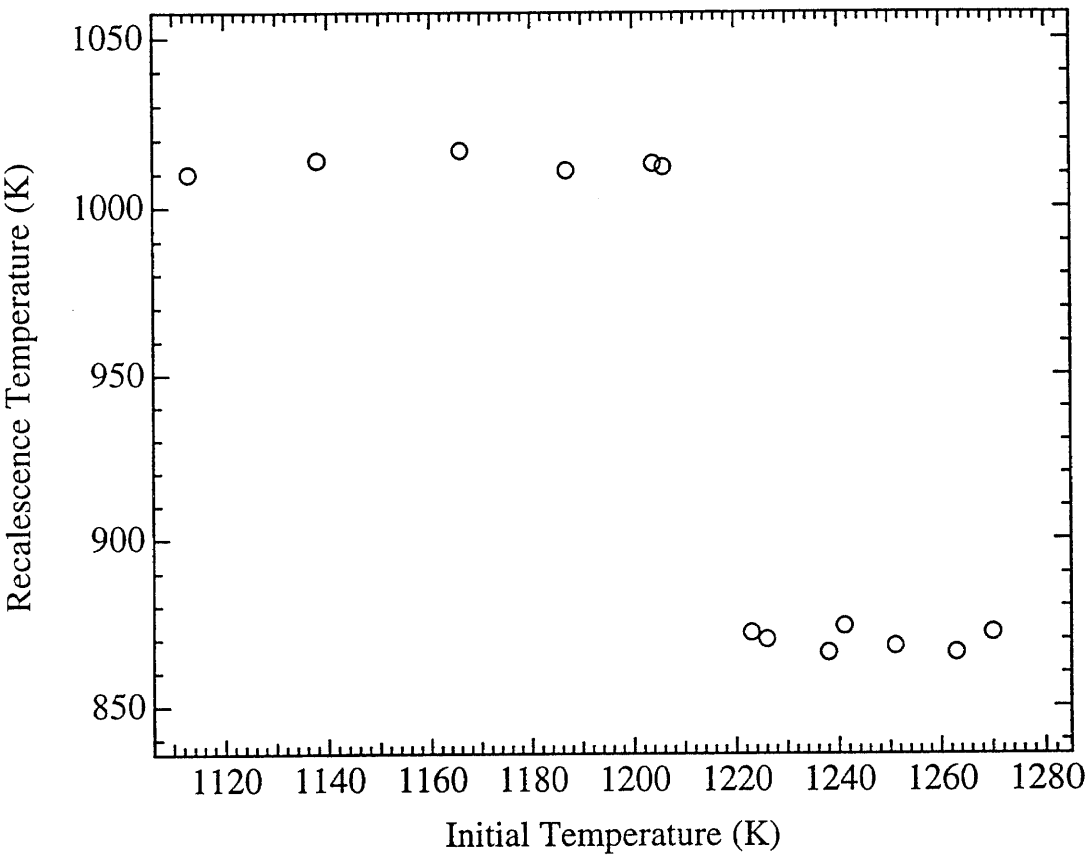

Fig. 5.4 Recalescence temperature versus initial temperature of the 27.4 mg $Zr_{52.5}Ti_5Cu_{17.9}Ni_{14.6}Al_{10}$ sample of 250 atom ppm oxygen. A clear initial temperature threshold for maximum undercooling is observed around 1215 K.

undercooling. Overheating effects have been previously reported on Ni-B,[14] Pd-Cu-Si,[15] and Fe-Ni-P-B[16] alloys in non-containerless processing studies and explained in terms of the progressive thermal break up of atomic clusters or associates with increasing temperature in the equilibrium melt. These clusters are presumed to have the symmetry of the nucleating crystalline intermetallic phase and act as nucleation sites for the crystal. It is argued that the clusters persist in the liquid above the melting point and are gradually broken up with increased overheating. In the present case, the well defined "threshold" soak temperature, hereafter referred to as T_{thr}, at about 146 K above the melting point, above which subsequent undercooling discontinuously increases, suggests a different interpretation. Equilibrium clustering in the melt would be expected to gradually diminish with increasing temperature. Further more, such clusters would reform and form reversibly with temperature changes. To investigate this possibility, the sample was heated above T_{thr} to 1230 K for 10 s, then cooled to 1100 K and held isothermally for 30 mins. Then the sample was allowed to cool by free radiative cooling. The recalescense temperate was found to be identical to that observed when the 30 min intermediate step at 1100 K was not carried out. This experiment shows that the heterogeneous nucleation sites once eliminated by overheating, do not reform when the sample is cooled below T_{thr}. Apparently, the heterogeneous nucleation sites involved do not form and reform reversibly in the equilibrium melt. Equilibrium atomic clustering in the melt can thus be ruled out as an explanation of the overheating effect.

A second explanation of the overheating effect in terms of liquid phase separation in the melt can be considered where T_{thr} would

correspond to crossing a miscibility gap. In this case, the 30 min intermediate step would be sufficient to permit phase separation to take place below T_{thr}. Thus, one would expect to observe less undercooling following the 1100 K step. As such, we rule out phase separation as an explanation as well.

A consistent explanation of the above observations is that the T_{thr} corresponds to the liquidus temperature of a second phase. When such a precipitate phase is present in the original sample, one must overheat above the liquidus of this phase to melt it. Once melted, the second phase can only reform by nucleation. If the precipitated phase is assumed to act as a heterogeneous nucleant during crystallization of the undercooled glass forming liquid, then this phase must nucleate once again (presumably by homogeneous nucleation) during subsequent undercooling.

The dependence of T_{thr} on the overall oxygen content of the alloy has been studied. This is shown in fig. 5.5. The figure shows T_{thr}, T_{recl} following overheating above T_{thr}, and T_{recl} without overheating above T_{thr}. The systematic dependence of T_{thr} on the logarithm of the oxygen concentration suggests a relationship between the liquidus of the precipitate phase and oxygen concentration, C_O. In particular, this liquidus temperature depends roughly linearly on the oxygen chemical potential (the chemical potential depends linearly on oxygen content for a dilute solution). This in turn suggests that the T_{thr} vs. C_O is the liquidus curve of an oxide phase. One notices, for example, that all samples undercooled from below T_{thr}, recalesce at the same temperature. Unmelted oxide precipitates act as a heterogeneous nucleation site for crystallization of the

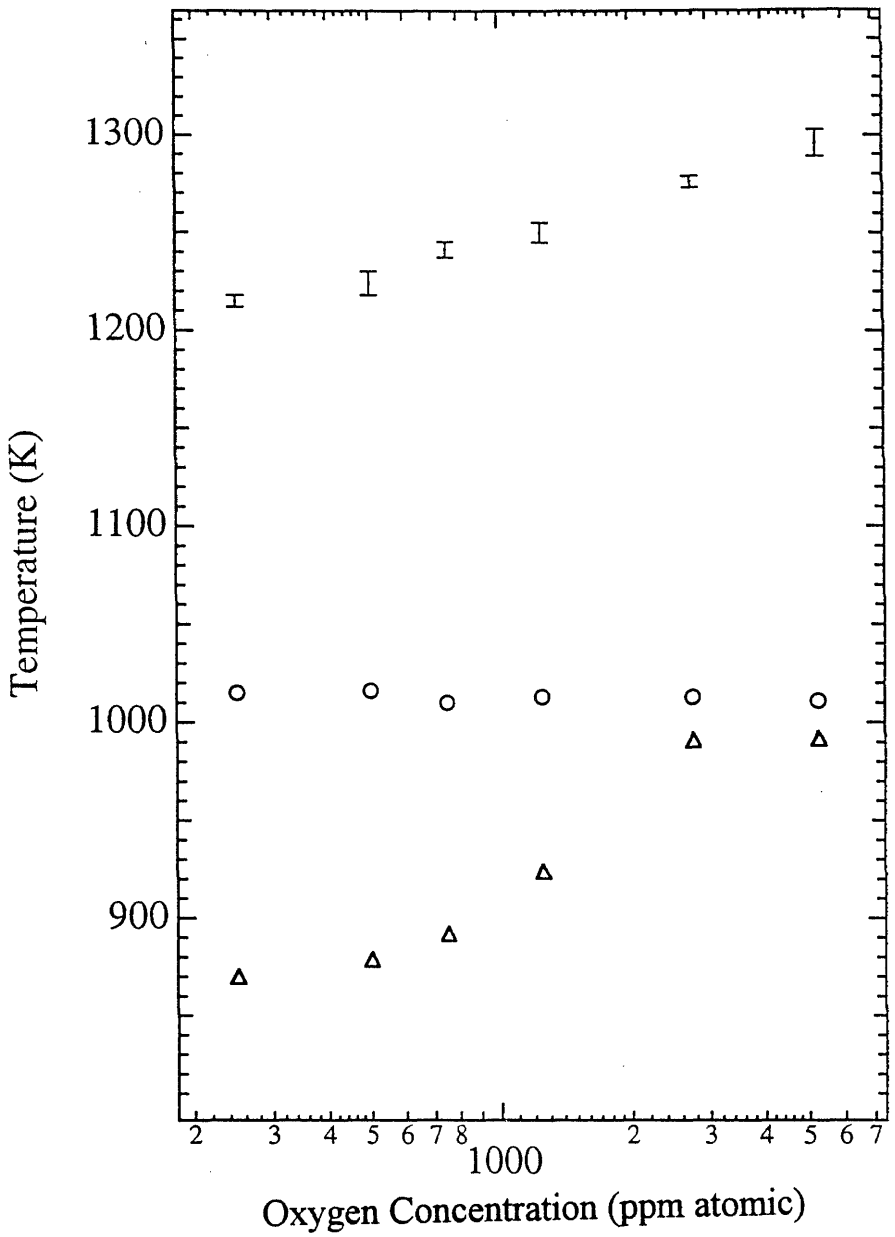

Fig 5.5 From top to bottom: initial temperature threshold for maximum undercooling, recalescence temperature for samples being cooled from below threshold, and recalescence temperature for samples being cooled from above threshold temperature versus oxygen concentration of the $Zr_{52.5}Ti_5Cu_{17.9}Ni_{14.6}Al_{10}$ samples respectively.

undercooled alloy. The nucleation temperature is determined only by the fact that such sites are present and not by their total number. This is not surprising since the density of such oxide particles in the melt is probably very high. Once the oxide precipitate is remelted by crossing its liquidus, T_{thr}, the heterogeneous nucleation sites are eliminated and must reform by homogeneous nucleation during subsequent undercooling of the sample. The homogeneous nucleation temperature for the oxide phase depends systematically on the degree of undercooling with respect to the oxide liquidus (see fig. 5.5). As such, the maximum undercooling achieved tends to decrease with increasing oxygen content in a manner which approximately follows T_{thr} as seen in fig. 5.5.

5.5 OXYGEN CONCENTRATION DEPENDENCE OF THE TTT DIAGRAMS

The TTT diagrams for crystallization of the undercooled melt (as determined by recalescence) were measured as a function of oxygen content. The sample was heated above T_{thr}, then cooled radiatively by blocking the iris of the xenon lamp. Following the procedure described in chapter 4, the crystallization times for samples with varying oxygen content at varying temperature were recorded. When the crystallization time becomes comparable to the radiative cooling time, a correction to the crystallization time is required since the duration of the isothermal step is no longer much longer than the radiative cooling time. The correction method has been discussed in chapter 4. Fig. 5.6 shows the resulting isothermal TTT diagrams obtained when the correction is applied to alloys with varying oxygen content.

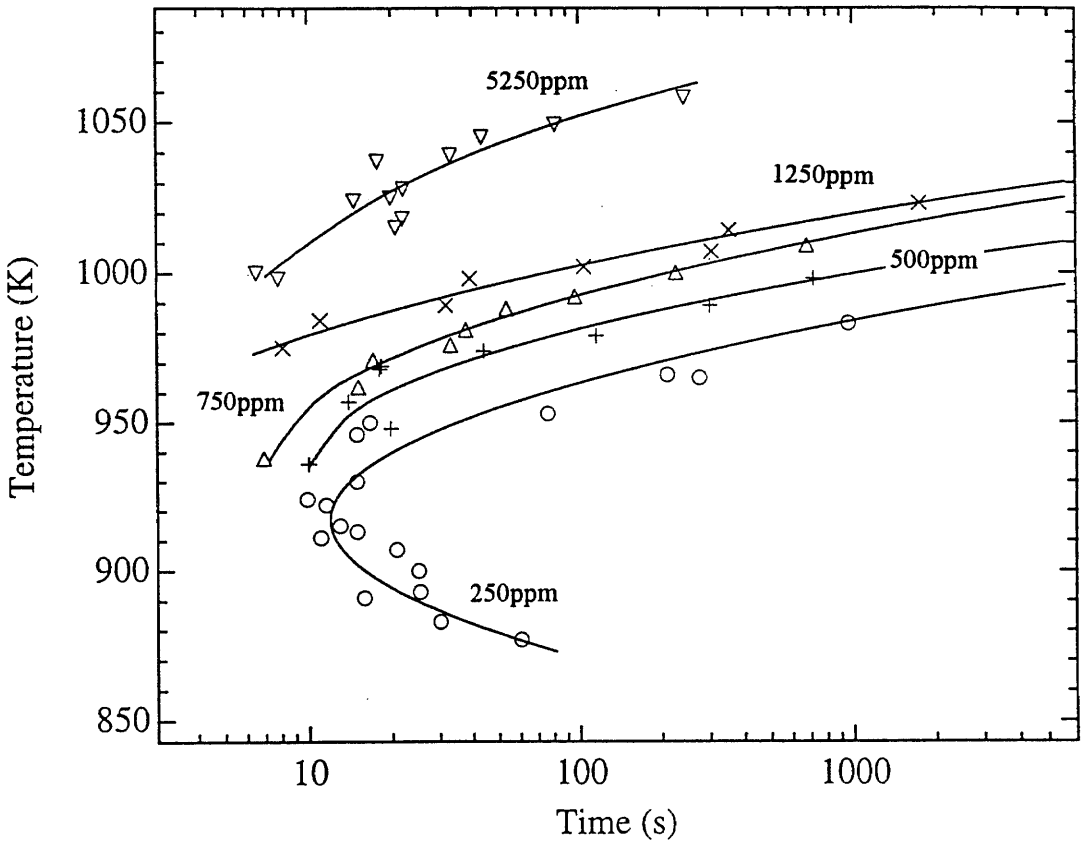

Fig. 5.6 From top to bottom: time-temperature-transformation diagrams of $Zr_{52.5}Ti_5Cu_{17.9}Ni_{14.6}Al_{10}$ alloys of 5250, 1250, 750, 500 and 250 atom ppm oxygen respectively.

Using the fitted TTT curves, the crystallization times for samples of different oxygen concentrations at a series of temperatures (under isothermal conditions) was estimated. The results are shown in fig. 5.7. The crystallization time decreases by orders of magnitude (at a given undercooled temperature) as one goes from 250 ppm to 5250 ppm oxygen. The trend in fig. 5.7 suggests that oxygen induced crystallization is the rate limiting process for even the cleanest sample studied here. This is consistent with the existence of an overheating effect and T_{thr} above the melting point in even the cleanest sample (250 ppm oxygen). When the cleanest sample is cooled from below T_{thr}, it recalesces at 1015 K. When cooled form above T_{thr}, recalescence requires 1000 s at 983 K. By extrapolation, it would take tens of hours or days to crystallize at 1015 K. This suggests that a sample of higher purity (< 250 ppm oxygen) would exhibit even greater undercooling and stability against crystallization.

5.6 IMPLICATIONS

In studies of crystal nucleation in undercooled melts, investigators have frequently used the condition of maximum undercooling to indicate homogeneous nucleation. This is a necessary but not sufficient condition since further extension of experimental undercooling cannot be ruled out. We propose to use the existence of an overheating effect to rule out homogeneous nucleation. This may not be a sufficient condition; however, it is a stronger condition than the maximum undercooling criteria and is experimentally more accessible.

Currently, the use of microgravity and ground based containerless processing facilities have been employed in a broad effort to study crystal

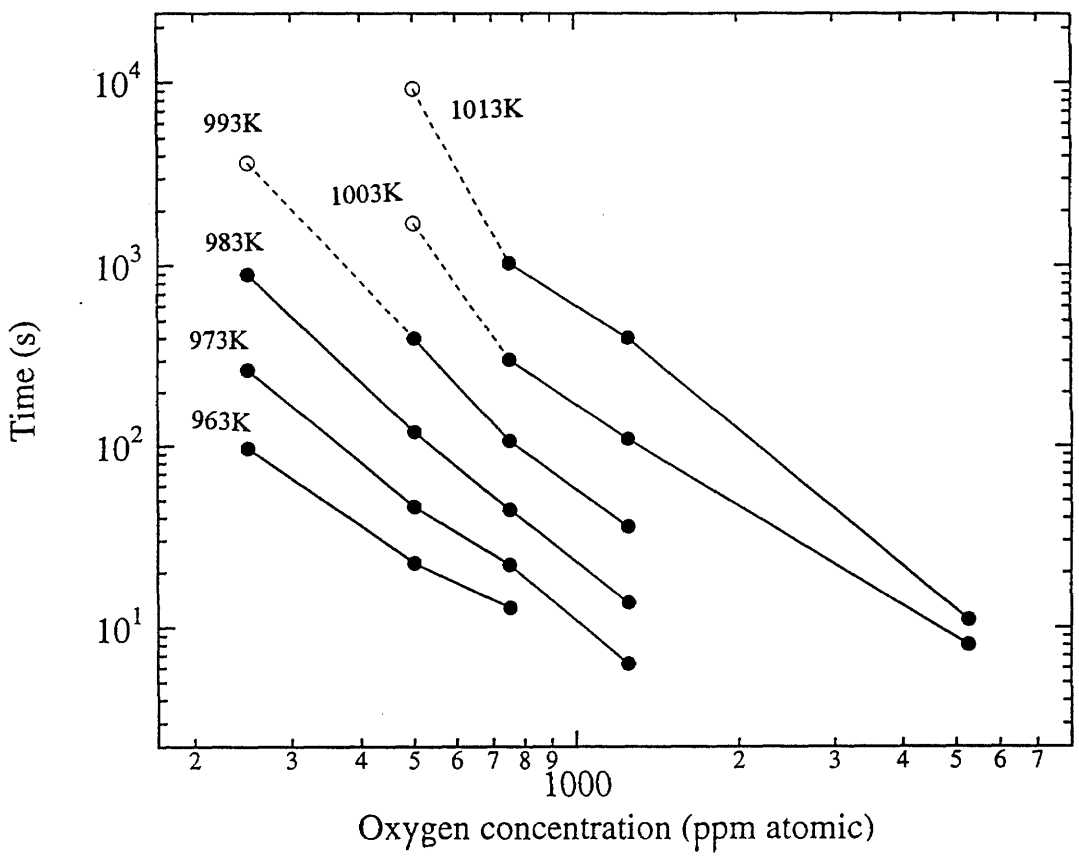

Fig. 5.7 From top to bottom: crystallization incubation time at 1013 K, 1003 K, 993 K, 983 K, 973 K, and 963 K versus oxygen concentration of the $Zr_{52.5}Ti_5Cu_{17.9}Ni_{14.6}Al_{10}$ alloys. Solid circles are from the measured TTT diagram. Open circles are extrapolated from the measured TTT diagram.

nucleation, undercooling, and physical properties of liquids such as surface tension, viscosity, atomic diffusion, etc.. Deep undercooling and stability of the liquid phase with respect to crystallization are necessary to obtain the most extensive data. The results presented in this chapter suggest that the use of the highest purity materials available and the overheating technique will enhance undercooling and improve the productivity of such investigations.

In the present experiments, it is not possible for us to predict at what oxygen purity level the heterogeneous nucleation of oxide precipitates will cease to be the rate limiting factor in crystallization kinetics of the melt. Extrapolation of the present data to lower oxygen levels suggests the reduction in nucleation rates, but the nature of the TTT diagram at lower levels cannot be predicted with confidence. The data which have been obtained show that the present alloy should in fact be viewed not as a 5-component system, but a 6-component system in which the dilute component oxygen plays a controlling role in determining glass forming ability. For glass forming alloys with high reduced glass transition temperature T_{rg}, other factors may be important. For instance, the viscosity of the melt in the undercooled regime may be very high in the undercooled region leading to reduced mobility of impurities and greater kinetic resistance to nucleation of a precipitate phase. High values of T_{rg} may thus still be an important factor in determining glass forming ability.

Impurity effects on crystal nucleation are expected to be common. It is likely that other impurities (e.g., carbon, nitrogen, etc.) may play an important role in nucleation of a variety of glass forming alloys similar to that played by oxygen in the present study. As such, reduction of impurity

levels may lead to improvements in the glass forming ability of a number of alloys and should be emphasized in the search for glass forming systems.

5.7 SUMMARY

In this chapter, a systematic study of the effects of oxygen impurities on crystal nucleation in a bulk glass forming system has been presented. Overheating the melt above a well defined threshold temperature, T_{thr}, is required to achieve maximum undercooling. T_{thr} depends systematically on oxygen content and is identified as the liquidus temperature of oxide precipitates. Heating above T_{thr} results in dissolution of the precipitates into the melt. In subsequent undercooling, the precipitates nucleate homogeneously at a temperature which depends on the oxygen content in solution in the melt. In both cases (overheating below or above T_{thr}), the precipitates are catalytic sites for heterogeneous nucleation for other intermetallic phases and control the crystallization behavior of the glass forming alloy. The systematic behavior of the TTT diagrams with oxygen content was also investigated for samples overheated above T_{thr}. The results suggest that the critical cooling rate for glass formation in this system depends dramatically on oxygen impurity levels.

REFERENCES

1. D. Turnbull, J. Chem. Phys. **20**, 411 (1952).
2. B. Chalmers, in *Principles of Solidification*, (John Wiley & Sons, New York, 1964), p.78.
3. H. W. Kui, A. L. Greer, and D. Turnbull, Appl. Phys. Lett. **45**, 615 (1984).
4. A. Inoue, T. Zhang, and T. Masumoto, Mater. Trans. JIM **31**, 425 (1990).
5. T. Zhang, A. Inoue, and T. Masumoto, Mater. Trans. JIM **32**, 1005 (1991).
6. A. Inoue, T. Nakamura, N. Nishiyama, and T. Masumoto, Mater. Trans. JIM **33**, 937 (1992).
7. A. Peker, and W. L. Johnson, Appl. Phys. Lett. **63**, 2342 (1993).
8. X. H. Lin, and W. L. Johnson, J. Appl. Phys. **78**, 6514 (1995).
9. X. H. Lin, and W. L. Johnson, to be published.
10. W. K. Rhim, S. K. Chung, D. Barber, K. F. Man, G. Gutt, A. J. Rulison, and R. E. Spjut, Rev. Sci. Instrum. **64**, 2961 (1993).
11. A. Gladys, M. Brohl, F. Schlawne, and H. Alexander, Z. Metall. **76**, 254 (1985).
12. M. Herlach, and F. Gillessen, J. Phys. **F17**, 1635 (1987).
13. Dunst, D. M. Herlach, and F. Gillessen, Mat. Sci. Eng. **A133**, 785 (1991).

Chapter 6
Discussions on Glass Formation in Multicomponent Alloy System

6.1 INTRODUCTION

Through the metallic glass development and property studies of resulting metallic glasses, it has been recognized that there are many factors that influence the crystallization of undercooled liquid alloys. These factors ultimately control the glass formation and cooling rate requirement. Some factors, such as lower reduced glass transition temperature, complexity of the alloy system, and strong glass behavior, hinder the crystallization and thus in turn promote the glass formation. Other factors, such as impurity induced heterogeneous nucleation, and decomposition in the undercooled liquid, enhance crystallization and thus in turn hurt the glass formation. In this chapter, these factors are discussed briefly and some possible ways to realize favorable factors and to avoid unfavorable factors are proposed.

6.2 REDUCED GLASS TRANSITION TEMPERATURE

Shortly after Duwez et al. showed that rapid quenching of certain eutectic (or near eutectic) alloy melts at cooling rates of 10^6 K/s resulted in suppression of crystal nucleation and formation of a glass[1], Turnbull et al. rationalized these results in terms of the classical theory of crystal nucleation in undercooled liquids which is summarized in ref. 2. Following his earlier theoretical analysis, Turnbull argued that the rate of

homogeneous crystal nucleation in undercooled metal alloys should become too low to measure in the laboratory when reduced glass transition temperature T_{rg} approaches a value of 2/3.

In Turnbull's treatment of crystallization of the undercooled liquid, polymorphic homogeneous crystallization was assumed. In fact, this polymorphic nucleation assumption is not valid for most glass forming alloys, because the glass forming alloys very frequently have compositions near eutectics and composition fluctuation and/or elemental diffusion are necessary for nucleation. It is also evident that for some (if not all) undercooled liquids, the crystallization starts by heterogeneous nucleation triggered by impurity particles. Surprisingly, the parameter T_{rg} is still the best indicator for GFA of alloys. This is because that in Turnbull's treatment, the increasing driving force for crystallization and viscosity of the undercooled liquid with decreasing temperature were considered. These two parameters are also the dominant factors for non-polymorphic nucleation and heterogeneous nucleation. Therefore, T_{rg} correlates well with the GFA of real alloys.

Since T_g does not generally vary as rapidly as T_m with composition change, to search good metallic glass forming alloys, the most intuitive approach is to search for deep eutectics. However, all the deep binary eutectics have been studied thoroughly and no bulk metallic glasses have been found. All the recently discovered bulk metallic glasses are ternary or higher order alloys. Unfortunately, our knowledge about ternary or higher order phase diagrams is very limited. This situation will not change in the near future. Thus, a simple approach is to combine deep binary eutectics to obtain deeper higher order eutectics using some

empirical guidelines for selecting alloy systems. Many of the known bulk metallic glass forming alloys are combinations of binary eutectic alloys.

It has been recognized for a long time that large difference between the components' atomic size favors glass formation.[3] Recently, Inoue et al.,[4] and Peker[5] used atomic size difference argument to interpret the exceptional good glass forming abilities of newly found bulk metallic glasses. Here, I will try to rationalize this argument in terms of theory of physical metallurgy.

Molar Gibbs free energy of mixing of a regular solution of A and B elements is:

$$\Delta G_{mix} = RT(X_A \ln X_A + X_B \ln X_B) + \Omega X_A X_B \qquad (6.1)$$

where R is gas constant, T is temperature, X_A and X_B are the mole fractions of components, Ω is a parameter independent of temperature and composition. Using this formula, one can structure a phase diagram for elements A and B. The phase diagram of A and B is dependent on the values of Ω for crystalline and liquid mixture. Shown in fig 6.1 are several phase diagrams calculated for a hypothetical system A-B containing a crystalline and a liquid phase with melting temperature of T_A=800 K and T_B=1200 K and with entropies for fusion for both A and B set to 10 J/molK, which is typical value for metals.[6] The parameters Ω_s and Ω_l have been varied systematically to generate various panels of fig. 6.1. These phase diagrams suggest that when mixture in liquid phase is favorable and mixture in crystalline phase in unfavorable, a deep eutectic results.

According to the semi-empirical Hume-Rothery rule,[7,8] the larger the atomic size difference of component elements, the smaller the solid solubility. When the atomic size difference exceeds 14-15%, solid

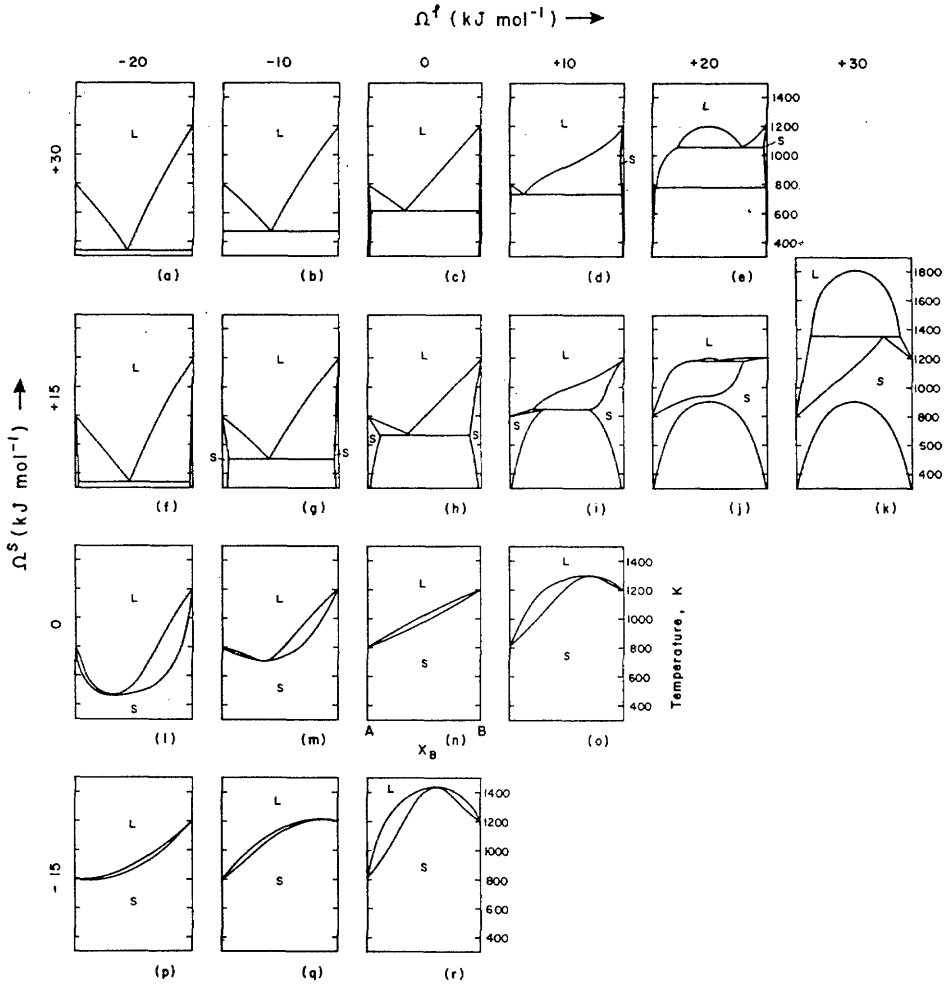

Fig. 6.1 Topological changes in the phase diagram for a system A-B with regular solid and liquid phases, brought about by systematic changes in the regular solution parameters Ω_s and Ω_l. (reproduced from ref. 6).

solubility becomes restricted. This is known as 15% rule. Combining Hume-Rothery rule with regular solution theory, one can understand why large atomic size difference among components favors glass formation. Since elements with large atomic size are not soluble in the solid state, a eutectic phase diagram results. This in turn tends to satisfy the T_{rg} criterion for glass formation.

Another factor affecting the phase diagram is the electronegativity of the elements. As the electronegativity difference between components increases, the atomic interaction among the components, represented by the negative heat of mixing, increases. When the crystal structures of the pure elements are different, a more negative heat of mixing for the liquid phase than that for the crystalline phase is expected, and a deeper eutectic results. However, in above arguments, the formation of intermediate phases is neglected. When the electronegativity difference is too large, and thus the affinity between two elements is too strong, very stable intermetallic compound forms, and the liquidus temperature rises again. Therefore, the electronegativities among the component elements must be different, but also within a certain range, in order to favor a good glass forming alloy. One piece of evidence for this argument is that boron forms glasses with later-transition-metals (such as Fe, Co, and Ni), but not with early-transition-metals (such as Ti and Zr). The reason for this can be seen in table 6.1, which lists the atomic radius and electronegativity values of some selected elements.[9] The electronegativity deference are 0.2 between B and Ni, but 0.5 between B and Ti. Therefore, B-Ni phase diagram, as shown in fig 6.2,[10] has many low lying eutectics, whereas, the B-Ti phase diagram, as shown in fig. 2.14, has a high lying liquidus line covering the

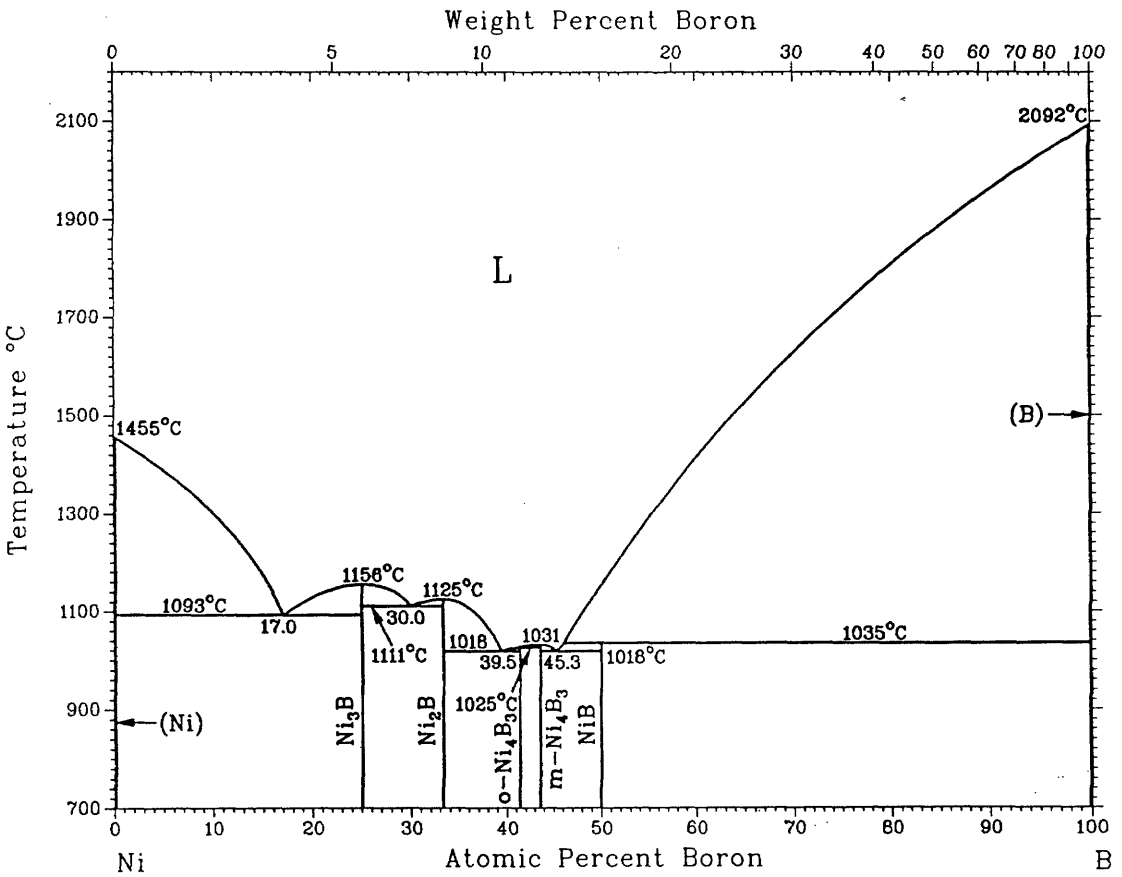

Fig. 6.2 Phase diagram of B-Ni. (reproduced from ref. 10).

whole composition range corresponding very stable Ti-B compounds. Thus, Ni-B alloys are good glass formers, but Ti-B alloys are not. Comparing B with Be atoms, both of them are much smaller than Zr and Ti atoms. Addition of Be or B would be both expected to enhance the GFA of Ti-Zr-Cu-Ni alloys from the atomic size rule. In fact, addition of Be greatly enhances GFA of the alloys, whereas, addition of B ruins GFA. The contradictory roles of B and Be can be rationalized by their different electronegativity values.

	Ti	Zr	Ni	Cu	Be	B
Atomic Radius	1.47	1.60	1.24	1.28	1.12	0.98
Electronegativity	1.5	1.4	1.8	1.9	1.5	2.0

Table 6.1 Atomic radius and electronegativity values of some selected elements. (reproduced from ref. 10).

6.3 COMPLEXITY OF THE ALLOY AND DIFFUSION CONTROLLED CRYSTALLIZATION

Looking at the short list of bulk glass forming alloys, one immediately recognizes that a high order alloy is a necessity for bulk glass formation. Besides the fact that higher order alloys may have a deeper eutectic than lower order alloys, the complexity of a high order alloy, itself has a positive effect on glass formation as described by "confusion principle".[11] In the crystallization of a glass forming alloy, since the crystal

compositions are generally different from the liquid, nucleation only occurs in the region in which the concentration of each element simultaneously satisfies the requirements of the crystalline phase, through either fluctuation or decomposition. The more elements the system has, the less the probability this will happen. Thus the more sluggishly the crystallization occurs, the better the glass forming ability. This "confusion principle" is an important correction to the T_{rg} dependence of glass forming ability.

In the crystallization of a near eutectic alloy, some phases are easier to form than others. The Laves phase, which has a broad homogeneity range, in the Ti-Zr-Cu-Ni system is one example. The eutectic alloy is not necessarily the best glass former. Good balance between having low melting temperature and keeping certain a distance from the composition of the easy-forming crystalline phases results in good glass forming alloys.

Adding new elements to an alloy has been proven to be an effective way to improve the glass forming ability. In selecting elements, the atomic size rule and electronegativity rule must be considered. Besides these rules, I would like to discuss what a "real" new element is to an alloy. Taking Zr-Cu-Ni alloy as an example, both Ti and Hf are complete soluble with Zr.[10] All these elements have deep eutectics with Ni and Cu, as show in figs. 2.1, 2.2, 2.3, 2.4, 6.3[10], and 6.4[10]. It has been proven that combining Ti with Zr results in bulk glass formation in Ti-Zr-Cu-Ni system, and even better glass forming ability in Zr-Ti-Cu-Ni-Al and Zr-Ti-Cu-Ni-Be systems with the help of Al and Be. Then, a question raises naturally: how about adding Hf. Comparing binary phase diagrams of Zr and Hf with Cu and Ni, one finds that most of the binary Hf-Ni and Hf-Cu

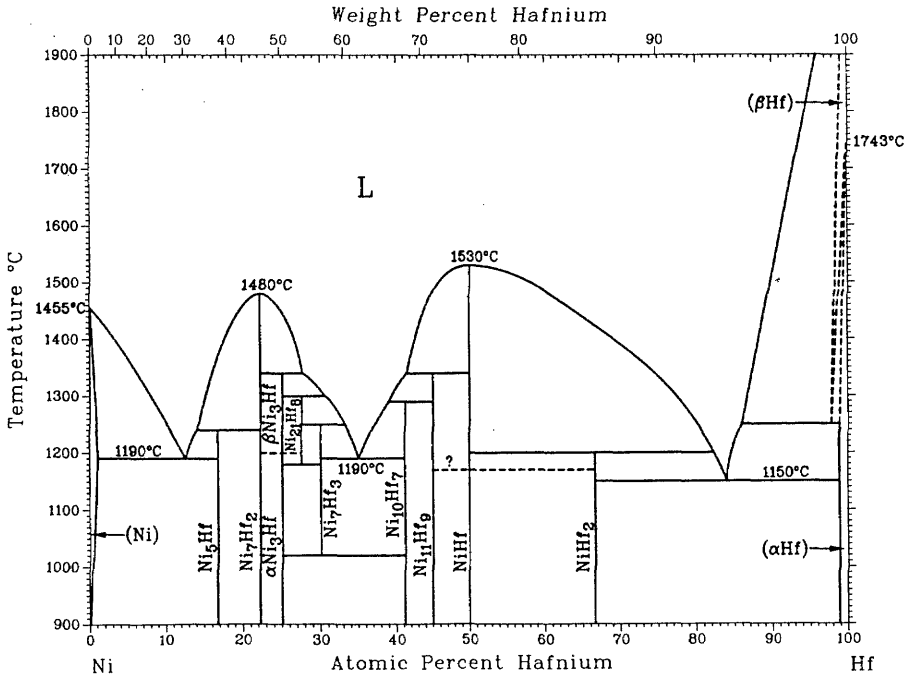

Fig. 6.3 Phase diagram of Hf-Ni. (reproduced from ref. 10)

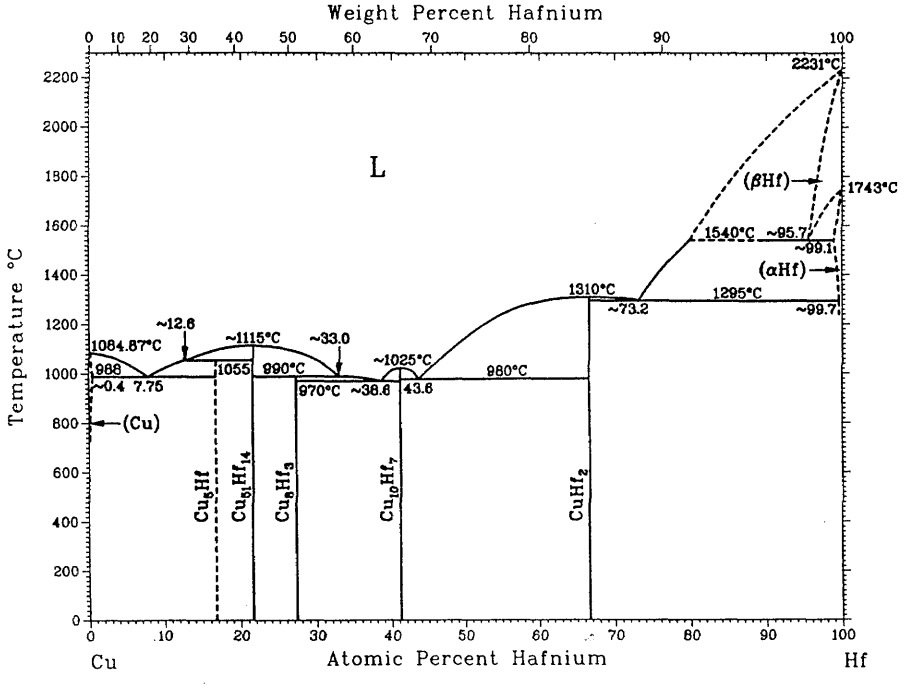

Fig. 6.4 Phase diagram of Hf-Cu. (reproduced from ref. 10)

phases are of the same crystal structures as the corresponding Zr-Ni and Zr-Cu phases. Therefore, the intermetallic compounds of Hf with Cu and Ni are expected to be completely soluble with corresponding Zr bearing compounds. No higher order eutectic is expected to appear by adding Hf in Zr alloys. On the other hand, because Hf and Zr are interchangeable in all intermediate phases, only the right total concentration of Zr and Hf is required to form any of these crystalline phases. Hence, adding Hf to Zr alloys does not make crystallization more difficult to occur from the point of view of the confusion principle, since it is not necessary to distinguish Hf and Zr in forming the crystalline phases. Therefore, while Ti is considered as a new element to Zr-Cu-Ni system, Hf is not. Replacing part or the whole of the Zr content in the glasses with Hf can tilt some properties of the glasses, such as density and glass transition temperature, but can not change the glass forming ability drastically. This example suggests that a "real" new elemental addition to an alloy system should have some new and distinct interaction relation with some of the components. This in turn will enhance glass formation.

6.4 IMPURITY INDUCED HETEROGENEOUS NUCLEATION

Generally all molten alloys contain some impurities, which may come from the elemental materials used or from the alloying processing. The impurities may appear as particles suspending in the melt. They may also be dissolved in the melt and then precipitate out during the process of undercooling. When crystalline embryos of the alloy can wet the impurity particles, i.e., when m defined by equation 5.3 is less than 1, the impurities will catalyze the crystallization. If the concentration of the impurity is

high enough, impurity induced crystallization will become the rate controlling process.

There are many kinds of impurities, such as O, N, P, S, B, etc. in metallic alloys. Some of the impurities may cause heterogeneous nucleation in certain alloys. Since Ti forms very stable compound with B, it may also be viewed as a harmful impurity for B bearing glass forming alloys such as Fe-B. The impurity does not need to be present at a high concentration to become the controlling factor for the crystallization process. As in the case of oxygen impurity in Zr based alloy, 250 ppm is more than necessary to cause heterogeneous nucleation, though this is the impurity level for the purest laboratory materials. Therefore, heterogeneous nucleation induced crystallization is expected to be common for many alloys, and will in turn determine the glass formation. Whether there is, in fact, any bulk alloy that crystallizes through homogeneous nucleation, is questionable. As such, when the critical cooling rates for glass formation are discussed, the impurity levels of the alloys must be addressed. This may be one of the factors explaining the disagreement about the maximum sizes specimens obtained for certain metallic glasses among different research groups.

In practical applications, in order to solve or suppress the impurity effect on the glass formation, using reasonable pure materials and processing melts under vacuum or inert atmosphere are necessary. For some impurities which dissolve into the melt at elevated temperature, such as the oxide particles in Zr based alloys, overheating the melt before quenching is very important. While purifying the elemental materials is difficult and expensive on a large scale, considering the differing heats of

formation, it is possible to transfer one kind of impurity to another kind of impurity by adding trace amounts of a new element. If the newly formed impurity phase is a liquid or glass itself (such as B_2O_3 and SiO_2) at the glass transition temperature of the alloy, it should then have less catalytic effect for the crystallization of the alloy. Even if the new formed impurity is crystalline, if the crystal embryos of the alloy do not wet the impurity surface or have a higher wetting angle than the original impurity, the catalytic effect of the impurity is neutralized or suppressed. In order to do this, the interfacial energies between liquid and crystalline alloy, liquid alloy and different impurity substrates, and crystalline alloy and different impurity substrate must be known. More emphasis in the future should be put on interfacial energy studies.

6.5 STRONG GLASS BEHAVIOR AND DECOMPOSITION IN THE UNDERCOOLED LIQUID

The recently found bulk metallic glasses have a large supercooled region when heated above the glass transition temperature. The thermal stability of these glasses enables physical properties to be measured far into the undercooled liquid region.

Bakke et al. measured the viscosity of the $Zr_{46.75}Ti_{8.25}Cu_{7.5}Ni_{10}Be_{27.5}$ undercooled liquid over a temperature range of 120 K.[12] Their result show that this glass tends to be a "strong" glass. This means that the viscosity in the range between T_g and T_m is higher than what has been previously assumed for other metallic glasses. The high viscosity of the undercooled melt makes the atomic transport more sluggish. Thus, crystallization can be more easily avoided. However, the origin of the strong glass behavior

remains unknown. One can only suspect that high T_{rg} and large dispersed atomic size distribution may make the atomic packing of the alloy very compact. As such, the free volume in the melt is very small. This in turn gives the alloy high viscosity value. How to apply this finding to alloy development is unknown.

In a deeply undercooled liquid, certain short range order at specific compositions may give rise to a low enthalpy value, resulting in a local minimum of free energy. Then, the melt will decompose into those compositions corresponding to local minima of free energy. The short range atomic orders in the liquid may be directly related to that of some crystalline phases having the same short range orders. In this case, the decomposed undercooled liquid or glass will crystallize into the corresponding crystalline phases polymorphicly. The composition requirements for crystallization are much easier to reach by decomposition than by random fluctuation. The "complexity" effect on the crystallization is partially offset by decomposition. As such, the crystallization can be greatly enhanced. Decomposition has been found to occur in the $Zr_{41.2}Ti_{13.8}Cu_{12.5}Ni_{10}Be_{22.5}$[13] alloy. One would expect an even better GFA for $Zr_{41.2}Ti_{13.8}Cu_{12.5}Ni_{10}Be_{22.5}$ alloy if decomposition did not occur. Effective ways should be developed to suppress liquid phase separation.

REFERENCES

1. W. Klement IV, R. H. Willens, and P. Duwez, Nature **187**, 869 (1960).
2. D. Turnbull, Contemp. Phys., **10**, 473 (1969).
3. H. A. Davies, in *Amorphous Metallic Alloys*, Edited by F. E. Luborsky, (Butterworths, London, 1983), p 8.
4. A Inoue, T. Zhang and T. Masumoto, J. Non-Cryst. Solids **156-158**, 473 (1993).
5. A. Peker, *Ph. D. Thesis*, California Institute of Technology, 1994.
6. A. D. Pelton, and W. T. Thompson, Prog. Solid State Chem., **10**, Part 3, p 119.
7. W. Hume-Rothery, J. Inst. Metals **35**, 295 (1926).
8. W. Hume-Rothery, R. E. Smallman, and C. W. Haworth, *The Structure of Metals and Alloys*, 5th Ed., (The Institute of Metals, London, 1969), p 349.
9. Sargent-Welch Co., *Periodic Table*, 1968.
10. T. B. Massalski ed., *Binary Alloy Phase Diagrams*, 2nd edition, ASM International (1990).
11. A. L. Greer, Nature **366**, 303 (1993).
12. E. Bakke, R. Busch, and W. L. Johnson, Appl. Phys. Lett. **67**, 3260 (1995).
13. R. Busch, S. Schneider, A. Peker, and W. L. Johnson, Appl. Phys. Lett. **67**, 1544 (1995).

Appendix I

Glass transition and crystallization temperatures of some representative Ti-Zr-Cu-Ni glass forming alloys determined by DSC at a heating rate of 20K/min. The missing crystallization temperatures are due either to the absence of crystallization peaks up to 873K, or to the crystallization temperature being too close to 873 to be determined accurately. Here 873K is the maximum working temperature of the DSC.

Composition				T_g (K)	T_{x1}(K)	T_{x2}(K)	T_{x3}(K)	T_{x4}(K)
Ti	Zr	Cu	Ni					
35	10	55	0	668	697	760	805	
33	13.4	49.6	4	674	694	758	800	
34	11	47	8	671	717	778	813	
33.4	11.9	42.7	12	671	724	780		
9.9	43.3	42.8	4	657	691	742	791	
9.5	45.2	37.3	8	653	690	729	769	
9.5	48.9	29.6	12	637	678	709	748	782
10	50	20	20	644	680	749	759	780

Appendix II

Vicker's hardness of some representing Ti-Zr-Cu-NI glass forming alloys determined using a load of 500 gram.

Composition				$H_v(kg/mm^2)$
Ti	Zr	Cu	Ni	
36.9	5.8	53.3	4	562
33	5.8	57.2	4	626
33	9.6	53.4	4	618
34	11	47	8	628
39.6	5.5	46.9	8	596
35.9	5.5	50.6	8	616
32.2	5.5	54.3	8	642
28.5	9.2	54.3	8	670
32.2	9.2	50.6	8	618
28.5	12.9	50.6	8	626
9.5	37.8	44.7	8	616
9.5	41.5	41	8	553
9.5	45.2	37.3	8	519
9.5	48.9	33.6	8	501
10	55	25	10	462
5.8	45.2	41	8	536
5.8	48.9	37.3	8	523
5	55	32	8	487
10	50	20	20	499
10	50	15	20	558

Appendix III

Representative bulk glass forming Zr-Ti(Nb)-Cu-Ni-Al alloys that can be cast into at least 1 mm thick glassy strips.

Zr	Ti	Nb	Al	Cu	Ni	comment
45	7.5	5	7.5	19.5	15.5	
50	7.5	5	7.5	16.5	13.5	
55	7.5	5	7.5	13.5	11.5	
47.5	5	5	7.5	19.5	15.5	
52.5	5	5	7.5	16.5	13.5	P
57.5	5	5	7.5	13.5	11.5	P
50	4	3.5	7.5	19.5	15.5	P
55	4	3.5	7.5	16.5	13.5	P
60	4	3.5	7.5	13.5	11.5	P
50	0	7.5	7.5	19.5	15.5	
55	0	7.5	7.5	16.5	13.5	P
60	0	7.5	7.5	13.5	11.5	P
45	0	7.5	7.5	20	20	
45	0	5	7.5	23.5	19	
50	0	5	7.5	20.5	17	P
55	0	5	7.5	18	14.5	P
60	0	5	7.5	15	12.5	P
45	0	10	7.5	20.5	17	
50	0	10	7.5	18	14.5	
55	0	10	7.5	15	12.5	

Zr	Ti	Nb	Al	Cu	Ni	comment
52.5	0	7.5	7.5	14	18.5	
57.5	0	7.5	7.5	12	15.5	
45	0	7.5	5	23.5	19	
50	0	7.5	5	20.5	17	P
55	0	7.5	5	18	14.5	P
60	0	7.5	5	15	12.5	P
45	0	7.5	10	20.5	17	
50	0	7.5	10	18	14.5	
55	0	7.5	10	15	12.5	P
60	0	7.5	10	12.5	10	P
52.5	0	5	7.5	19.25	15.75	P
52.5	0	3.5	7.5	20	16.5	P
57.5	0	5	7.5	16.5	13.5	A
57.5	0	3.5	7.5	17.5	14	P
57	0	5	8	16.5	13.5	A
57	0	5	8.5	16.2	13.3	A
57	0	5	10	15.4	12.6	A
56.5	0	5	7.5	17	14	P
56.5	0	5	8.5	16.5	13.5	A
57	0	5	11	14.9	12.1	A
52.5	0	5	12.5	16.5	13.5	P
55	0	5	12.5	15.1	12.4	A
57.5	0	5	12.5	13.8	11.2	A
60	0	5	12.5	12.4	10.1	P
52.5	0	5	15	15.1	12.4	P

Zr	Ti	Nb	Al	Cu	Ni	comment
55	0	5	15	13.8	11.2	P
57.5	0	5	15	12.4	10.1	P
60	0	5	15	11	9	
50	0	7.5	7.5	17.5	17.5	
55	0	7.5	7.5	15	15	P
50	0	7.5	7.5	15	20	
55	0	7.5	7.5	13	17	P
52.5	0	5	8.5	14.6	19.4	P
55	0	5	8.5	13.5	18	P
57.5	0	5	8.5	12.4	16.6	P
52.5	0	5	8.5	20.4	13.6	A
55	0	5	8.5	18.9	12.6	A
57.5	0	5	8.5	17.4	11.6	A
60	0	5	8.5	15.9	10.6	P
55	0	5	8.5	18	12	A
57.5	0	5	10	16.5	11	A
54	0	5	10	18.6	12.4	A
56	0	5	10	17.4	11.6	A
52.5	0	5	12.5	18	12	P
55	0	5	12.5	16.5	11	A
57.5	0	5	12.5	15	10	A
52.5	0	7.5	10	16.5	13.5	P
57.5	0	7.5	10	13.75	11.25	P
52.5	0	2.5	10	19.25	15.75	
55	0	2.5	10	17.9	14.6	

Zr	Ti	Nb	Al	Cu	Ni	comment
57.5	0	2.5	10	16.5	13.5	
60	0	2.5	10	15.1	12.4	
52.5	5	0	7.5	19.3	15.7	P
55	5	0	7.5	17.9	16.4	A
57.5	5	0	7.5	16.5	13.5	A
52.5	5	0	10	17.9	14.6	A
55	5	0	10	16.5	13.5	A
57.5	5	0	10	15.1	12.4	P
50	5	0	10	19.3	15.7	P
45	9	0	6	30	10	
50	9	0	6	20	15	P
55	9	0	6	15	15	P
60	9	0	6	10	15	P
45	12	0	8	20	15	
50	12	0	8	15	15	
55	12	0	8	10	15	
45	5	0	5	37	8	
50	5	0	5	30	10	
55	5	0	5	20	15	P
60	5	0	5	15	15	P
65	5	0	5	10	15	P
45	7.5	0	7.5	30	10	
50	7.5	0	7.5	20	15	P
55	7.5	0	7.5	15	15	P
60	7.5	0	7.5	10	15	P

Zr	Ti	Nb	Al	Cu	Ni	comment
45	10	0	10	20	15	
50	10	0	10	15	15	
55	10	0	10	10	15	P
60	10	0	10	10	10	
45	6	0	9	30	10	P
50	6	0	9	20	15	P
55	6	0	9	15	15	P
60	6	0	9	10	15	
45	8	0	12	20	15	
50	8	0	12	15	15	P
55	8	0	12	10	15	P
45	4.5	0	10.5	30	10	
50	4.5	0	10.5	20	15	P
55	4.5	0	10.5	15	15	P
60	4.5	0	10.5	10	15	P
40	6	0	14	30	10	
45	6	0	14	20	15	
50	6	0	14	15	15	P
55	6	0	14	10	15	P
55	7.5	0	7.5	20	10	P
55	7.5	0	7.5	10	20	P
55	7.5	0	7.5	17	13	P
57.5	7.5	0	7.5	15.1	12.4	P
60	7.5	0	7.5	13.8	11.2	P

REMARKS:

P: a five gram sample can be solidified to a partially glassy ingot by turning off the power of arc melter or induction melter.

A: a five gram sample can be solidified to a fully glassy ingot by turning off the power of arc melter or induction melter.